COMPUTED TOMOGRAPHY OF CATS WITHOUT GENERAL ANESTHESIA: FEASIBILITY, PROTOCOL DEVELOPMENT AND ASSESSMENT OF CATS WITH THORACIC DISEASE

BY

CINTIA RIBEIRO DE OLIVEIRA

THESIS

Submitted in partial fulfillment of the requirements
for the degree of Master of Science in VMS-Veterinary Clinical Medicine
in the Graduate College of the
University of Illinois at Urbana-Champaign, 2011

Urbana, Illinois

Adviser:

Professor Robert O'Brien

ABSTRACT

This study consisted of three phases. On phase one, the VetMouseTrap™, a novel device that allows computed tomography (CT) of awake cats and provides a clinically supportive environment, was designed. Ten normal cats were used to test the device for safety parameters, including ambient internal oxygen, carbon dioxide levels and temperature. The final design of the VetMouseTrap™ was a transparent acrylic tube with easy access for oxygen administration at therapeutic levels with ports on both ends of the device and easy access for intravenous lines. The device is safe and met the clinical needs of cats. In phase two, CT protocols were developed and tested in awake normal cats using the VetMouseTrap™. Twenty two awake normal cats were imaged using a 16 multi-slice helical CT unit to evaluate dose equivalent protocols. Two different x-ray tube potentials (kV's), 80 and 120, and 2 different helical pitches, 0.562 and 1.75, were evaluated. The signal intensity of the pulmonary parenchyma (SI_{lung}), signal intensity of background ($SI_{backgr.}$), contrast, noise, signal-to-noise ratio (SNR), and contrast-to-noise ratio (CNR) were calculated. Three evaluators ranked the images for quality parameters including sharpness of liver margins, motion artifact, helical artifact and windmill artifact. The CT examinations were successfully completed in 90.9%of (20/22) normal cats. No artifacts directly related to the device were detected and 94% (75/80) of examinations were judged to have an absence of or minimal motion artifact. A statistically significant difference was found for SNR (P = 0.001) and CNR (P = 0.001) between all protocols. The higher pitch protocols had significantly lower noise and higher SNR and CNR, lower motion artifact, but greater helical artifacts.

The findings of the study suggest that a protocol using 80 kV, 130 mA, 0.5 s, and 0.562 pitch with a 1.25 mm slice thickness, and 0.625 mm slice reconstruction interval is recommended.

On phase three, thoracic CT was performed in 54 cats and thoracic radiography in 50 cats, and these imaging modalities were compared for imaging awake cats with signs of thoracic disease. The final diagnosis was obtained with cytology, histopathology, necropsy, or response to therapy. Cats were imaged in the VetMouseTrap™ using a 16 multi-slice helical CT system. The cats used in phase two served as control for imaging evaluation. The images were anonymized, randomized, and evaluated in consensus by two radiologists. The most common final diagnoses were lung neoplasia, lower airway disease, and cardiomyopathy (9 each). Other disease groups included mediastinal mass (8), infection (7), trauma (4) and hernia (3). CT provided additional correct diagnoses in 28% (14/50) and additional information in 76% (38/50) of the cats. Additional correct diagnoses achieved only with CT were most common for cats with trauma (n=3) and lower airway disease (n=4). The most common additional findings were lung hyperlucency (n=10), lung nodules (n=4), lung masses (n=4), bronchiectasis (n=4), and mediastinal lymphadenopathy (n=3), and the majority of these were found in cats with lower airway disease (n=8), pulmonary neoplasia (8) and mediastinal mass (6). Survey CT clinically changed the diagnosis or prognosis in 20 of the 50 cats that underwent both modalities. Contrast CT was performed without complications and most commonly in cats with lung neoplasia (n=6), mediastinal mass (n=4), and infectious (n=3) diseases, providing additional correct diagnosis in 2 cats not achieved with survey CT. Based on the results, survey and contrast thoracic CT using the VetMouseTrap™ in diseased cats is safe and clinically useful.

DEDICATION

To my parents, Beth and Lupércio, whose unconditional love, support and encouragement made everything I ever dreamed about possible. I am blessed to have you as my parents.

To my siblings, Dani e Dú, always by my side giving me support and showing me the way, albeit allowing me to take my own steps.

You are my heroes and my role models.

Aos meus pais, Beth e Lupércio, pelo amor, suporte e incentivo incondicionais, que tornaram possível conquistar tudo o que eu sonhei na vida. Eu sou abençoada por tê-los como pais.

Aos meus irmãos, Dani e Dú, que sempre estiveram ao meu lado e me apoiaram, me mostrando o caminho porém permitindo que eu desse meus próprios passos.

Vocês são meus heróis e meus exemplos de vida.

ACKNOWLEDGEMENTS

I'm deeply grateful to my mentor Dr. Bob O'Brien for his encouragement, guidance and confidence in my work. Bob, you taught me much of what I know about radiology, but also that I was capable of more than I could ever think. My profound appreciation for your advice, support and patience in every aspect of this study.

I am greatly indebted to Dr. Frank Ranallo for his invaluable help in designing this study and for the many physics lectures he provided, even being away. My great appreciation for his endless patience and countless hours on the phone answering my questions.

I also would like to thank my advisory committee, Drs. Maureen McMichael and Mark Mitchell, for their help, understanding and dedication to the completion of this study. Thank you Dr McMichael for your advice when I needed it, and Dr. Mitchell for your invaluable statistical guidance.

Many thanks to Sue Hartman, RT(R)CT, whose input on computed tomography techniques made this study a better one, and to the UIUC radiology team, Dr. Jodi Matheson and techs Caroline, Melinda, Sam, Beth, Stephanie, Jill; your support and laughter made some sad moments turn into fun ones.

TABLE OF CONTENTS

Page

INTRODUCTION

In humans, computed tomography (CT) is established as the primary imaging modality for patients with clinical signs of thoracic disease.[1, 2] Computed tomographic high contrast resolution and its lack of anatomic superposition provide unique diagnostic information that is unobtainable with conventional radiographic techniques.[3-8] Computed tomography allows better distinction among specific tissue densities and detection of subtle changes in organ size, shape, margin contour, and position.[3, 4, 8] Therefore, CT plays a key role in the diagnosis and evaluation of various thoracic syndromes and diseases such as pneumothorax, pleural and pericardial effusion, collapse of a lung lobe, congenital anomalies, pulmonary parenchymal and bronchial diseases, cysts, abscesses and primary or metastatic neoplasia of the lungs, pleura, mediastinum, lymph nodes, and chest wall. Furthermore, CT is a useful preoperative technique, a precise staging tool, and improves the use of biopsies by allowing detection of lesions not identifiable by other imaging modalities.[8]

In veterinary medicine, survey thoracic radiography is the standard imaging modality for evaluating the thorax.[3, 9] This is due, at least in part, to the need for general anesthesia when performing CT. General anesthesia has inherent risks and causes varying degrees of atelectasis that can mimic or obscure underlying disease.[10-13] Additional scans in different positions may be necessary to evaluate the patient fully, thereby increasing imaging and anesthesia time.[14]

The use of CT for the diagnosis of thoracic diseases in veterinary medicine is still under investigation with an increasing number of published clinical reports involving thoracic CT.[8] Its use to diagnose thoracic diseases in anesthetized cats has been described.[3-5] However, since the

need for general anesthesia makes this imaging modality contraindicated in a large number of patients presented in emergency conditions, including those in respiratory distress, the evaluation of these patients is usually limited and dependent on tolerance from the patient to the stress and handling necessary for thoracic radiography examination.

Chapter 1 discusses the advances in CT technology and the physical principles of CT, including image formation, image quality and artifacts. A discussion of CT in veterinary medicine is presented.

Chapter 2 discusses the development of a device, the VetMouseTrap^{TM}, for performing CT imaging in feline patients without the need for sedation or general anesthesia. The imaging and clinical requirements of the device are described, with emphasis on normal as well as diseased cats, including their special needs. Since the VetMouseTrap^{TM} was designed, safety parameters such as temperature and levels of carbon dioxide were evaluated inside the device.

Chapter 3 discusses the development of CT protocols for thoracic CT imaging of awake feline patients. Four CT protocols were developed and evaluated in 20 normal cats for the impact of kV, pitch, and patient size on image quality using the VetMouseTrap^{TM}. Image quality parameters such as CT related artifacts, motion artifact, contrast and noise were evaluated and compared for each protocol. The feasibility of performing CT imaging in awake animals was tested and discussed.

Chapter 4 discusses the use of whole-body CT in the evaluation of feline patients presented in emergency with respiratory distress, or presented with clinical signs of thoracic disease. Fifty-four cats presented with different underlying thoracic diseases were evaluated and CT images compared with thoracic radiography in 50 cats for additional information. The feasibility of performing CT in awake diseased cats was also evaluated.

CHAPTER 1

LITERATURE REVIEW

1.1 Recent advances in computed tomography

The introduction of spiral CT in the early 1990s represented a major evolutionary step in the development of CT imaging techniques in humans. With spiral CT volume data could be acquired without misregistration of anatomic detail, which resulted in a revolution for diagnostic imaging and the basis for CT angiography and the noninvasive assessment of vascular disease.[15] The ability to acquire volume data resulted in the development of three-dimensional (3D) image processing techniques including multiplanar reformation (MPR), maximum intensity projection, and volume-rendering techniques. In addition, the detection of lung and liver lesions have substantially improved. Helical CT has improved over the past eight years with faster gantry rotation, more powerful x-ray tubes, and better interpolation algorithms.[15, 16]

Multi–detector row CT also dramatically expanded into areas such as cardiac imaging with electrocardiographic (ECG)-gating capability, previously considered beyond the capability of third-generation CT scanners since they were based on the mechanical rotation of an x-ray tube and detectors. With a gantry rotation time of 0.5 second or less, and dedicated imaging reconstruction approaches, the temporal resolution for acquisition of a CT image was improved to 250 milliseconds and less, which proved to be sufficient for motion-free imaging of the heart in the mid- to end-diastolic phase when the patient had a slow to moderate heart rate (i.e., up to 65 beats per minute).[15]

The advent of multi-detector helical CT (MDCT) technology also dramatically transformed noninvasive imaging of the airways in both adults and pediatric patients.[17, 18] With high-resolution multiplanar reconstructions of the airways, many of the potential limitations of axial CT imaging could be surmounted. These post processed imaging methods are a complement to the axial original images and can be easily generated in real time at the CT workstation.[17] Post processing techniques are particularly advantageous for evaluating the airways, since image reconstructions can be created in any plane of imaging, including the long axis of the airway, providing a more useful anatomic representation of airway pathology. Three-dimensional reconstruction techniques can include external and internal renderings of the airways. External 3D rendering of the airways, or CT bronchography, depicts the inner surface of the airways and its relationship with adjacent structures. When compared with conventional axial images, external 3D reconstructions have been shown to enhance the evaluation of airway disorders by increasing the recognition of mild and focal airway stenosis, providing supplemental information about the shape, length, and severity of airway stenosis, improving the understanding of airway anatomy, and increasing the diagnostic confidence of findings seen on transverse images. Internal 3D rendering of the airways, or virtual bronchoscopy, enables navigation through the lumen of the airway to the sixth-order and seventh-order subdivisions, providing an endobronchial perspective similar to that of conventional bronchoscopy. Virtual bronchoscopy is useful for the assessment of airway stenosis, guidance of transbronchial biopsies, evaluation of aspirated foreign bodies, confirmation of anatomic airway abnormalities, and screening for tracheobronchomalacia.[17]

1.2 Limitations of conventional radiography

Film/screen radiography has several limitations that limit its ability to visualize low-contrast tissues and structures with acceptable levels of patient radiation exposure. These limitations include inefficient high scatter-to-primary x-ray ratios, and superimposition and decreased conspicuity.[19] Due to large beam areas, scattered photons represented 50% or more of the x-rays absorbed by the screens, even with a grid able to remove high levels of scatter. Scatter effectively reduces subject contrast by creating a background intensity unrelated to the overlying anatomy. Radiography renders a 2-dimensional image of a 3-dimensional volume, and as a consequence, over- and underlying tissues and structures are superimposed, generally resulting in reduced conspicuity as well as subject contrast.[19]

1.3 Physics of computed tomography

Development of the first CT commercially viable CT scanner occurred in 1967 by Godfrey Hounsfield, an engineer at British EMI Corporation. Hounsfield was studying situations in which large amounts of potential information were inefficiently used- a description of conventional radiography. He estimated that by taking careful measurements of x-ray transmission through a subject at many positions across the subject and at a sufficient number of angles, it should be possible to determine attenuation differences of 0.5%—possibly sufficient to distinguish between soft-tissues. After verification of his hypothesis with a laboratory apparatus, the first clinical CT scanner was built and installed in England in September of 1971.[19-21] The prototype took 160 parallel readings through 180 angles, each 1° apart, with each scan taking a little over 5 minutes. The images required 2.5 hours to be processed by algebraic reconstruction techniques on a large computer. The scanner had a single photomultiplier detector and operated on the Translate/Rotate principle.[21]

Computed tomography is based on x-ray densitometry and uses the same basic principles as conventional radiography.[22] X-rays result from the conversion of the kinetic energy attained by electrons accelerated under a potential difference- the magnitude of which is termed voltage with units of volts (V) into electromagnetic radiation, as a result of collisional and radioactive interactions. An x-ray tube provides the proper environment and components to produce x-rays, whereas an x-ray generator provides the source of electrical voltage and user controls to energize the x-ray tube. In the x-ray tube, 2 electrodes, the cathode and anode, are situated a small distance apart, about 1–2 cm, in a vacuum environment made of either glass or metal. Connected to the cathode and the anode are negative and positive high voltage cables from the x-ray

generator. A separate, isolated circuit connects the cathode filament (a coiled wire structure similar to a coiled light-bulb filament) to a low-voltage power source.[23]

The first step for x-ray production requires free electrons to be available in the environment of the x-ray tube to allow electrical conduction between the electrodes. The electron beam emitter consists of the cathode filament set in a metal focusing cup, the cathode cup. Activating the filament circuit causes intense heating of the filament due to its electrical resistance and promotes release of electrons. The application of a high voltage, typically ranging from 50,000 to 150,000 V (50–150 kV),supplied by the x-ray generator to the cathode and anode activate the electrons, and they are immediately accelerated to the electrically positive anode along a path determined by the filament and focusing cup geometry. Tube current, defined as the number of electrons traveling between the electrodes, is expressed in milliampere (mA) units. Typical tube currents for CT operation have a selectable range of 50–300 mA, depending on the type of examination and required image quality. Each electron attains a kinetic energy (in keV) equal to the applied tube voltage, which typically is set to a single value that ranges from 50 to 150 kV depending on the examination. In CT, 120–130 kV is usually used, but 80-, 100-, and 140-kV settings are also available on some CT scanners. Thus, the tube voltage (kV), tube current (mA), and exposure duration (s) are operator selectable parameters for x-ray production.[23] The last step for x-ray production occurs when the highly energetic electrons interact with the x-ray tube anode or target. Targets used in x-ray tubes are generally made of tungsten, primarily due to its high atomic number and extremely high melting point which is necessary for efficient x-ray production and tolerance of high power deposition, respectively.[23]

The focal spot is the area of electron interaction and emanation of x-rays from the target surface. Typical dimensions are 1.0- to 1.2-mm (large) and 0.3- to 0.6-mm (small) focal spots.

The use of a small focal spot minimizes geometric blurring of patient anatomy with magnification. However, the small focal area constrains x-ray tube output and heat loading factors, primarily due to heat concentrated in a small area. Larger focal spots have higher instantaneous x-ray production capacity and are preferred, as long as blurring does not adversely affect resolution. Computed tomography scanners usually have larger focal spots (1.2-mm nominal size), which provide good geometric resolution that is compatible with the sampling resolution of the discrete CT detector array. A collimator constructed with movable lead shutters is situated adjacent to the x-ray tube output port to determine the x-ray beam shape incident on the patient. For CT, the collimator shutters determine the slice thickness setting for a specific examination. A collimator light or laser beam positioned at a "virtual" focal spot location provides a visible indication of the x-ray beam. An important factor for image quality in CT is the coincidence of the slice thickness defined by the collimators to the light beam and the x-ray profile transmitted to the detector array, which must be periodically verified for accuracy during regular quality control checks. X-rays are emitted in all directions from the anode structure, however only a small fraction of the reflected x-rays emerging through the collimator-defined area are used for image formation, the remaining x-rays must be attenuated. Protection from scatter radiation is provided by a lead shielded x-ray tube housing, which absorbs essentially all but those x-rays emerging from the x-ray tube port and collimator assembly.[23]

In computed tomography, the X-ray intensity behind the object is measured to form a projection image. This is achieved with the use of X-ray detectors, ionization chambers filled with xenon gas, or scintillation detectors in the form of crystals or ceramics, usually cesium iodide or gadolinium oxysulfite, respectively.[22] Measurements of x-ray transmission through the subject are made by the detector at several locations. The x-ray beam path through the subject

corresponding to each measurement is called a ray. The set of measurements made and their associated rays is a view.[19] The number of measurements for today's scanners is typically over 750.[19]

When developing CT, Hounsfield divided a slice into a matrix of 3-dimensional rectangular boxes (voxels) of tissue. Conventionally, the X and Y directions are within the plane of the slice, and the Z direction is along the axis of the patient (slice thickness direction). The Z dimension of the voxels corresponds to the slice thickness. The X and Y voxel dimensions depend on the size of the area over which the x-ray measurements are obtained (scan field) as well as on the size of the matrix (the number of rows and columns) into which the slice is divided.[19] Attenuation in CT depends on the effective atomic density, the atomic number of the absorber and the photon energy. Computed tomography uses heterogeneous beam (polychromatic beam) in which the photons have different energies. As the beam passes through equal thicknesses of material, the attenuation is not exponential as both the quantity and quality of the photons change. The lower-energy photons are absorbed, which allows the higher-energy photons to pass through.[20]

The attenuation of a monochromatic x-ray beam through a homogeneous object is described by the Lambert-Beer law:

$$I = I_o e^{-\mu x}$$

where *I* is the transmitted photon intensity, I_o is the original intensity, *x* is the length of the x-ray path through the object, and μ is the linear attenuation coefficient of the material traversed. This expression changes for inhomogeneous materials such as human tissue:

$$I = I_o e^{-\int(\mu_p + \mu_c)x}$$

Where μ_p represents the linear attenuation coefficient resulting from photoelectric effect and μ_c represents the linear attenuation coefficient resulting from compton scattering. Line integrals of the linear attenuation coefficients, μ, can be obtained by taking the negative logarithm of the above expression. A line integral at angle θ through the object is the ray sum, a set of which at a given θ constitutes a projection. The computational problem in CT is to determine the linear attenuation coefficient at a given point from a large set of projections obtained at θ varying about the object which indicates the amount of attenuation that has occurred in each voxel of the reconstruction matrix.[19, 20, 24]

The attenuation values are calculated and represented as picture elements (pixels) in shades of gray. A pixel represents a two-dimensional image (X and Y) of a three-dimensional voxel within the patient, the third dimension being the slice thickness of the examined cross-section of the patient. The sizes of the pixels in the displayed image (image matrix) are not necessarily the same as those in the reconstruction matrix but may be interpolated from the reconstruction matrix to meet the requirements of the display device or to graphically enlarge (zoom) the image.[19, 22]

A convention in CT is to replace the attenuation value calculated for each voxel of the reconstruction matrix with an integer (CT number) calculated as follows:

$$\text{CT number (in Hounsfield units, HU)} = K \cdot (\mu_{tissue} - \mu_{water}) / \mu_{water}$$

In this equation, μ_{tissue} is the attenuation coefficient of the measured tissue, μ_{water} is the attenuation coefficient of water, and K is an integer constant, standardized as 1,000. Because attenuation coefficients are affected by x-ray beam energy, proper x-ray generator calibration is

important for accurate and reproducible CT numbers. Scanners today determine μ_{water} from periodic calibration scans of water or water-equivalent phantoms.[19, 20]

Displaying the full possible range of CT numbers (-1,000 to +1,000) presents a problem: even today, displays often show only about 250 shades of gray, of which fewer (as few as 100) may be visually discernible. If the full CT number range of 2,000 (-1,000 to +1,000) is spread evenly over 200 discernible gray levels, each level represents a range of 10 CT numbers. However, a 0.5% attenuation difference , which CT has the ability to distinguish, corresponds to a CT number difference of 5 Hounsfield units. Many soft-tissue structures would be displayed with the same gray level as their surroundings and thus would not be visible. A material must differ from its surroundings by at least 1% to ensure a different gray level. Tissues of most common interest in CT generally are in the range of -100 to +100 CT numbers. If instead discernible gray levels were limited to the CT number range of -100 to +100, then no bone details (all white) and no lung details (all black) would be visible. The solution for this is windowing, by which a viewer may decide how gray levels are to be allocated by specifying a window width (the range of CT numbers to display) and a window level (or window center). Adjustable window settings may then be altered to view other CT number ranges.[19]

1.4 CT generations

Over time different generations of scanners have been developed. The first generation scanners used one X-ray tube that produced a pencil shaped beam falling on a single detector. Together they translated through 180 steps in the axial or also called transverse plane and then rotated 1^{o} at a time through 360^{o} around the patient (two-dimensional XY-plane). In total this procedure took a scan time of 3–5 min for one slice.[22] The reconstruction algorithm for first generation CT scanners was based on the parallel beam geometry.[20] Second generation scanners used a narrow fan beam falling on a small curved array of detectors. Together they translated and then rotated through 360^{o} but needed fewer angular steps to produce the image, thus reducing the scan time to 20 seconds per slice. This information could then be used to reconstruct the images in different planes performing multiplanar reformatting (MPR). However, image noise and artifacts due to the long scan times deteriorated the image quality. Third generation CT scanners were also based on a fan beam geometry but used a rotate–rotate conformation which rotated continuously 360^{o} around the patient. The tube produced a wide fan-shaped X-ray beam that fell on a larger array of many detectors. The fourth generation scanners used a rotating fan beam with a stationary ring of detectors. In this type of machine the tube alone rotates through 360^{o} around the patient while the broad fan-shaped X-ray beam falls on a fixed ring of thousands of detectors that are attached to the housing of the machine. In both the third and fourth generation scanners the acquisition time are reduced to 1 second per slice but due to its conformation the third generation scanners are prone to ring artifacts from miscalibration or failure of one or several detectors.[20, 22]

1.5 Conventional versus spiral/helical CT scanners

In conventional CT or slice-by-slice or step-and-shoot CT, the x-ray tube and detectors rotate for 360^{o} degrees or less to scan one slice while the table and patient remain stationary. The CT examination time was dominated by interscan delays. After each 360^{o} rotation, cables connecting rotating components (x-ray tube and, if third generation, detectors) to the rest of the gantry required that rotation stop and reverse direction. Cables were spooled onto a drum, released during rotation, and then respooled during reversal. Scanning, braking, and reversal required at least 8–10 s, of which only 1–2 were spent acquiring data. The result was poor temporal resolution (for dynamic contrast enhancement studies) and long procedure times.[19]

Some of the limitations of conventional CT included the following: 1) longer examination times because of the stop-start that is necessary for table indexing and cable unwinding; 2) certain parts of the anatomy could be omitted because of inconsistent respiration phase; 3) inaccurate generation of 3-dimensional images and multi-planar reformatted images which is attributed to the inconsistent levels of inspiration from scan to scan; 4) only a few slices are scanned during maximum contrast enhancement when contrast studies are performed.[20]

The fact that conventional CT was so time consuming led to the development of a technique in which a volume of tissue is scanned by moving the patient continuously through the gantry of the scanner while the x-ray tube and detectors rotate continuously several times. As a result, the x-ray beam traces a path around the patient and this beam geometry is called spiral or helical CT.[20] The continuous rotation of the tube only became possible with the invention of the slip-ring technique in the 1980s, reducing the gantry rotation time substantially.[22]

1.6 Single versus multi-slice CT scanners

Spiral/helical CT scanners can be single or multi-detector. A single-detector helical scanner has a data acquisition system (DAS) that allows registration of only one slice of the scanned body part per gantry rotation. The slice thickness is defined by the distance between collimators, which usually ranges from 1 to 10 mm. With multidetector (also called multi-slice CT, or multisection CT) the single detector is replaced by multiple rows of detectors. The multiple rows of detectors allow for registration of more than one slice per gantry rotation. A scanner's number of channels and the gantry rotation time determine the number of slices that can be acquired per unit time. A single-detector scanner with a gantry rotation time of 1 second can acquire one slice per second, whereas a 16-detector scanner with 0.4-second rotation time can acquire up to 38 slices per second.

In multi-detector scans, the detector arrays can be of equal detector row widths in the longitudinal direction, called a fixed-array detector, or unequal detector row widths, called adaptive-array detector. An example of a scanner with this design is the LightSpeed 16 scanner (GE Medical Systems). It provides 16 sections with either 0.625- or 1.25-mm collimated section width. The total coverage in the longitudinal direction is 20 mm at the isocenter.[15] Different section widths are available to adjust the optimum scan speed, longitudinal resolution, and image noise for each application. To select different section widths, the scanners combine several detector rows electronically to a smaller number of sections according to the selected beam collimation and the desired section width. With a single-detector row CT scanner, different collimated section widths are obtained by means of pre-patient collimation of the x-ray beam.[15, 16]

There are two ways slice thickness can be described: either as nominal slice thickness or as effective slice thickness. Nominal slice thickness refers to the physical width of the detector elements that build up the slice information in the DAS. Depending on reconstruction algorithm and table speed during scanning (pitch) a phenomenon called slice broadening occurs. Slice broadening leads to thicker slices than what the nominal slice width indicates, in which case the term effective slice width is appropriate.[16] In single-detector scanners, the pitch of helical scan refers to the ratio of the table translating distance per gantry rotation to the nominal slice thickness. A pitch of 1 indicates contiguous scan through the patient where the radiation beam spirals through the patient continuously with no overlap and gap. A pitch less than 1 indicates overlapping scan and a pitch greater than 1 indicates scan with gap. In MDCT, the most accepted definition of pitch is:

$$\text{Pitch} = \frac{\text{Table translation (mm) per rotation}}{\text{Total nominal slice width}}$$

16

In a "step-and-shoot" sequential mode, any multiple of the collimated width of one detector section can be obtained by adding the detector signals during image reconstruction. In a spiral mode, the effective section width, which is usually defined as the full width at half maximum (FWHM) of the spiral section-sensitivity profile (SSP), is adjusted independently in the spiral interpolation process during image reconstruction. Thus, from the same data set both narrow sections for high spatial-resolution detail or for 3D post processing and wide sections for better contrast resolution or quick review and filming may be derived.[15]

Multi-detector CT scanners can generate volume data that are of high spatial resolution and are isotropic in nature, meaning that each image data element or voxel, is of equal

dimensions in all three spatial planes, which obviates the need to obtain transverse, dorsal or sagittal planes directly. A single-detector spiral CT with a 1-second gantry rotation is unable to fulfill these requirements, except for very limited scan ranges.[15]

In spiral CT, inconsistent data that are obtained from 360^{o} degree spiral scan rotation are used directly in the reconstruction process, which results in visible motion artifacts that arise from the continuous movement of the patient during scanning. Therefore, spiral CT requires an interpolation of the acquired measurement data in the longitudinal (through-plane) direction to estimate a complete CT data set at the desired plane of reconstruction.[20] The most commonly used single-section spiral interpolation schemes are the 360-degree and 180-degree linear interpolation methods. The 360-degree linear interpolation method makes use of the 360-degree periodicity of the projection data and for each projection angle, a linear interpolation is performed between those two projections on either side of the image plane that are positioned closest to the image plane and are 360-degree apart (i.e., measured in subsequent rotations).[15] The main limitation with the 360^{o} degree linear interpolation algorithm is related to the image quality of the planar slice since this algorithm broadens the SSP and therefore degrades image quality.[20] The 180-degree linear interpolation technique explores the fact that for each measurement ray, an interpolation partner is already available after approximately half a rotation, after the x-ray tube and detector have exchanged positions, called complementary ray. In spiral CT, z-axis resolution is determined by the collimated beam width (as in sequential scanning) and also by the effective section width, which is established in the spiral interpolation process. Single-section spiral CT is based almost exclusively on 180-degree linear interpolation, due to the narrower SSP of this algorithm, despite its increased susceptibility to artifacts and increased image noise.[15]

Image reconstruction is more complicated in MDCT than it is in single-detector CT. As the width of the detector increases in MDCT, the x-ray beam must diverge to produce the equivalent of multiple fan beams along the longitudinal direction and therefore reach multiple rows of detectors. In this way a two-dimensional projection on the array is formed and the scanning geometry is referred to as cone beam geometry. In MDCT, spiral projections are sampled by multiple detector channels, the sampling interval depending on scanning pitches along the longitudinal axis, and the planar image formation involves spiral interpolation along a complex sampling path. A number of algorithms have been developed for MDCT reconstruction when the collimation is narrow, or less than 10 mm. These algorithms assume that projection rays measured in different detector rows are parallel to each other and perpendicular to the longitudinal axis. A complete set of projection data for a chosen transaxial plane is formed by interpolation in the longitudinal direction. Similar to the single-detector spiral CT, multichannel interpolation may also be performed as 360-degree or 180-degree linear interpolation algorithms according to the spiral interpolation strategy. There are two disadvantages with 360- and 180-degree linear interpolation, one being that it has a prefixed trade-off between the spatial resolution, noise, and pitch. The 180-degree linear interpolation algorithm maintains a narrow slice sensitivity profile at the cost of image noise. The 360-degree linear interpolation algorithms, however, reduce the image noise at the cost of a wider SSP. The two algorithms share the following disadvantages: no flexibility to choose desirable image quality (section widths and noises) independent of pitches, and insufficient dose use in image reconstruction as not all projections are fully used in the reconstruction. Modified algorithms have been developed for a more complete usage of all detector channels. With these algorithms the section profile and

the image noise can be fixed for all pitch values. Multiple slice widths from a single collimation can be obtained.

It has been demonstrated that cone-beam artifacts can be tolerated if the maximum number of simultaneously acquired sections does not markedly exceed four. As a consequence, the image-reconstruction approaches of all commercially available four-section CT systems neglect the cone angle of the measurement rays.[15] For CT scanners with 16 or more detector rows, modified reconstruction approaches accounting for the cone-beam geometry of the measurement rays have to be considered. The mishandling of beam geometry can introduce cone-beam artifacts, such as streaks and altered reconstruction density. These artifacts may substantially degrade the image quality, particularly when the target regions are away from the scan center. In this case, dedicated cone-beam reconstruction algorithms must be used to eliminate the artifacts.[15, 16]

1.7 Image quality in computed tomography

Several physical parameters are used to characterize the image quality of a CT scanner: high-contrast spatial resolution, low-contrast-resolution, temporal resolution, CT number uniformity and accuracy, noise and artifacts. These parameters are influenced by the CT system performance and some of them by the operator's selection of protocol such as x-ray tube voltage, tube current, slice thickness, helical pitch, reconstruction parameters and scan speed.[20] Trade-offs are constantly made between image quality, dose to the patient, system limitations and clinical indications. For instance, factors that improve resolution usually increase noise and decrease the signal-to-noise ratio.[20, 25]

High-contrast spatial resolution

The high-contrast spatial resolution of a CT scanner describes the scanner's ability to discriminate objects of different attenuation at small separation distances.[20, 25] Spatial resolution of CT is much lower than that of screen-film radiography, but CT has in turn much higher contrast resolution.[25, 26] The in-plane resolution of a CT scanner is usually described as the spatial frequency that can be discriminated with a 10% detection of true contrast, and is measured in terms of line pairs per centimeter (lp/cm) or line pairs per millimeter (lp/mm).[20, 24, 25, 27] To characterize the spatial resolution, the point spread function (PSF) or line spread function (LSP) in the scan plane are frequently employed.[28] Because the CT acquisition and reconstruction process is band limited (high-frequency contents are suppressed or eliminated), the reconstructed image of a bar pattern is a blurred version of the original object.[20] The PSF is used in image deblurring techniques, and it is applied to simulate the imaging of small structures. The study of small structures is relevant to the correct interpretation of clinical data, as well as in

estimating the accuracy attained in quantifications of object spatial dimensions and attenuation. Such studies require the precise determination of the PSF.[28]

The magnitude of the bar pattern reduces as the frequency (lp/cm) of the bar pattern increases. If the spatial frequency is plotted as a function of the image fidelity, a smooth curve is obtained, referred to as the modulation transfer function (MTF) of the system. The modulation transfer function of a system can be derived by taking the Fourier transform of the point spread function (PSF) or line spread function (LSF) and can be used to compared the performance of different CT systems, different reconstruction parameters and for evaluating the accuracy of size and density measurements of fine details in images.[20, 27]

Some of the most important factors that affect the in-plane spatial resolution are the x-ray focal spot-size and shape, size of the detector channels, scanner geometry, sampling frequency and patient motion.[29, 30] Patient motion can blur diffuse edges and can cause streaking artifacts if the motion is of a high-contrast object.[30] Although most of these factors are largely determined by CT manufacturers, operators have control in some factors. For instance, most CT scanners have more than one x-ray focal spot to account for an increased tube loading. By properly selecting the x-ray tube current the operator has the option to use either the small spot, which provides higher spatial resolution, or the large spot, which provides lower spatial resolution.[20]

The in-plane resolution is also strongly influenced by the reconstruction algorithm. Image reconstruction involves two mathematical procedures: convolution and back-projection. If the projection profiles are back-projected without correction, blurring results. To sharpen the image a convolution process is applied to modify the frequency contents of the projection before back-projection. Another parameter, the convolution algorithm, or kernel, is operator dependent and also affects the appearance of imaged structures. The kernel can be used to enhance high

frequency contents for the sharpest images, or to suppress high frequencies for reduction of noise and aliasing, resulting in a smoother image.[20, 29] The reconstruction field of view (FOV) is another factor that affects the spatial resolution. The sampling interval (pixel size) has to be sufficiently small to support the reconstruction and visualization of small objects. Pixel size is related to FOV by the following equation:

$$\text{Pixel size} = \frac{\text{Field of view}}{\text{Matrix size}}$$

[20]

The cross-plane spatial resolution is described by the slice sensitivity profile, and in many cases the SSP is replaced by the full width half maximum. The FWHM represents the distance between two points on the SSP curve whose intensity is 50% of the peak. Like the in-plane spatial resolution, after the SSP is calculated, the modulation transfer function can be calculated by taking the Fourier transform of the SSP. With the advent of multi-slice CT scanners, as the spatial resolution in all planes become isotropic, it is convenient to specify both the in-plane and cross-plane resolution in a similar way, such as using the modulation transfer function.[20]

Low-contrast resolution

Low-contrast resolution is the ability of the CT scanner to detect low-contrast objects whose density is slightly different from the background, or the ability to discriminate differences in tissue attenuation.[20, 24] The contrast between an object and its background depends primarily on the attenuation properties, but also on several physical factors such as the spectrum of the x-ray tube, the amount of beam hardening and scatter.[29] Low contrast resolution as the opposite of spatial resolution, is much higher in CT than in radiography since CT scans thin slices and eliminates the problem of superimposition that is present with radiography.[29]Computed tomography can image tissues that vary only slightly in density and atomic number. While

radiography can discriminate a density difference of about 10%, CT can detect differences from 0.25% to 0.5%. The low-contrast performance or low-contrast detectability (LCD) of the scanner is usually defined as the smallest object that can be visualized at a given contrast level and dose.[20] Since the images are digital, the displayed contrast is modulated by the gray level transformation (window and level) after the image formation. This makes noise the main limitation on the perception of low-contrast details.[29] In CT the contrast level is specified in terms of the percent linear attenuation coefficient. A 1% contrast means that the mean CT number of the object differs from its background by 10 Hounsfield units.[20]

Temporal resolution

Temporal resolution refers to the ability of an imaging system to discriminate sequentially acquired projection data separated by small time intervals. With higher temporal resolution, more projection datasets can be acquired over a fixed gantry rotation interval, thus improving contrast resolution. Limited temporal resolution leads to image ghosting and "after-glow" or memory effects as well as streak artifacts, which degrade image quality and impair low-contrast detectability.[24]

Noise

There are several types of noise that can interfere with the interpretation of an image. Image noise can be divided in random noise, artifactual noise and structural noise. Although noise may infiltrate and corrupt the data at any point in the CT process, the ultimate source of noise is the random noise arising from the detection of a finite number of x-ray quanta in the projection measurements and that limits the ability to discriminate between two regions of different density.[29, 31]Since for a given CT geometry the number of transmitted x-ray quanta is proportional to the dose, the magnitude of the statistical noise depends on the dose. Because of

its unpredictable nature, such noise cannot be completely eliminated from the image and will always lead to some uncertainty in the interpretation of the image.[31] To reduce the uncertainties due to noise, the signal can be measured for a longer time, or the measurement can be repeated several times, which is effectively the same. If the noise is random its contribution to the total image signal will diminish over time or repeated measurements.[32]

Random noise can be divided in three types: quantum or statistical noise, electronic noise, and round-off or quantization noise that results from the limited dynamic range of the detector. The main contribution in CT is from quantum noise, which is due to the statistical nature of the x-rays.[29, 31] Some factors that influence the amount of quantum noise are: 1) the scanning technique, such as x-ray tube voltage, milliamperage per second (mAs), slice thickness, scan speed, helical pitch; 2) scanner efficiency, such as detector quantum efficiency, detector geometrical efficiency and amber-penumbra ratio; 3) patient size and 4) the reconstruction algorithm, with both the applied filter and the interpolation methods influencing the image noise. The scanning techniques dictate the number of x-ray photons that reach the patient, and the scanner efficiency determines the percentage of the x-ray photons exiting the patient that are converted into useful signals. The patient size will determine the amount of bone and soft-tissue in the scanning plane. Finally, the reconstruction algorithm can be use to either suppress or enhance high frequency components in the projection and most noise presents as high-frequency signals, therefore noise can be reduced or increased according to the algorithm choose.[20, 29]

To perform noise measurements, the standard deviation (SD) within a region of interest (ROI) in the reconstructed image can be calculated. Typically, the SD because of noise is a few Hounsfield units.[20, 29]

Electronic noise appears during the processing of electrical signals and it is due to inherent physical limitations of a particular system. These include noise in the detector photodiode, noise in the data acquisition system (DAS), scattered radiation, among others.[20]

Artifactual noise is due to some systematic 'error' in the method of the image formation.[32] There is a wide variety of artifacts that can be produced by CT scanners and some of this will be discussed below.

1.8 Computed tomography artifacts

Artifact can be defined as a distortion or error in an image that is unrelated to the subject being studied. The term artifact can also be applied to any systematic discrepancy between the CT numbers in the reconstructed image and the true attenuation coefficients of the object. Artifacts can degrade image quality, affect the perceptibility of detail or lead to misdiagnosis.[20, 33] Computed tomography images are inherently more prone to artifacts than conventional radiographs because the image is reconstructed from something on the order of a million independent detector measurements. The reconstruction technique assumes that all these measurements are consistent, so any error of measurement will usually reflect itself as an error in the reconstructed image.[33]

Artifacts in CT originate from a range of sources. Physics-based artifacts result from the physical processes involved in the acquisition of CT data. Patient- based artifacts are caused by such factors as patient movement or the presence of metallic materials in or on the patient. Scanner-based artifacts result from imperfections in scanner function. Helical and multisection technique artifacts are produced by the image reconstruction process.[33]

Beam hardening

Beam hardening is the term describing the shift of the transmitted x-ray spectrum to higher effective energy (E) with increasing attenuator thickness. The x-rays generated by the x-ray tube have a wide spectrum of energies. With increased thickness, not only the overall quantity of x-rays decreases but also the mean x-ray energy shifts, with the lower energy photons being absorbed preferentially than the higher energy photons. Therefore, the effective energy of the x-ray beam increases as it passes through tissue, a phenomenon called beam hardening. Computed tomography measures the linear attenuation coefficient which in turn is very

dependent on the energy of the x-ray beam.[30] The degree of beam hardening is strongly dependent on the characteristics of the attenuator. Higher atomic number (Z) absorbers such as bone and iodine cause more beam hardening per unit thickness than soft tissue, partially due to higher density, and partially due to the Z^3/E^3 dependency of photoelectric absorption. Beam hardening can produce subtle artifacts in CT, where variations in the attenuation coefficient that occur for different x-ray paths are not compensated for in the CT image reconstruction algorithm.[34] In the head, beam hardening artifacts typically manifest as dark streaks or areas of hypoattenuation.[15]

Partial volume

Partial volume artifacts are the result of a variety of different tissue types being contained within a single voxel. When the linear attenuation coefficient is different for two or more of these tissues, the attenuation that occurs and is measured is averaged. This partial volume averaging results in the calculation of a CT number that is not necessarily accurate for either tissue type which can result in artifacts.[20, 33] Partial volume artifacts can best be avoided by using a thin acquisition section width. This is necessary when imaging any part of the body where the anatomy is changing rapidly in the z direction. To limit image noise, thicker sections can be generated by adding together several thin sections.[33]

Windmill artifact

The windmill artifact is a z-aliasing artifact that occurs primarily in helical cone-beam CT. The helical cone-beam reconstruction involves interpolation between the detector rows for image reconstruction. Hence, windmill artifacts occur independent of the reconstruction approach.[15, 29] Windmill artifact appears as a typical pattern of black and white spokes

originating from high contrast features with curvature along the longitudinal z-axis. As helical pitch increases, the number of detector rows intersecting the image plane per rotation increases and the number of "vanes" in the windmill artifact increases.[33, 35] Windmill artifact can be reduced by decreasing the pitch and/or increasing the reconstruction section width relative to the collimation.[15]

Stair-step artifact

Stair step artifacts appear around the edges of structures in multiplanar and three-dimensional reformatted images when wide collimations and non-overlapping reconstruction intervals are used. They are less severe with helical scanning, which permits reconstruction of overlapping sections without the extra dose to the patient that would occur if overlapping axial scans were obtained. They are visible in longitudinal images as regular stair step disruptions along inclined edges and in 3 dimensional images as black or white helical winding along inclined surfaces, such as the skull.[29] Stair step artifacts can be virtually eliminated in multiplanar and three-dimensional reformatted images from very thin-section data;this is possible because of multisection scanners.[33]

Metal artifact

The presence of metal objects in the scan field or patient can lead to severe streaking artifacts. They occur because the density of the metal is beyond the normal range that can be handled by the computer, resulting in incomplete attenuation profiles. Additional artifacts due to beam hardening, partial volume, and aliasing are likely to compound the problem when scanning very dense objects.[20, 33]

Motion artifact

Patient motion causes misregistration artifacts, which usually appear as shading or streaking in the reconstructed image. Motion can be voluntary or involuntary. Steps can be taken to prevent voluntary motion, but some involuntary motion may be unavoidable during body scanning. However, there are special features on some scanners designed to minimize the resulting artifacts.[33]

Undersampling

The number of projections used to reconstruct a CT image is one of the determining factors in image quality. According to the sampling theorem, or Nyquist criterion, to faithfully represent a continuous signal (intensity profile of a patient), the sampling frequency must be at least twice the highest frequency component in the signal. If the interval between projections is too large, undersampling may occur; this can result in misregistration of information relating to sharp edges and small objects, leading to an effect known as view aliasing, where fine stripes appear to be radiating from the edge of a dense structure. View aliasing can be minimized by acquiring the largest possible number of projections per rotation. On some scanners, this can be achieved only by using a slower rotation speed, while on others the number of projections is independent of rotation speed.[20, 33]

Ring artifacts

If one of the detectors is out of calibration on a third-generation scanner, the detector will give a consistently erroneous reading at each angular position, resulting in a circular artifact. A scanner with solid-state detectors, where all the detectors are separate entities, is in principle more susceptible to ring artifacts than a scanner with gas detectors, in which the detector array consists of a single xenon-filled chamber subdivided by electrodes.[33]

1.9 Computed tomography in veterinary medicine

Experimental CT studies in veterinary medicine began in the late 1970s together with the first clinical experiences in canine patients with neoplasia or central nervous diseases.[22] In sequence, several studies describing the anatomy of the brain, head, orbital region, nasal cavity thorax and abdomen were published.[8, 22, 36, 37] Computed tomography may be considered nowadays as one of the most important tools for the imaging work-up of neurology, orthopedic and oncology canine and feline patients. In small animals with acute trauma, particularly in complex anatomical areas such as the head, spine or pelvis, CT has been established as a standard imaging method. With the increasing availability of radiation therapy in veterinary medicine, CT has also become the principal tool used to stage a tumor, assess response, and guide radiation therapy. CT can yield a three dimensional, exactly scaled matrix of quantitative data and can provide important information on radiation interaction properties correlating directly with X-ray absorption in the tissues, which is essential for dose calculations in radiation therapy. The main CT applications in small animals including intracranial and extracranial lesions, the spine, appendicular skeleton, abdominal and thoracic diseases was reviewed.[22]

Computed tomography of the thorax in small animals can reveal details of anatomy with or without the use of IV contrast medium injection. Except for some smaller blood vessels, nerves and details of the heart, most of the bony and soft tissue structures of the thorax can be identified. Computed tomography of the thorax is used most commonly to improve detection of subtle pulmonary lesions, to differentiate thoracic masses from accumulations of mediastinal or pleural fluid, to evaluate the mediastinum or thoracic wall and to assess for the presence of foreign material.[4-6, 38] It has also been successfully used to guide fine-needle aspirates and tissue-core biopsies of intrathoracic lesions. Indications include lesions close to vascular structures,

lesions not well identified on radiographs or with fluoroscopy, and lesions surrounded by air which would not be identified with ultrasonography.[22, 39]

Protocols for helical CT and high-resolution CT have been published for the canine lung, with a described mean attenuation value of - 846 HU or - 713 HU for the normal canine lung.[9, 22, 40] Cross-sectional areas and ratios for the caudal lobar bronchi, pulmonary arteries, and veins were also established for dogs. The caudal lobar pulmonary veins were found to be significantly larger than their corresponding arteries.[9, 22] A novel classification system for high-resolution CT findings in the dog adapted from humans was introduced accounting for the lack in interlobular septa in dogs.[9, 22] Finally, the normal pulmonary artery tree and various thoracic vessels in dogs were illustrated using spiral CT angiography in a brief report. After the injection of contrast medium the time to peak enhancement was determined for various thoracic vessels and this was considered the optimal scan delay. The time to peak enhancement varied for different vessels and between individuals and a test bolus technique was recommended.[22] Similar studies specific for cats are lacking.

Clinical reports on thoracic CT for the diagnosis of thoracic diseases in dogs and cats are limited to anesthetized patients.[3-7] A small number of studies have described the CT appearance of thoracic diseases in cats, including the CT appearance of lung lobe torsion, cranial mediastinal masses (CMM), primary and metastatic lung neoplasia, atelectasis and alveolar pathology.[4, 5, 7, 41]

CHAPTER 2

A DEVICE FOR COMPUTED TOMOGRAPHIC IMAGING OF AWAKE CATS, THE VETMOUSETRAP™: DESIGN AND SAFETY EVALUATION

This work includes previously published material. The VetMouseTrap™: A Device for Computed Tomographic Imaging of the Thorax of Awake Cats. Oliveira, CR, Ranallo, FN, Pijanowski, GJ, Mitchell, MA, O'Brien, MA, McMichael, M, Hartman, SK, Matheson, JS, O'Brien, RT. E-pub 2010 Veterinary Radiology & Ultrasound.[42]

2.1 Introduction

It would be advantageous if the benefits of CT for thoracic imaging could be applied more frequently. In pediatric CT the high speed of multidetector CT imaging has decreased the need for sedation significantly.[43, 44] In veterinary medicine, the use of multidetector helical CT scanners allows CT examinations to be performed in a very fast period of time and therefore brings the possibility to scan sedated or awake patients.

The purpose of this study was to design a clinically supportive device that minimizes movement of awake feline patients during CT examination and provides a safe environment for these patients. We hypothesized that the device would: 1) allow CT examination of non-sedated, unanesthetized cats with minimal to no motion artifact; 2) create no CT artifact; 3) improve the clinical environment of the imaged patient compared to radiography; and 4) be a safe environment not causing temperature elevation or high levels of carbon dioxide.

2.2 Materials and Methods

A device to facilitate thoracic CT imaging of awake cats, the VetMouseTrap™ (University of Illinois at Urbana-Champaign, Urbana, Illinois) was designed and tested. Environmental parameters within the device, including temperature, carbon dioxide and oxygen levels, where measured using 10 clinically normal cats.

When developing the device, both the clinical and imaging needs of patients were considered. The clinical needs required the device to: 1) allow access for oxygen administration at therapeutic levels; 2) allow access for intravenous lines without the need to disconnect the lines when placing or removing the patient from the device; 3) be symmetric, providing ports for catheter and oxygen access on both ends of the device; 4) be transparent, allowing visual observation of the patient; 5) have a closure mechanism that allowed quick removal of the patient; 6) have a secure closure mechanism preventing patient escape; 7) provide a low heat environment; 8) avoid clinically relevant elevation of carbon dioxide; 9) be portable; and 10) be easily disinfected. The imaging needs were that the device: 1) have low CT attenuation, 2) have symmetrical round design in cross section to avoid edge or hardening artifacts, 3) have a narrow and short design to limit movement of the patient, 4) have no metal parts, 5) be rugged enough for daily use in both the emergency room and a clinical imaging environment, and 6) allow additional padding to compensate for patients of different body size and patient behavior characteristics.

Different material types and shapes were tested for attenuation and artifact production, and varying lengths and diameters were tested for patient compliance, ruggedness, and clinical utility.

To test the final device design for ambient internal oxygen, carbon dioxide levels and temperature, 10 cats were evaluated. These were clinically healthy young adults ranging in size from 3.3 to 7 kg (mean 4.9 kg). The cats were placed inside the device and the following parameters were measured at times 0, 5, 10, 15, 20, 25 and 30 minutes: carbon dioxide (CO_2), fraction of inspired oxygen (FiO_2), internal chamber temperature and subject respiratory rates. An anesthesia monitor* was used to measure the above parameters. The tubing that would normally fit onto a special cuff on the endotracheal tube was placed into one of the intravenous (IV) line access ports at one end of the device. The monitor recorded end tidal CO_2 ($ETCO_2$), which was extrapolated as the carbon dioxide level within the device. The FiO_2 was measured via the same tubing. A probe to measure temperature was placed into one of the oxygen ports of the device. Oxygen was provided via an oxygen flow meter, with humidifier, at a rate of 2 liters/min into an oxygen port on the other end of the device. Cats were not restrained inside the device.

Statistical analyses were performed using 2 commercial software programs§. The Kolmogorov-Smirnov test was used to evaluate the distribution of the data. Normally distributed data were reported by mean, standard deviation (SD), and minimum-maximum values, while non-normally distributed data were reported by median, 10-90% and minimum-maximum values. For $ETCO_2$, FiO_2, temperature, and respiratory rate, non-normally distributed data were analyzed using Friedman's test, while a repeated measures general linear model was performed for normally distributed data. Post-hoc tests were used to compare differences to time 0 when significant. A $P < 0.05$ was considered statistically significant.

2.3 Results

The final design of the VetMouseTrap^{TM} was a transparent acrylic tube with a wall thickness of 5 mm, outer diameter of 21 cm, and length of 40 cm (Figure 1). The tube was cut lengthwise during construction, resulting in a top and base portion. The base portion has supportive legs with rounded edges. The construction has no moving parts or hinges and has a secure closure without additional metallic or plastic components. The closure is affected by intimate interlocking upper and base components. The sides are not sealed, which allows excess gas to escape, and prevents pressure, heat and humidity accumulation. The cats can be monitored visually throughout the imaging procedure and removed quickly in case of an emergency. Oxygen and catheter line access is simple. Catheter line access is via a slot in the base which, after closure with placement of the top component, results in an oblong small 6 x 6 mm hole. The device has low attenuation (approximately 54 Hounsfield units) and did not cause visible artifacts during CT image acquisition.

The mean age of the cats was 7.5 years and the mean body weight 4.5 Kg. End tidal carbon dioxide, FiO_2, temperature inside the device, and respiratory rates of the cats are presented in Tables 1 and 2. During the measurements, one cat was active after being placed in the device and kept moving during the 30 minute interval. The other 9 cats remained quiet most of the time, with no overt signs of stress.

There was a statistically significant difference in $ETCO_2$ levels at time 0 compared to times 5-30 min.; however, there was no difference in $ETCO_2$ levels over time after 5 min. The maximum CO_2 level inside the device at all times was 19 mmHg. There was a significant difference of FiO_2 levels at time 0 compared to times 5-30 minutes with the levels increasing over time. There was a significant difference in FiO_2 levels comparing measurements at 5

minutes to 10, 15 and 25 minutes. No difference was found comparing measurements at 5 minutes to 20 or 30 minutes.

Similarly a significant difference in temperature was found at time 0 compared to times 5-30 minutes, with the temperature increasing over time. The highest measurement, of 29 ºC, was found at 20, 25 and 30 min. Respiratory rate was recorded in 9 of the 10 cats, and no difference was found over time. Mean respiratory rate at time 0 was 53 breaths per minute (bpm), while at time 30 minutes it was 47 bpm.

2.4 Discussion

The goals of the present study were to describe the design of a new low attenuating transparent device that functions as a clinically supportive environment and to evaluate the safety of the device. Based on physiologic measurements, the VetMouseTrap™ was safe and well tolerated by the cats. The difference of $ETCO_2$ levels at time 0 compared to times 5-30 min was expected since initially no cat was inside the device and therefore the levels of $ETCO_2$ for all but one cat, were 0 mmHg. There was no statistical significant difference in $ETCO_2$ levels over time after 5 minutes, indicating that the levels of CO_2 inside the device do not increase for up to a period of 30 minutes. Although not statistically significant, decreasing CO_2 levels were found at the maximum times (25 and 30 min.) compared to initial times. The maximum CO_2 level inside the device at any time was 19 mmHg.

The significant difference of FiO_2 levels found at time 0 compared to times 5-30 minutes with increasing levels of oxygen up to 25 minutes indicates the device worked properly as an oxygen provider. An oxygen flow rate of 2 L /min provided a mean FiO_2 inside the device of 53% at 5 minutes and 68% at 25 minutes with a maximum of 95% FiO_2 (FiO_2 at room air = 21%).[45, 46]

There was a significant difference of temperature levels inside the device over time with the highest mean of 26.8°C at 30 minutes. Overall, the mean temperature was within a narrow and safe range of 23.5°C to 26.8°C. There was no significant change in respiratory rate of the cats indicating that the temperature and CO_2 rise were not significant to cause any increase in respiratory rate and effort. This is most important for cats in respiratory distress as the device should not contribute to increased respiratory rate or effort.

Respiratory rates were mildly above the normal range after time 0 (20–44 bpm), possibly indicating some degree of stress.[47] However the fact that they were higher at 0 minutes compared to any other time could indicate that the cats were stressed by other reasons such as being in the hospital and being handled, rather than by the device itself. After 20 minutes inside the device the respiratory rates began to decrease and achieved the lowest mean at the maximum time (30 minutes).

One limitation of this study is that the measurements of FiO_2 inside the VetMouseTrap™ could have been affected by the fact that some cats turned around constantly resulting in temporary blocking of the flow of oxygen.

The VetMouseTrap™ is a device that provides effective oxygen and catheter-based therapy while keeping safe temperature and CO_2 levels, permitting CT imaging of non-sedated, unanesthetized cats.

Footnotes:

[*] Datascope Mindray DS USA Inc., Mahwah, NJ

[§] MedCalc Software, Mariakerke, Belgium; SPSS, IBM Company, Chicago, IL

2.5 Figure

Figure 1. The VetMouseTrap™: Ports for catheter access (thin arrows) and oxygen administration (thick arrows) are present on both ends of the device. The device is transparent, portable, easy to clean, narrow, has no metal components and a symmetric design.

2.6 Tables

Table 1- CO_2 and FiO_2 Measurements Inside the VetMouseTrap™

	CO_2 (mmHg)			**FiO_2 (%)**		
Time (min.)	Mean	SD	Min-Max	Mean	SD	Min-Max
0	0*	0 – 5**	0 - 6	20.7*	20 - 30**	20 - 33
5	10.5	4.1	6 - 19	53.2	17.1	30 - 85
10	10.1	4.1	3 - 16	64.2	14.2	44 - 85
15	11.1	3.9	7 - 17	66.8	17.7	36 - 93
20	11.5	4.9	3 - 17	61.1	20.4	32 - 95
25	9.2	4.1	5 - 18	68.1	19.5	40 - 95
30	9.7	4	4 - 18	65.9	15.6	42 - 86

*Median, **80% Percentile, CO_2 = carbon dioxide, measured as end-tidal carbon dioxide
FIO_2 = fraction of inspired oxygen; FiO_2 at room air = 21%, SD = standard deviation
Min-Max= minimum-maximum

Table 2- Temperature Inside the VetMouseTrap™ and Respiratory Rate of Cats

	Temperature (^oC)			**RR(bpm)***		
Time (min.)	Mean	SD	Min-Max	Mean	SD	Min-Max
0	23.5	0.9	22 - 24	52.9	14.8	24 - 72
5	25.4	1.5	23 - 27	51.3	13.8	30 - 66
10	25.9	1.2	24 - 28	47.6	14.3	28 - 66
15	26.1	1.1	25 - 28	50.7	18.5	28 - 80
20	26.4	1	25 - 29	47.3	15.8	28 - 66
25	26.7	1	25 - 29	47.3	14.6	28 - 66
30	26.8	1	26 - 29	46.9	14.7	28 - 68

*RR = respiratory rate in breaths per minute- recorded in 9 cats
SD = standard deviation, Min-Max= minimum-maximum

CHAPTER 3

PROTOCOL EVALUATION FOR WHOLE-BODY COMPUTED TOMOGRAPHY OF NORMAL AWAKE CATS USING THE VETMOUSETRAP™

This work includes previously published material. The VetMouseTrap™: A Device for Computed Tomographic Imaging of the Thorax of Awake Cats. Oliveira, CR, Ranallo, FN, Pijanowski, GJ, Mitchell, MA, O'Brien, MA, McMichael, M, Hartman, SK, Matheson, JS, O'Brien, RT. E-pub 2010 Veterinary Radiology & Ultrasound.[42]

3.1 Introduction

The advent of multidetector CT technology that has led to greatly decreased examination time, substantially increased longitudinal resolution by means of reduced slice thickness and slice reconstruction interval, and improved multiplanar and 3 dimensional (3-D) reconstruction.[40] With multidetector CT scanners, isotropic pixels allow reformatted images to have the same quality as those acquired in the plane imaged directly.[48]

The purposes of this study were to evaluate the impact of kV, pitch and patient size on image quality during helical CT imaging of the thorax in awake cats using the VetMouseTrap™. The initial hypotheses were: 1) the protocols with lowest kV would have the best contrast; 2) the protocols with higher pitch would have less motion artifact; 3) the size, conformation and body weight of the cat would have no impact on image quality, regardless of protocol; and 4) no pulmonary atelectasis would be detected.

3.2 Materials and Methods

The VetMouseTrap™ was used to scan normal awake cats with 4 different dose equivalent CT protocols. Twenty-two clinically healthy cats were imaged within the device. Computed tomography was performed without sedation or general anesthesia using a 16 slice helical CT scanner† and the VetMouseTrap™.

The cats were placed inside the VetMouseTrap™ prior to the CT examination. The device was secured to the CT table with standard CT table velcro straps. These also provided additional security to the top portion of the device. Supplemental foam wedges were added as necessary to encourage the cats to remain in a neutral sternal position within the device. Cats were not restrained inside the device and were monitored visually throughout the procedure. Oxygen was provided at a flow of 2 liters/min for all animals during the procedure. To avoid pre-scan scouts, images were acquired of the entire VetMouseTrap™, which resulted in a whole-body study. The CT table was kept at a pre-determined height of 170 cm, and the device was always placed on a same pre-determined position on the CT table. Post-image acquisition, the cats were removed from the device. Two cats exhibited signs of overt stress inside the device and were excluded from the study.

In the remaining 20 cats, 2 different kV settings and 2 different helical pitch settings were tested resulting in 4 dose equivalent protocols. The goal was to test a low and a high kV (80 and 120) and 2 extremes of pitch (0.562 and 1.75), while keeping the CT dose index ($CTDI_{vol}$) of the scans constant. The scan rotation time for all imaging in this study was 0.5 seconds. The initial protocol was set as 80 kVp, a pitch of 1.75 and 400 mA. To get a protocol with the same kV and a pitch of 0.562, we decreased the mA by the same factor we decreased the pitch (0.32), resulting in 128 mA which the machine automatically changes to 130 mA, resulting in both protocols

having aproximatelly the same effective mAs (mA x rotation time / pitch) of 114. To change the kV we used information from the technical data sheet of the CT scanner[‡]. According to this data sheet, to change the kV from 80 to 120, while keeping the CTDIvol constant, the mA needed to be decreased by multiplying by a factor of 0.36. The next protocols were: 120 kV, a pitch of 1.75, and 144 mA (400 x 0.36) and 120 kV, a pitch of 0.562, and 46 mA (128 x 0.36). This CT scanner only allowed mA settings in increments of 5 and so automatically changed the previous mA settings as follows: 128 to 130, 144 to 145 and 46 to 45.

A detector configuration of 16 x 0.625 mm and beam collimation of 10 mm were used along with a "small" scan field of view. The image reconstruction parameters were: a display field of view of 25 cm, a 1.25 mm slice thickness, a 0.625 mm slice reconstruction interval, and the "detail" algorithm. The protocols were repeated if severe motion artifact was detected by subjective evaluation during the scan. The original scanned images were manipulated on a separate workstation to obtain symmetric transverse plane images of the thorax. Subsequent multiplanar reformatting was performed to obtain dorsal and sagittal images, reconstructed with a 0.625 mm slice thickness and a 0.312 mm slice reconstruction interval.

The CT protocols were non-randomized for the first 10 and randomized for the second 10 cats. The data from randomized and non-randomized cats were evaluated for statistical significant differences.

For each protocol, total scan time and radiation dose measurements were recorded, the latter based on the scanner-generated CT dose index volume values (CTDIvol) for a 16 cm phantom. The total time spent on CT was recorded for each cat from the time the cat entered the CT room until the time the cat left the CT room. Cats were removed from the VetMouseTrap™ immediatelly after leaving the CT room.

Quantitative image analysis was performed using a GE Advantage Workstation†. All measurements were made on the original 1.25 mm thickness transverse images by one investigator (CRO). Signal intensity of the pulmonary parenchyma (SI_{lung}) was defined as the attenuation (CT numbers in Hounsfield units) measured by placing a circular region of interest (ROI) in the dorsal pulmonary parenchyma at the level of the caudal thorax. The ROI size was 22 mm^2, the largest possible that could be drawn while avoiding the inclusion of bronchi and vessels.

Signal intensity of background ($SI_{backgr.}$) was defined as the attenuation measured by placing a circular ROI in the paraspinal muscle at the level of the caudal thorax.[49] The ROI size was 45 mm^2, the largest possible that could be drawn while avoiding the inclusion of adjacent bones. To minimize bias from a single measurement for both SI_{lung} and $SI_{backgr.,}$ the measurements were made at 5 different locations in 5 subsequent images and the mean value was used for further calculations.

Contrast was calculated as $SI_{lung} - SI_{backgr.}$ The background noise was calculated on a phantom. The phantom was a round plastic container measuring 14.5 cm in diameter (approximately the diameter of the chest in a cat) and with a 2.0 mm wall thickness that was filled with water . Regions of interest of 400 cm^2 were placed in the center of the phantom in 5 subsequent images for each protocol. Averaged numbers were used for further calculations.
Signal-to-noise ratio (SNR) was calculated by dividing the mean CT number of the lung by the background noise (SI_{lung}/noise). Contrast-to-noise ratio (CNR) was calculated as follow: CNR = ($SI_{lung} - SI_{backgr.}$)/noise.[49]

The lateral and dorsoventral diameter of the thorax (chest width and chest height respectively) were measured for each cat at the level of the widest dimension of the thoracic

cavity by placing the cursor on the edge of the skin. For cats aligned with the limbs in contact with the chest, the limbs were included in the measurements.

All images were initially evaluated qualitatively by one investigator (CRO). The CT protocols were hidden from each image. During this first review, any artifacts encountered were recorded. These included blurred liver margins, helical-helical, motion and windmill artifacts. Windmill artifact consists of black/white patterns that spin off of high contrast features that vary along the longitudinal (z-) axis. When the images are viewed in cine mode, the artifact appears to spin like a windmill. In dorsal or sagittal images, they appear as bands.[35] The helical helical artifact appeared as large areas in the lung with no attenuation. Helical helical artifact, like windmill, is related to the need for data interpolation in helical scanning, which can result in areas of artificially high or low CT numbers near regions of large CT number changes.

For subsequent analysis, all data sets were evaluated by 2 board certified radiologists and one certified CT technician. Images were randomized and displayed in transverse plane in lung window (window level = -500, window width = 1500). Readings were performed independently for liver margins, windmill and helical helical artifact, and in consensus for motion artifact; evaluators were not aware of CT acquisition parameters for any image. A standardized questionnaire was used for image evaluation as follow: 1) liver margins: sharp - 0, blurred - 1; 2) helical helical artifact: absent – 0, present – 1; 3) windmill artifact: absent – 0, present – 1; 4) motion artifact: absent – 0, minimal – 1, moderate – 2, severe – 3. Motion artifact was ranked according to the following locations: cranial thorax, if the motion artifact appeared predominantly cranial to the heart but not including the heart; middle thorax, if the motion appeared predominantly cranial to liver but not including the liver; and caudal thorax, if the motion appeared predominantly from where the liver begins until the end of the thorax. Images

were assigned the most severe score. The overall score for motion artifact for each cat was considered the highest score among the locations. For each protocol, the percentage of slices affected by motion was calculated for each cat in which motion was found. Finally, for liver margins, helical-helical, and windmill artifacts the number of times each score appeared combining all 3 evaluators was calculated and compared among each protocol.

Statistical analyses were performed using 2 commercial software programs[§]. The Kolmogorov-Smirnov test was used to evaluate the distribution of the data. Normally distributed data were reported by mean, standard deviation (SD), and minimum-maximum values, while non-normally distributed data were reported by median, 10-90% and minimum-maximum values. A 2-way ANOVA test was used to compare the protocols between the randomized versus non-randomized cats for SI (muscle and lung), noise, contrast, SNR and CNR.

A one-way ANOVA test was performed to compare the protocols for SI (muscle and lung), noise, contrast, SNR and CNR data. Regression analysis was used to compare SI in muscle and lung, noise, contrast, SNR and CNR with the variables protocol, age, weight, width and height of thoracic cavity, and total time at CT. For liver, helical, and windmill artifacts, Kappa test was used to assess the level of agreement between evaluators and interpreted as follow: < 0 Less than chance agreement, 0.01–0.20 Slight agreement, 0.21– 0.40 Fair agreement, 0.41–0.60 Moderate agreement, 0.61–0.80 Substantial agreement, 0.81–0.99 Almost perfect agreement. [50] Differences in the protocols between the evaluators were compared using the chi-square test for homogeneity. When one box was less than 5, the Fisher exact test was used.

A Kruskal Wallis test was used for the comparison of protocols for overall motion and to compare motion among the 3 different locations in the chest. Since a difference was found for

overall motion among the protocols, a Mann-Whitney test was used to compare each protocol. A $P < 0.05$ was considered statistically significant.

3.3. Results

Demographic and morphologic parameters of the cats are shown in Table 3. The mean age of the cats was 7.5 years and the mean body weight 4.5 Kg. There was no statistical significant difference between randomized versus non-randomized cats and the statistical analysis was performed adding these 2 groups. The mean total time at CT was 12.5 minutes, with a range of 5-28 minutes. With the exception of 5 cats, the total time at CT was below 15 minutes.

The CT protocols are displayed in Table 4. In 20 out of 22 cats CT was completed without complications. Two cats had signs of overt stress and attempted to escape from the VetMouseTrap™. The first attempt to image one of these cats resulted in extreme motion artifact; the CT examination was terminated. The second cat remained in dorsal recumbence and was pushing the top of the device with all four limbs and CT examination was not attempted. These 2 cats were excluded from the study. The remaining 20 cats had no signs of physical or respiratory distress and remained in a sternal resting position for almost the entire CT examination. Some cats moved their head from side to side and some would flip 180^{o} inside the device and then remain still. Approximately 50% of cats had at least one protocol repeated due to motion artifact. The images were acquired from cranial to caudal in most cats. Most original transverse plane images were characterized by mild to moderate obliquity before on-line manipulation. Presumed pulmonary atelectasis was present in 1 cat and seen in all protocols for this cat. This appeared as a small region of patchy alveolar pattern in a dependent region of the lung.

The results for the quantitative evaluation are displayed in Table 5. A statistically significant difference was found for SNR and CNR between all protocols. Among the same kV, protocols with the higher pitch had the highest SNR and CNR and among the same pitch,

protocols with higher kV had the highest SNR and CNR. The contrast was higher in protocols with lower kV although the difference was not statistically significant. There was no statistically significant difference for SI_{lung} between any protocols. The results for CTDIvol were similar for all 4 protocols (Table 4). Results of regression analysis are summarized in Table 6. There was a statistically significant although weak positive correlation of body weight with $SI_{backg.}$ and noise, and negative correlation with CNR. Similarly, width of the thorax had a weak positive correlation with SI_{lung} and noise, and negative correlation with CNR and SNR. Age had a significantly although weak positive correlation with SNR and CNR, and negative with SI_{lung}. Height of the thorax was not correlated with any of the parameters.

Qualitative results are summarized in Tables 7 - 9. The interobserver agreement was moderate to substantial for evaluation of liver margins, substantial for helical helical artifact and substantial to almost perfect for windmill artifacts[50]. For overall motion, protocols with high pitch had significantly less motion artifact compared with protocols using low pitch. For location of motion artifact, there was no statistical difference based on the reader's score for any protocol in any location. Overall, 75 out of 80 (94%) examinations were judged to have absent or minimal motion artifact.

There was a statistically significant difference for windmill and helical helical artifacts between protocols with 1.75 and 0.562 pitch, with 0.562 pitch protocols having less windmill and helical-helical artifacts (Figures 2-5). There was also a significant difference for liver margins between protocols with different pitch, with higher pitches showing sharper liver margins than lower pitches (Figures 6a-d).

3.4 Discussion

The VetMouseTrap™ allowed cats to be imaged without direct manipulation, and CT examination was deemed less stressful than thoracic radiographs since there was minimal stress of restraint and no stress of positioning. Computed tomographic examinations were successfully performed in 20 of 22 cats when placed inside the VetMouseTrap™. The remaining cats tolerated the device very well and remained still for almost the entire CT examination.

The CT protocols used in this study were adapted from human pediatric CT. When performing CT imaging of awake cats, two similarities can be found with human pediatric CT: the need to depict very small anatomic structures, such as peripheral bronchi, and the fact that both awake cats and children often can be uncooperative patients producing motion artifact. To address these two problems we compared protocols with a low and high kVp to test for differences in image contrast and with a low and high pitch to test for differences in image artifacts.

In humans, a reduction in kV is associated with an increase in image contrast. Changes in kV alter both the quality as well as the quantity of photons. By changing tube voltage, the number of photons produced changes and the photons have a different energy.[43] In this study protocols with lower kV had better contrast although not statistically significant, but slightly lower SNR and CNR compared with protocols with higher kV. The higher SNR can be explained by the increased tube voltage on 120 kV, but the higher CNR in protocols with higher kV was not expected. An important consideration is the fact that the contrast measurements were performed between soft tissue and air in the lung. This contrast is not strongly dependent on kV since by definition the CT contrast scale has a difference of 1000 (HU) Hounsfield units between air and water at all kV settings. In looking at contrast or CNR between soft tissues or bone one

would expect an increase or improvement at lower kV. Also in situations in which contrast media are used, the image contrast and CNR will be substantially increased at lower kV. It is well-documented in humans that besides increases in soft-tissue contrast, low kV CT protocols enhance the iodine-induced contrast and thus reduces the amount of iodinated contrast media needed to image lower-weight patients, because the attenuation of iodine based contrast media increases with reduced x-ray energy.[51-53] Although statistically significant, the difference in SNR and CNR related to kV in this study was very small and probably not clinically relevant. The impact of this difference on the subjective evaluation of image quality was not assessed. The higher SNR, CNR and slightly lower noise in the protocols with 1.75 pitch can be explained by the fact that increasing pitch causes widening of the slice sensitivity profile (SSP), a measure of the ability of the CT scanner to precisely limit the information that makes up the image to a defined slice of tissue. If the individual detector collimation does not change, images acquired with higher pitch are effectively thicker slices.[43, 54] The slice thickness has a strong influence on the number of photons used to produce the image. Thicker slices use more photons and have better SNR.[26] This means that the apparent advantage of higher pitch in SNR and CNR is artificial and only obtained through decrease in the longitudinal resolution.

Patient motion can cause significant artifacts, which usually appear as shading or streaking in the reconstructed image.[33] Motion is decreased with shorter imaging time in two ways. First, the amount of motion during each single slice acquisition decreases. Second, the ability of the patient to cooperate is improved with a shorter overall duration of the scan, at least in humans. Scan time can be decreased by using a faster gantry rotation.[43] The scan time also affects the longitudinal (Z axis) coverage. The longitudinal coverage can be calculated by

multiplying the longitudinal beam collimation, pitch, and scan time, and dividing by the gantry rotation time.[16]

The selection of pitch is a trade-off between patient coverage and accuracy. Larger pitches reduce scanning time allowing more coverage of a patient per unit of time, but slice data must be interpolated using scan data that is farther from the actual slice, producing more artifacts.[19,55] In pediatric thoracic CT although no single helical CT technique has gained universal acceptance, in general, a pitch of at least 1.3 is used and many authors use a pitch from 1.3 to 1.6.[43] When evaluating CT protocols for pulmonary nodule detection in dogs, pitches of 1.5 and 2 were tested and both resulted in good image quality.[55] In evaluation of CT protocols for the cervical and lumbar spine of dogs, increasing pitch from 0 to 2 was associated with significantly poorer scores for half of the examined categories.[56]

To minimize motion artifact we used the fastest available rotation time (0.5 seconds) and tested protocols with higher pitch. We hypothesized that images acquired with 1.75 pitch would result in less motion artifact, supported by the results of all evaluators. Most CT examinations judged to have moderate or severe motion artifact were obtained with protocols using 0.562 pitch. This difference was expected as the scan time using 1.75 pitch was approximately 30% of the scan time using 0.562 pitch. However, even though a statistically significant difference was found between high and low pitch for motion artifact, overall, motion artifact was considered to be absent or minimal for the majority of examinations regardless of protocol and moderate or severe motion were present in a very small percentage of examinations (Table 9). Furthermore, all images were considered of excellent diagnostic quality, even those ranked as having moderate or severe motion. Finally, all CT examinations were ranked by the worse score present,

regardless of number of slices affected. In this regard, only 6% (5/80) of the examinations had motion artifact present in 10% or more of the total number of slices.

Liver margins were considered consistently blurred on the low pitch protocols, but the degree of blurring was very mild and did not seem to affect the overall image quality.

Although protocols with a higher pitch had less motion artifact, substantial helical and windmill CT artifacts were found using these protocols with a moderate to good interobserver agreement. Helical and windmill artifact were significant in most images with 1.75 pitch and these artifacts were almost absent in the images acquired with 0.562 pitch.

It is a common understanding that the windmill artifact is due to the need for data interpolation in helical scanning. Generally, the amplitude of the windmill artifact decreases as the number of detector rows increases: the windmill artifact in 64-slice is less than in 16- slice CT.[57] Both windmill and helical-helical artifacts gradually increase as pitch is increased.[15]As helical pitch increases, the number of detector rows intersecting the image plane per rotation increases and the number of "vanes" in the windmill artifact increases, but the strength of the artifact in each vane decrease proportionately.[33] The most recommended practice to avoid this artifact is to scan using the thinnest possible individual detector collimation, in other words, fine longitudinal sampling, and reconstructing thick images, such as 1 and 2 mm or thicker images. For example, a detector collimation of 16 x 0.625 mm is preferable to 16 x 1.25 mm or 8 x 2.5 mm. Obtaining thicker images than the individual detector collimation is equivalent to longitudinal filtering, which means a substantial compromise on the longitudinal resolution, but also a decrease in image noise.[58]

Near isotropic images could be acquired by reformatting the 0.625 mm slice thickness images in dorsal and sagittal planes for the thorax and dorsal and transverse planes for the head.

Recent advances in multidetector CT technology have made the acquisition of isotropic data feasible with use of a narrow configuration of the detector array so that only the smallest detector elements are exposed.[59] Through several generations of CT scanners, long-axis resolution was consistently inferior to short-axis, or transverse, spatial resolution. Spatial resolution in the transverse plane is limited by pixel size. Within a matrix of 512 x 512 and a scanning field of view of 25 cm, the pixels that constitute each axial image are squares with a length of approximately 0.49 mm on each side. Using the "detail" reconstruction algorithm, the spatial resolution due to the algorithm is about 0.6 mm. Thus, a slice thickness in the range of 0.5– 0.8 mm is required to achieve similar spatial resolution in all three dimensions. If the thickness of the axial slice is taken into account, the square pixels are converted to three dimensional voxels. When data are reconstructed to achieve similar dimensions in all 3 planes it consists of cube-shaped voxels and the images are considered to be isotropic. Isotropic imaging minimizes the importance of patient positioning and obviates the need to obtain transverse, dorsal and sagittal planes directly because reformation in any desired plane will have a spatial resolution similar to that of the original plane.[15, 16, 48, 59, 60] This is especially important when imaging awake cats since the original images are acquired in a nontraditional oblique plane depending on the position of the cat inside the device.

We hypothesized that the images would have no lung lobe atelectasis since the cats were scanned without sedation or general anesthesia and this was confirmed in all but one cat, in which atelectasis probably ocurred as a result of recumbency.

When developing the protocols we used information from the technical data sheet of the CT scanner[‡] to adjust the scan parameter to provide the same CTDIvol for each of the four protocols used. When performing the scans we recorded the CTDIvol generated by the CT

scanner and the displayed results were in fact similar for all 4 protocols. The CT Dose Index (CTDI) is the dose measured in a 16 or 32 cm acrylic phantom (the CTDI phantom), while the CTDIvol is a weighted average of surface and central dose measurements in the phantom so as to approximate the average dose to the phantom volume when the effect of pitch on dose is also taken into account. The CTDIvol is widely used in human adult and pediatric CT to evaluate different protocols on a single CT scanner since an initial comparison of different techniques can be easily performed. Improvements in image quality for a consistent dose, as well as decreases in dose while maintaining acceptable image quality can be suggested, and then evaluated in regular use.[43] When choosing protocols for CT in humans there is always a trade-off between image quality and dosage. Radiologists and technicians must balance protocol selection between resolution, noise, and contrast to achieve good image quality and keep patient exposure as low as reasonably achievable.[61] In veterinary medicine radiation exposure is not as much of a concern as it is in humans, however, studies evaluating radiation dose and safety associated with routine imaging diagnosis are lacking. We decided to choose protocols with a relatively low and constant dose since the cats would be submitted to multiple scans.

In pediatric CT there is a recommendation for using a sharper algorithm for reconstruction of lung images.[43] Sharper algorithms delineate object margins more clearly at the expense of increased image noise. Less sharp algorithms reduce noise, allowing larger low contrast object to become more visible although edges will be more blurry and fine detail lost. A moderately sharp ("detail") algorithm was used in this study, which is somewhat sharper than smooth or standard algorithms, but less sharp compared to "bone' algorithms. This algorithm was chosen to deliver the best compromise between resolution and image noise.[19]

Although positive, the correlation found between body weight and noise, and width of the chest and noise was very weak and probably not clinically relevant. This correlation could be explained by the fact that cats in this study had a wide range of body weight and thoracic cavity width and this could increase image noise if tube current and voltage are not changed. If the noise increases and contrast and signal intensity do not increase proportionally, it is expected that CNR and SNR will vary in the opposite direction.

The mean total time in the CT scanner in this study was similar to time to perform a 3 view thoracic study in our institution in a cooperative cat with experienced holders, which is on average 10 minutes. However, in a clinical situation when only one protocol would be used the total time in the CT scanner when scanning awake cats would be significantly reduced. Furthermore, CT examinations were believed to be less stressful for the cats, since no direct manipulation was necessary, and safer for personnel due to the absence of radiation exposure.

Although motion artifact was almost absent, some cats were scanned multiple times when the images were initially considered non-diagnostic. When dealing with an uncooperative patient, the advantages of performing CT without general anesthesia, such as the possibility to scan a patient that otherwise would not be submitted to CT due to clinical instability, absence of lung atelectasis, and faster and less expensive examinations, could be considered a trade-off with the potential radiation hazard and increased tube usage that could result from multiple scans.

During the CT scan the thoracic region could have been out of the isocenter of the CT machine in some examinations since pre-scan scouts were not made and it was not possible to predict where the cat would be positioned inside the VetMouseTrap™. This could have been responsible, at least in part, for some image degradation. When testing pitch we decided to used two extreme values and 0.938 and 1.375 pitches, not tested in this study, could potentially result

in a better balance between helical and motion artifacts. It could also have been of interest to assess if a qualitative difference would have been detected between the two different kVps however this was not done in this study. Finally, the protocols evaluated here can vary significantly with different CT machines and should only be used as a guideline.

In conclusion**,** the VetMouseTrap™ allowed whole-body images to be successfully acquired in a very short period of time with excellent spatial resolution in all three planes and negligible motion artifact. Presumed lung lobe atelectasis was present in only one cat and deemed to be very mild. Protocols with 1.75 pitch had significant windmill and helical-helical artifact that compromised image quality and therefore are not recommended. With 0.562 pitch, windmill and helical artifacts were almost absent and motion, although statistically higher compared to 1.75 pitch, was overall minimal and not considered to be clinically relevant. Based on these results and on the literature, we recommend a protocol of 80 kV, 130 mA, 0.5 s, and 0.562 pitch with a 1.25 mm slice thickness, and a 0.625 mm slice reconstruction interval for helical thoracic CT examination of awake cats using the VetMouseTrap™. Protocol adjustments for cats with different body weights and conformations do not seem to be necessary. Future studies are needed that would evaluate the full range of available pitches and assess the subjective difference in image quality between 80 and 120 kV. The VetMouseTrap™ has the potential to make a significant impact on the safety of the diagnostic imaging and case management of cats with respiratory compromise.

Footnotes

[†]GE Healthcare, Buckinghamshire, United Kingdom

[‡]LightSpeed 4.X, LightSpeed 16, Technical Reference Manual, CE 0459

[§] MedCalc Software, Mariakerke, Belgium; SPSS, IBM Company, Chicago, IL

3.5 Figures

Figure 2. Transverse CT image of the caudal thorax of cat 7 using protocol 1 (80 kV, 0.562 pitch). Window width = 1600, window level = -600.

Figure 3. Transverse CT image of the caudal thorax of cat 10 using protocol 2 (80 kV, 1.75 pitch). The vanes of the windmill artifact are visible (thin arrows). The helical-helical artifact is also visible (thick arrow). Window width = 1600, window level = -600.

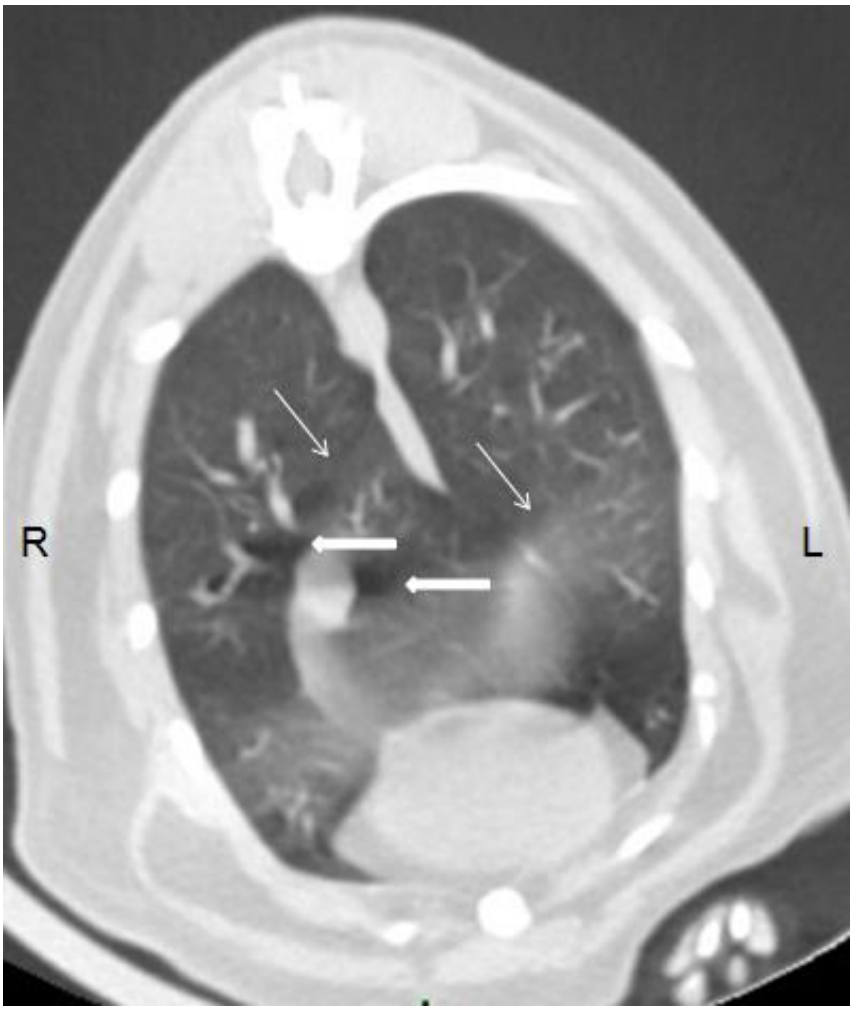

Figure 4. Transverse CT image of the caudal thorax of cat 1 using protocol 3 (120 kV, 0.562 pitch). No windmill or helical helical artifacts were detected. There is mild blurring of the liver margin (arrow). Window width = 1600, window level = -600.

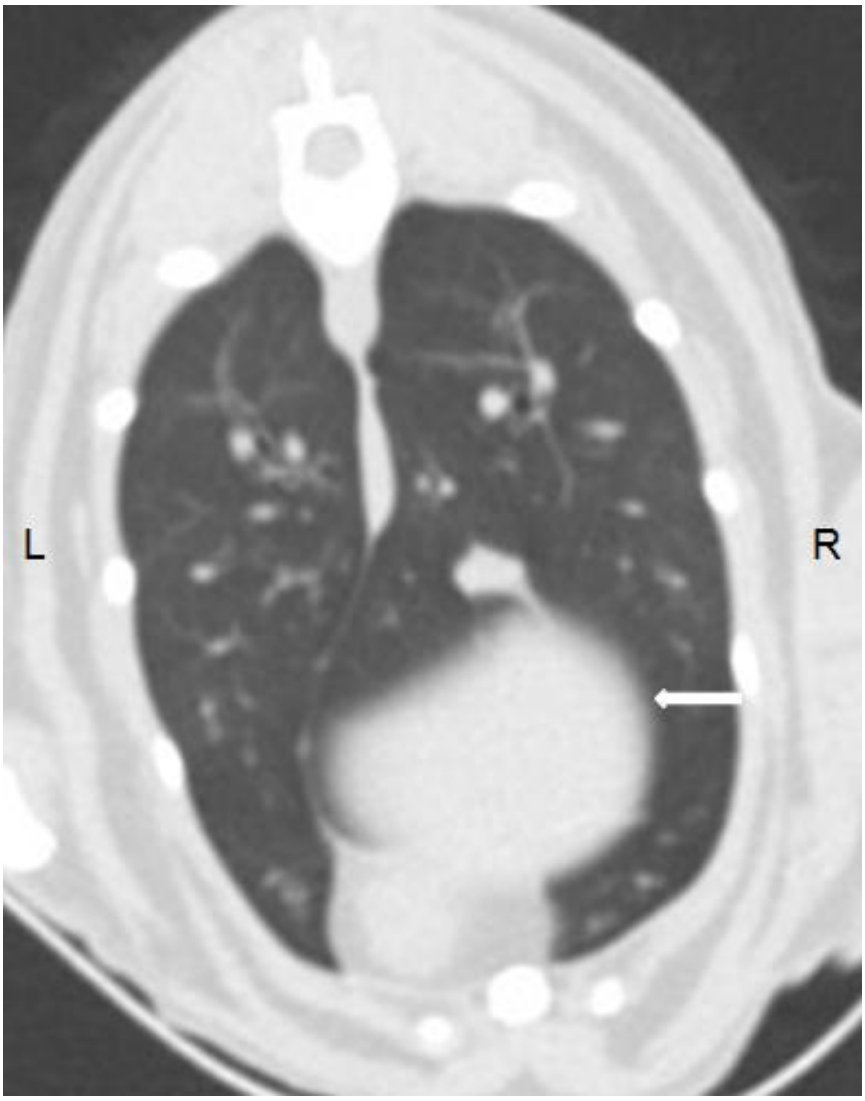

Figure 5. Transverse CT image of the caudal thorax of cat 5 using protocol 4 (120 kV, 1.75 pitch). Multiple regions of helical helical artifact are visible (arrows). Window width = 1600, window level = -600.

Figures 6a – d. Transverse CT images of the caudal thorax of cat 11 with CT protocols 1 (a), 2 (b), 3 (c) and 4 (d). Liver margins are blurred in protocols 1 and 3 (this arrows), and sharp in protocols 2 and 4 (thick arrows). Note "vane" from windmill artifact (asterisk) with procotol 2 (figure 5b). Window width = 1600, window level = -600.

Figure 6a. CT protocol 1: 80 kV, 0.562 pitch- Note blurred liver margins (arrows).

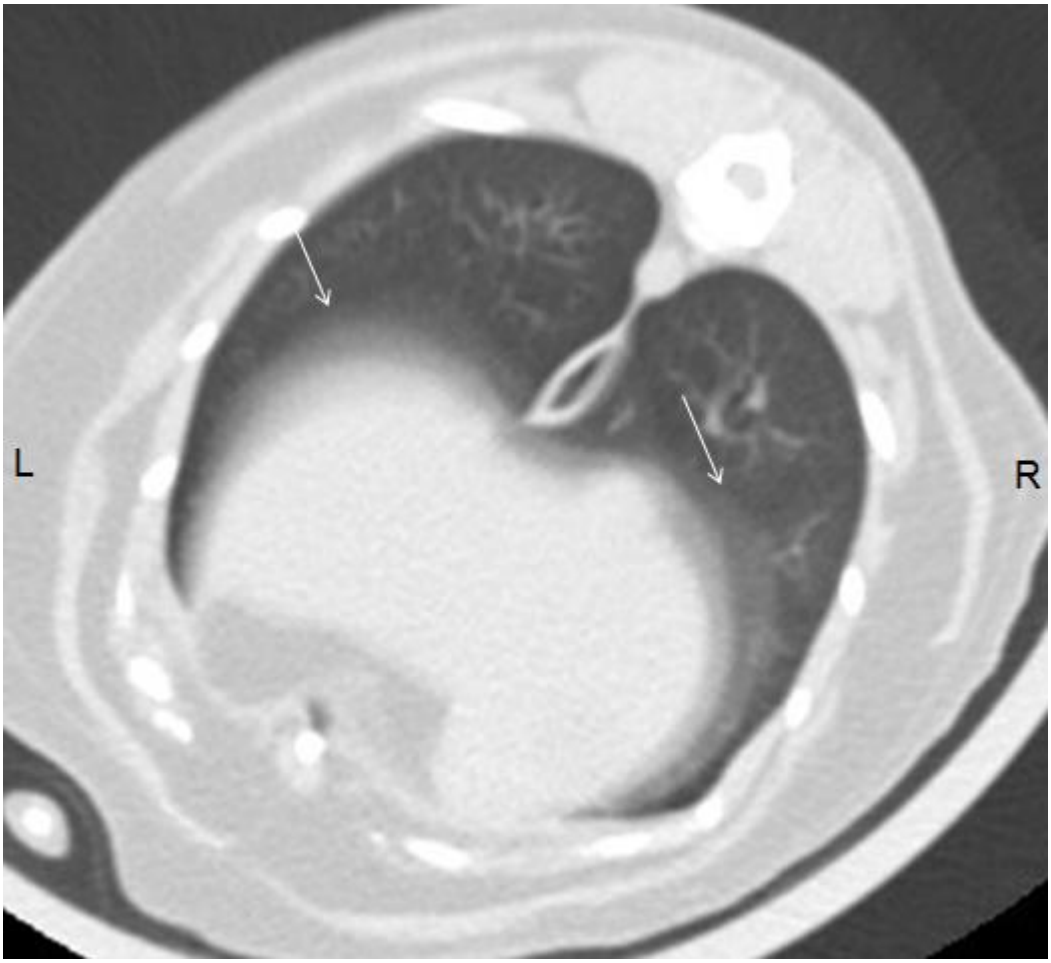

Figure 6b. CT protocol 2: 80 kV, 1.75 pitch- Note sharp liver margins (arrow) but "vanes" of windmill artifact are present (asterisk).

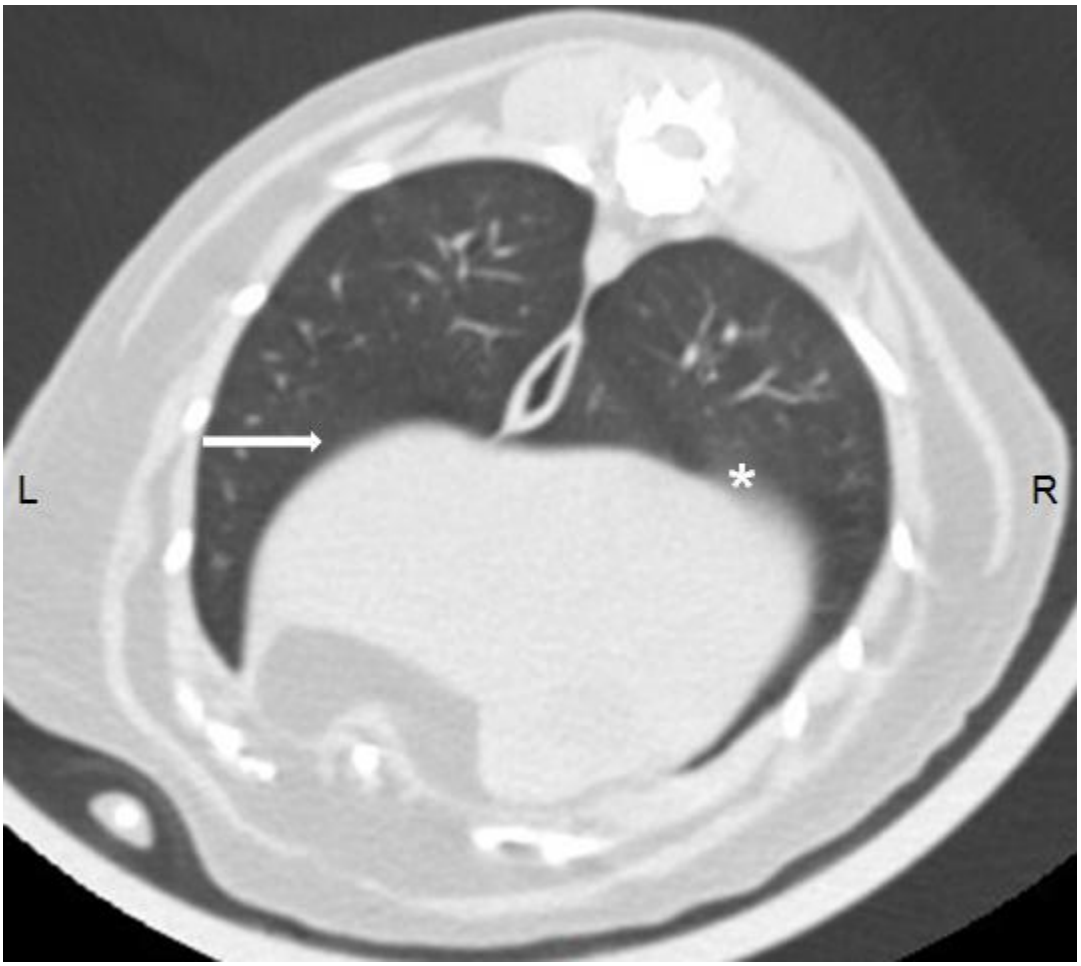

Figure 6c. CT protocol 3: 120 kV, 0.562 pitch- Note blurred liver margins (arrows).

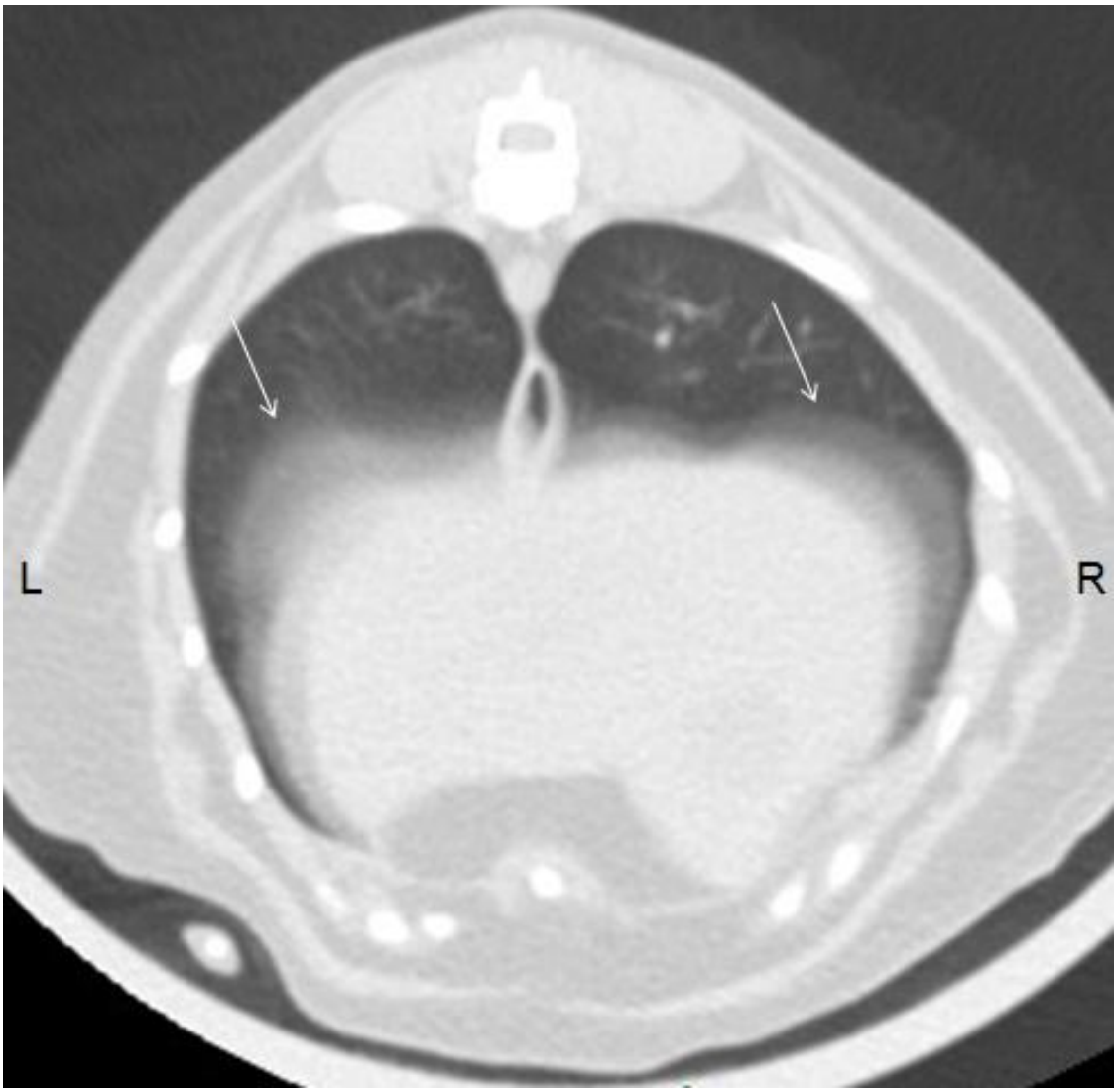

Figure 6d. CT protocol 4, 120 kV, 1.75 pitch- Note sharp liver margins (arrows).

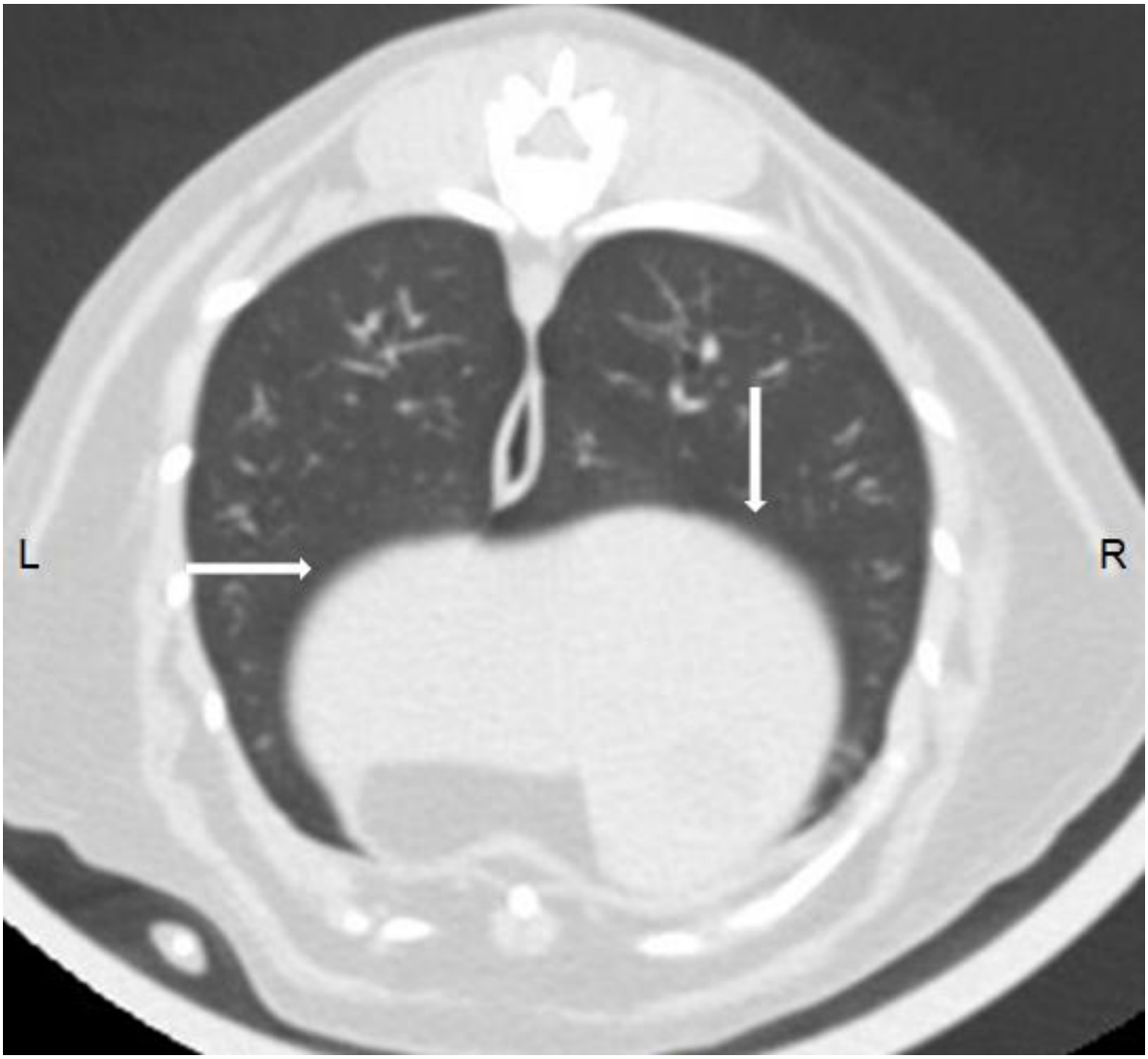

3.6 Tables

Table 3- Data Distribution of Cats

	Mean	**SD**	**95% CI**	**Min-Max**
Age (y)	7.5	4.5	5.4 – 9.7	1 – 15
BW (Kg)	4.6	1	4.2 – 5.1	3 – 6.1
WC (cm)	12.8	2.7	11.6 – 14	8.4 – 17.5
HC (cm)	14.3	1.4	13.7 – 15	11.9 – 16.5
Total time at CT (min.)	12.7	6	9.9 – 15.6	5 – 28

BW = body weight, WC = width of chest, HC = height of chest,
SD = standard deviation, CI = confidence interval,
Min-Max= minimum-maximum

Table 4- CT Protocols

	Protocol 1	**Protocol 2**	**Protocol 3**	**Protocol 4**
Tube Voltage (kV)	80	80	120	120
Pitch	0.562	1.75	0.562	1.75
Tube Current (mA)	130	400	45	145
mAs	65	200	22.5	72.5
Effective mAs	116	114	40	41
Rotation time (s)	0.5	0.5	0.5	0.5
Field of view (cm)	25	25	25	25
Slice thickness (mm)	1.25	1.25	1.25	1.25
Increment (mm)	0.625	0.625	0.625	0.625
Total Scan time (s)	36.7	11.9	36.7	11.9
$CTDI_{vol}$ (mGy)	8.71	9.39	8.36	8.66

$CTDI_{vol}$ = volume CT dose index

Table 5- Quantitative Results

	Protocol 1		**Protocol 2**		**Protocol 3**		**Protocol 4**	
	Mean	SD	Mean	SD	Mean	SD	Mean	SD
SI_{lung}	- 827.8[a]	53.5	- 831.2[a]	59.2	- 814.3[a]	56.2	- 822.6[a]	59
$SI_{backgr.}$	61.9[a]	3.2	62.4[a]	4.9	60.4[ab]	2.5	58.7[b]	5.4
Contrast	765.9[a]	53.2	768.8[a]	58.5	753.9[a]	57.4	763.9[a]	61.4
Noise	20.4	0.09	17.8	0.2	18.5	0.2	16.3	0.1
SNR	40.5[a]	2.6	46.7[b]	3.2	44[c]	3	50.6[d]	3.5
CNR	37.5[a]	2.6	43.2[b]	3.3	40.7[c]	3.1	47[d]	3.8

Within a row protocols with different letters show statistically significant difference
SI_{lung} = signal intensity in the lung, $SI_{backgr.}$ = signal intensity in the background,
SNR = signal-to-noise ratio, CNR = contrast-to-noise ratio

Table 6- Pearson's Correlation Coefficient

	SI_{lung}	**$SI_{backgr.}$**	**Noise**	**SNR**	**CNR**
Protocols	0.06*	- 0.3	- 0.5	0.4	0.3
Age (y)	- 0.4	- 0.25*	- 0.22*	0.3	0.3
BW (Kg)	0.37*	0.5	0.3	- 0.43*	- 0.4
WC (cm)	0.4	0.07*	0.3	- 0.4	- 0.4
HC (cm)	- 0.14*	0.16*	- 0.01*	0.06*	0.06*

*Not statistically significant

Table 7- Kappa Statistic Interobserver Agreement

Evaluator*	**Liver Margins**	**Helical Artifact**	**Windmill Artifact**
A-B	0.59	0.72	0.90
A-C	0.70	0.72	0.75
B-C	0.72	0.74	0.80

*Evaluator A and C: Board-certified radiologists
*Evaluator B: Certified CT technician

Table 8- Percentage of Slices Affected by Motion Artifact

Protocol	**1**	**2**	**3**	**4**
Cats				
1	3% (8/241)	0%	9% (23/243)	0%
6	10% (25/243)	0%	15% (35/230)	0%
8	10% (17/174)	0%	0%	0%
9	7% (15/216)	0%	0%	0%
10	7% (16/229)	0%	6% (13/233)	0%
11	0%	0%	9% (21/243)	0%
12	0%	0%	10% (21/206)	0%
13	9% (19/207)	0%	8% (16/198)	0%
14	0%	0%	8% (17/202)	0%
15	0%	4% (6/162)	0%	0%
16	6% (11/185)	0%	4% (7/175)	0%
17	6% (11/198)	19% (37/199)	0%	7% (14/198)
20	0%	0%	9% (18/192)	0%

Cats 2, 3, 4, 5, 7, 18 and 19 had no images affected by motion

Table 9- Frequency of Scores Combining All Evaluators

	Liver Margins				**Helical Artifact**				**Windmill Artifact**			
Protocol	1	2	3	4	1	2	3	4	1	2	3	4
Score												
0	5^a	49^b	4^a	53^b	47^a	2^b	50^a	3^b	57^a	1^b	53^a	3^b
1	55^a	11^b	56^a	7^b	13^a	58^b	10^a	57^b	3^a	59^b	7^a	57^b

Within a row protocols with different letters show statistically significant difference
Liver Margins: sharp-0, blurred-1, Helical Artifact: absent-0, present-1, Windmill Artifact: absent-0, present-1

CHAPTER 4

WHOLE-BODY COMPUTED TOMOGRAPHY IN AWAKE CATS WITH THORACIC DISEASE

This work includes material previously submitted for publication. Whole-Body Computed Tomography in Awake Cats with Thoracic Disease. Oliveira, CR, Mitchell, MA, O'Brien, RT. Submitted November 2nd 2010 to Veterinary Radiology & Ultrasound

4.1 Introduction

In humans, CT is established as the primary imaging modality for patients with clinical signs of thoracic disease.[1, 2] Computed tomographic high contrast resolution and its lack of anatomic superposition provide unique diagnostic information that is unobtainable with conventional radiographic techniques.[3-8] Computed tomography allows better distinction among specific tissue densities and detection of subtle changes in organ size, shape, margin contour, and position.[3, 4, 8] Therefore, CT plays a key role in the diagnosis and evaluation of various thoracic syndromes and diseases such as pneumothorax, pleural and pericardial effusion, collapse of a lung lobe, congenital anomalies, pulmonary parenchymal and bronchial diseases, cysts, abscesses and primary or metastatic neoplasia of the lungs, pleura, mediastinum, lymph nodes, and chest wall. Furthermore, CT is a useful preoperative technique, a precise staging tool, and improves the use of biopsies by allowing detection of lesions not identifiable by other imaging modalities.[8]

Clinical reports on thoracic CT for the diagnosis of thoracic diseases in dogs and cats are limited to anesthetized patients.[3-7] General anesthesia limits the clinical use of CT and is contraindicated in many emergency conditions, especially for patients with respiratory distress.

General anesthesia has inherent risks and additional disadvantage of causing lung atelectasis. In human patients with normal lung function before anesthesia, 90% develop dependent atelectasis even with positive pressure ventilation during general anesthesia and is considered the major cause of impairment of gas exchange and lung compliance.[11]

A small number of studies, each using a small number of animals, have described the CT appearance of thoracic diseases in cats. These previous studies described the CT appearance of lung lobe torsion, cranial mediastinal masses (CMM), primary and metastatic lung neoplasia, atelectasis and alveolar pathology in anesthetized cats.[4, 5, 7, 41] Recently, the use of CT in awake normal cats was described. In this study, CT images of awake cats were collected using a low-attenuating and clinically supportive device (VetMouseTrap™). Computed tomography imaging was completed in 91% (20/22) of the cats and image quality in all completed sets considered of excellent quality with minimal motion artifact.[42]

The purposes of the present study were to: 1) test the clinical usefulness of the VetMouseTrap™, and 2) compare CT and thoracic radiography findings in a clinical group of cats with signs of respiratory disease.

4.2 Materials and Methods

Cats presenting to the Emergency Department of the Veterinary Teaching Hospital of the University of Illinois with recent historical or current clinical signs of respiratory disease were initially stabilized and thereafter imaged in the VetMouseTrap™ without sedation or general anesthesia using a 16 slice helical CT system*. Inclusion criteria for historical evidence of respiratory disease included information presented by the owner, physical exam findings of the referring veterinarian (RDVM) or response to specific therapy by either the owner or RDVM. Inclusion based on current signs of respiratory disease was dependent on clinical judgment of the primary receiving clinician. These signs included demonstration of increased respiratory rate or effort, cyanosis, open-mouth breathing, extension of head and neck, anxious behavior, decreased tolerance to handling, cough, auscultation of abnormal breathing sounds, abdominal breathing, or nasal discharge.[62] Cats displaying signs consistent with dyspnea included at least two of the aforementioned signs, excluding cough and nasal discharge. All cats had a final diagnosis based on echocardiography, cytology, histopathology, necropsy, or clinically based on response to specific therapy.

The cats were separated into eight clinical classifications based on final diagnosis: 1), pulmonary neoplasia 2), lower airway disease, 3) cardiomyopathy 4) mediastinal mass 5) infection, 6) trauma, 7) hernia, 8) other. Clinical history and presenting or historical physical examination signs was obtained for each cat. Folllow-up was obtained on all cases up to the time of writing this manuscript by searching the medical records, contacting the referral veterinarian or owner.

The VetMouseTrap™ device was used for CT imaging of all cats without sedation or anesthesia. Cats were typically placed inside the device whilst in the emergency room of the

Small Animal Clinic and transported to the Radiology Department receiving constant oxygen administration. Therapeutic thoracocentesis was performed, as clinically necessary, in cats with suspected pleural effusion or pneumothorax prior to imaging. Additional supportive therapy was performed as clinically indicated. Cats were placed in the the VetMouseTrap™ without additional restraint and monitored visually throughout the CT procedure. Oxygen was provided at a flow of 2 liters/min by oxygen tubing in the VetMouseTrap™ at the head end of the patient for animals during the procedure, as deemed clinically necessary. Images were acquired of the entire VetMouseTrap™ resulting in a whole-body study in all cats. The CT protocols used were: 0.562 pitch, with either 80 kV and 130 mA, or 120 Kv and 45 mA, collimation of 16 x 0.625 mm, gantry rotation speed of 0.5 second, 25 cm field of view, 1.25 mm slice thickness with 0.63 mm increment and "detail" algorithm.

Intravenous iodinated† (2ml/Kg) contrast CT studies were performed as clinically indicated or as requested by the clinician. Contrast CT images and multiplanar reconstruction (MPR) images were not compared with survey radiographs to 1) avoid the inherent bias of contrast CT versus noncontrast radiology, and, 2) demonstrate the utility of survey CT in cats imaged in the VetMouseTrap™. Multiplanar reconstruction and contrast images were retrospectively evaluated for additional diagnoses and additional CT findings, compared to survey CT.

Thoracic radiographs were made in both left and right lateral views and either dorsoventral or ventrodorsal views using routine radiographic techniques. The duration of time from initial presentation in the hospital to initiation of imaging was compared between the two imaging modalities. The attending clinician decided which modality was used first.

Image analysis

All imaging studies were evaluated on a PACS workstation[‡] by consensus of two radiologists. Twenty clinically healthy cats, imaged with radiographs and survey CT as part of a preliminary research study, were included in the evaluation to avoid bias. The image sets were anonymized and randomized. Information about the studies, patient name, age, clinical signs, and date of examination were blinded.

CT images were evaluated using a standardized questionnaire in bone window (window center 800, window width 2000), soft tissue (center 60, width 360) and lung window (center -600, width 1600). Evaluators answered the questions as present, absent, or indeterminate. Specific pathology and motion artifact were subjectively graded as absent, mild, moderate or severe. Evaluators provided the reasons for indeterminate findings and if technique or positioning was judged inadequate. Lung patterns were evaluated for location and distribution. Readers were asked to provide a radiographic diagnosis.

Statistical analysis

A commercial software[§] was used for statistical analyses. The Kolmogorov–Smirnov test was used to test for normalcy of the data. Normally distributed data were reported by mean and minimum–maximum values, while non-normally distributed data were reported by median and minimum–maximum values.

A Chi-square test was used to test for statistically significant differences between the proportion of males/females, spayed/non-spayed, pedigree/non-pedigree and dyspneic/non-dyspneic cats. When one box contained less than 5 cats, the Fisher exact test was used.

The Independent Sample t test was used to compare age among dyspneic versus non-dyspneic cats. A Wilcoxon test for paired samples was used to compare the time from presentation to performing radiographs with the time from presentation to performing CT.

For the imaging evaluation, the results of radiographs analyses were compared with the results of CT using Kappa inter-rater agreement test and interpreted as follow: < 0 Less than chance agreement, 0.01–0.20 Slight agreement, 0.21– 0.40 Fair agreement, 0.41–0.60 Moderate agreement, 0.61–0.80 Substantial agreement, 0.81–0.99 Almost perfect agreement.[50] A comparison of proportions was performed for indeterminate findings and for image quality evaluation for each imaging modality including technique adequate, positioning adequate, motion artifact and complete study. The results for image quality evaluation were reported as percentage with 95% confidence interval (CI) and Chi-square. A $P < 0.05$ was considered statistically significant for all statistical tests.

4.3 Results

Fifty-four cats were included in the study. The mean age of all cats was 9.5 years (min-max: 0.17 – 19 years) and the mean body weight 4.9 Kg (min-max: 2 - 8.4 Kg). A statistically significant difference was found between the proportion of males (39/54, 72.2%) and females (15/54, 27.8%) ($P = 0.0017$), spayed (50/54, 92.6%) versus non-spayed (4/54, 7.4%) ($P < 0.0001$), pedigree (7/54, 13%) versus non-pedigree (47/54, 87%) ($P < 0.0001$) and dyspneic (41/54, 75.9%) versus eupneic (13/54, 24.1%) ($P= 0.0002$). There was not a statistically significant difference between the age of the cats with dyspnea versus eupneic cats ($P= 0.194$). The breeds included in the study were: Domestic Short Hair (DHS, n=32), Domestic Long Hair (DLH, n= 10), Mixed (n= 4) and Domestic Medium Hair (DMH, n= 1). Pedigree cats included: Siamese (n= 3), Himalayan (n= 1), Maine Coon (n= 1), Devon Rex (n= 1) and Burmese (n= 1).

The most frequent final diagnoses were lung neoplasia (16.7%, n=9), lower airway disease (16.7%, n=9), and cardiomyopathy (16.7%, n=9). Forty-one cats had a final diagnosis, and final confirmation was based on the following diagnostics: necropsy (n=14), cytology (n= 13), echocardiogram (n=7), histopathology (n=5) or surgery (n= 2). In the remaining 13 cats, a presumed diagnosis was made based on response to therapy and follow-up.

Of the 54 cats with CT imaging, fifty cats had both CT and radiography performed, from which 46 had complete (3 view) radiographic studies and survey CT imaging performed within 24 hours of each other. Eight cats were excluded from the statistical analysis for comparison between the imaging modalities (Kappa evaluation), but evaluated for additional information provided: correct diagnosis, image quality, and time from presentation to performing study.

The time from presentation to radiography and CT was not normally distributed. There was a significant difference ($P = 0.0427$). in the time from presentation to the hospital to

radiography (median: 175 minutes, min-max 8 – 2025) compared with CT(median: 237.5 minutes, min-max 26- 2057). From the 50 cats with both CT and radiographs, 46 had both imaging sessions performed on the same day, 3 cats had these imaging modalities performed a day apart, and one cat had referral veterinarian radiographs performed 8 days before CT. Excluding the latter cat, more cats (65%, 32/49) had radiography performed prior to CT. Radiography was the most common initial imaging modality in dyspneic cats in 68.4% (26/38).

Imaging findings

Overall accuracy of the correct final diagnosis was higher for survey CT (42/54; 77.8%) than radiography (29/50; 58%) (Table 10). The group with the highest percentage of correct diagnosis provided by CT compared with radiography was lower airway disease, where 88.9% (8/9) of correct diagnoses were made with CT compared with 50% (4/8) for radiography. The group for which CT had the highest accuracy overall was CMM (100%, 8/8). Cardiomyopathy was the group for which CT provided the lowest percentage of additional information (37.5%, 3/8), nevertheless CT had a high diagnostic accuracy in this group achieving the correct diagnosis in 88.9% (8/9) of the cats. Criteria for radiographic and CT diagnosis is displayed in Table 11.

Twenty-six of the 37 (71.3%) findings had fair or poor agreement between CT and radiography (Table 12). Survey CT provided additional information in 76% (37/50) of cases. Radiography failed to detect pulmonary metastases (n=5 cats), primary lung tumors (n=4 cats), thoracic lymphadenopathy (n=3 cats) and CMM (n=1 cat). CT identified 2 cats with both sternal and cranial mediastinal lymphadenopathy, and one cat with only sternal lymphadenopathy (Figure 7). Atelectasis was seen in six cats; four cats with CMM, one cat with pulmonary contusions and one cat with fibrosing pleuritis.

A total of 21 cats had pleural effusion based on at least one imaging modality. The majority of cats with pleural effusion were in the cardiomyopathy group (33.3%, 7/21), followed by mediastinal masses and lung neoplasia, 23.8% each (5/21). The majority of cats in the cardiomyopathy (77.8% ,7/9), cranial mediastinal (62.5%, 5/8) and lung neoplasia (55.6%, 5/9) groups had pleural effusion.

The majority of indeterminate answers occurred for radiographic studies (Table 13). The most common indeterminate answers were mediastinal lymphadenopathy (16%, 8/50), diaphragmatic hernia (DH) (16%, 8/50), mediastinal mass (10%, 5/50) and cardiomegaly (10%, 5/50),all in cats with concurrent pleural free fluid or CMM. Two indeterminate answers on survey CT were in one cat in which the diaphragm could not be delineated and this was the reason for the uncertainty about the presence of diaphragmatic tenting or flattening. When comparing the proportions for image quality (Table 14), only 4% (2/50) of the radiographic studies were considered inadequate technique, one due to the presence of gloves on the primary beam and the second due to a missing marker. All CT studies were considered of adequate technique. A total of 16% (8/50) of the radiographic studies, significantly more ($p = 0.0099$) than CT studies,were considered inadequately positioning. Reasons for inadequate positioning included: oblique lateral or VD projections, entire cat radiography, only a VD projection or incomplete lateral projection. The most common positioning error was obliquity on VD projection, seen in 4 cats, including 3 dyspneic cats. The majority of inadequate positioning was for studies performed on dyspneic cats 75% (6/8). The positioning on all CT studies was considered adequate. All cats were in sternal recumbency during the CT imaging, and mild obliquity did not affect image quality. Motion artifact was not found in any radiographic study, but was present in 50% (27/54) of the CT studies and was statistically significant ($P < 0.0001$). In

85% (23/27) of the CT studies, motion artifact was considered mild and in 16.6% (4/27) moderate. Motion was seen in a small number of CT slices and did not affect image quality in any case.

Contrast CT imaging was performed in 19 cats, two of which had no survey CT imaging. Cats that received contrast were in the groups: lung neoplasia (n=6), mediastinal mass (n=4), infectious (n=3), cardiomyopathy (n=2), hernia (n=2), lower airway disease (n=1) and other (n=1, chylothorax). The same diagnosis was reached in 15 of 17 (88.2%) cats with both survey and contrast CT. In the remaining 2 cats, additional new diagnoses were one cat each with pyogranulomatous pneumonia with fibrosis and lower airway disease. Nine cats had additional information on contrast CT, including sternal and CM lymphadenopathy in eight cats, and cystic portions of the CMM in one cat with thymoma. From the 8 cats that had thoracic lymphadenopathy based on contrast CT, six had neoplasia (five cats with lung carcinoma, one cat with thymoma), one cat had a lung abscess with fibrosing pleuritis and one cat had restrictive cardiomyopathy with CHF.

Lung neoplasia

Nine cats were included in this group, with a mean age of 11.6 years (min-max 6-18). Seven of nine (77.8%) cats presented with dyspnea. Eight had primary lung tumors and one had metastases from intestinal lymphoma. The final diagnosis in all cats with primary tumor was carcinoma. Diagnoses were obtained based on cytology (n=5), necropsy (n=3) or histopathology (n=1).

Accuracy of survey CT and radiography was 88.9% (8/9). Additional diagnosis (1/9) with survey CT was abdominal neoplasia with lung and pleural metastasis (n=1).

The most common CT findings were: one to multiple lung masses (7/9), one to multiple soft-tissue nodules (4/9), pleural effusion (4/9) and patchy alveolar pattern (4/9). Lung masses were located in the right caudal lobe (n=5), right middle lobe (n=2), left caudal lobe (n=2), and one mass on the right and left cranial lobes each. Additional information obtained with CT (8/9) included soft-tissue attenuating pulmonary masses (n=4) (Figure 8) and lung metastasis (n=4) seen either as lung nodules (n= 2) or a patchy alveolar pattern (n=2).

Contrast CT was performed in six cats, with an additional CT finding of thoracic lymphadenopathy in five cats. This included both sternal and cranial mediastinal lymph nodes (n=2), both cranial mediastinal and tracheobronchial lymph nodes (n=1), sternal (n=1) and cranial mediastinal (n=1).

Lower Airway

Nine cats were included in the lower airway disease group, with a mean age of 12.9 (min-max 8-19). Three of the cats presented with dyspnea. Seven cats had a diagnosis of lower airway disease based on response to therapy and follow-up, and two cats based in histopathology (bronchiolitis and bronchitis in both).

Survey CT had higher accuracy 88.9% (8/9) than radiography 50% (4/8) for the diagnosis of lower airway disease. The most common CT findings werediffuse bronchial wall thickening, (8/9), patchy alveolar pattern (5/9) and bronchiectasis (4/9). Bronchial wall thickening was seen on CT as multiple thick soft-tissue linear opacities longitudinally, and had a thick ring shaped appearance transversely. Thick bronchi were seen more peripherally than normal bronchi. Additional information obtained with CT (8/8) included: bronchial wall thickening (n=4), bronchiectasis (n=4) and hyperlucency (n=3)(Figures 9a and b), pneumonia (n=3), and main stem bronchial (n=2) and tracheal (n=1) wall thickening with luminal stenosis (Figures 10a and

b). Contrast CT provided the correct diagnosis in the one cat with the false diagnosis of congestive heart failure on survey CT.

Cardiomyopathy

Nine cats were included in this group with a mean age of 11.9 years (min-max 6-17). All cats presented with dyspnea. Diagnoses in this group were restrictive cardiomyopathy (RCM) (n=4), hypertrophic cardiomyopathy (HCM) (n=3), arrythmogenic (n=1) and unclassified (n=1) cardiomyopathy. Final diagnosis was made based on: echocardiogram (n=7) and necropsy (n=2).

Accuracy of survey CT was 88.9% (8/9) and radiography 75% (6/8). Additional correct diagnosis with survey CT (2/8) were cardiomegaly with congestive heart failure, radiographic diagnosis being CMM with pleural metastasis (n=1) and pneumonia (n=1).

The most common CT findings were cardiomegaly (7/9) (Figures 11a and b), pleural effusion (7/9) and patchy alveolar pattern (6/9). Additional information obtained with CT (3/8) included cardiomegaly (n=2 cats, both with pleural effusion), pleural effusion (n=1) and consolidated alveolar pattern (n=1).

Eight of nine (88.9%) cats had imaging findings consistent with congestive heart failure, including pulmonary edema, pleural or peritoneal free fluid. Pulmonary edema was variable in appearance and location (Figures 12a, b and c). A multifocal nonconsolidated alveolar pattern (n=5) was either bilateral (n=3) or unilateral (n=2). In most cats the edema was seen in three or more lung lobes (n=5). The distribution was variably hilar, central, or sub-pleural region or in combination.

Pleural effusion was identified in seven cats by the presence of fluid attenuating material (10 – 15 HU) in the dependent aspect of the thorax and fissure lines. Peritoneal effusion was seen in two cats as multiple linear thin soft-tissue attenuating regions interspersed with the peritoneal

fat, or soft-tissue attenuating material accumulating on the dependent aspect of the abdomen, surrounding the organs and causing an overall increased soft-tissue attenuation of the abdomen.

The interventricular septum and left ventricular free wall (average 45 to 68 HU) were hyperattenuating compared to blood (average 20 to 40 HU) in four cats (figure 13a and b). Wall-chamber characterization was indistinct in 3 cats and not possible 2 cats.

Contrast CT was performed in two cats providing the additional finding of sternal lymphadenopathy in one cat. Contrast administration provided more clear identification of cardiomegaly and cardiac chamber enlargement with no complications.

Mediastinal mass

Eight cats were included in the mediastinal mass group, with a mean age 9.4 years (min-max 5-12). Six of eight cats (75%) presented with dyspnea. Diagnoses in this group were: thymoma (n=4), lymphoma (n=3) and carcinoma (n=1). The final diagnosis was based on cytology (n=6), histopathology (n=1) and necropsy (n=1).

Accuracy of survey CT was 100% (8/8) and radiography 85.7% (6/7). The most common CT findings in this group were soft-tissue mass in the cranial mediastinum (7/8) that was homogeneous (3), cystic (3) or mixed soft-tissue and mineralized (1), pleural effusion (5/8) and lung lobe atelectasis (4/8). Additional information obtained with CT (6/7) included lung atelectasis (n=3) (Figure 14), and one cat each with pulmonary metastasis, sternal and cranial mediastinal lymphadenopathy, neck mass and lung mass.

Contrast CT was performed in four cats. Additional findings were cystic portions of the CMM (thymoma) and sternal and cranial mediastinal lymphadenopathy (thymoma) in one cat each.

Infection

Seven cats were included in this group, with a mean age of 5 years (min-max 0.17 – 11.5). Six of the seven cats (85.7%) presented with dyspnea. Diagnoses in this group were aspiration pneumonia (n=1), suppurative tracheitis with suppurative bronchitis (n=1), suppurative tracheitis and bronchopneumonia (n=1), lung abscess with pleuritis (n=1), suppurative bronchopneumonia secondary to *Bordetella bronchiseptica* (n=1), pyogranulomatous pneumonia with fibrosis (n=1), and suppurative inflammation (n=1). The final diagnosis was based on necropsy (4), histopathology (n=1), cytology (1) and response to therapy and follow-up (n=1).

Accuracy of survey CT was 28.6% (2/7) and radiography 14.3% (1/7). Additional correct diagnosis with survey CT (2/7) were pneumonia with tracheitis and tracheal and bronchial collapse and stenosis (Figures 15a and b) (n=1) and bronchitis with pneumonia (n=1). Radiography had an additional correct diagnosis of pneumonia in a cat with pyogranulomatous pneumonia and fibrosis.

The most common CT findings in this group were patchy alveolar pattern (4/7), one to multiple lung masses (3/7), mixed patchy and consolidated alveolar pattern (2/7), and sternal and cranial mediastinal lymphadenopathy (2/7). Additional information obtained with CT (5/7) included sternal and cranial mediastinal lymphadenopathy (n=2), and one cat each with tracheal and main stem bronchial wall thickening with stenosis and collapse, lung mass, hyperlucent lung and lung nodule.

The location and type of alveolar pattern was variable. A patchy alveolar pattern was seen both unilaterally (n=3) and bilaterally (n=2). Distribution was often seen concurrently in both cranioventral and caudodorsal lung fields (n=4). A consolidated alveolar pattern (n=3) was

seen most commonly bilaterally (n=2), with either cranioventral (n=1), caudodorsal (n=1) or both (n=1) distributions seen concurrently. Lung masses were located in left cranial lobe (n=1), left caudal lobe (n=1) or right middle and left caudal (n=1).

Contrast CT was performed in 3 cats, adding a correct diagnosis of pneumonia in the cat with pyogranulomatous pneumonia with fibrosis and additional information of sternal and cranial mediastinal lymphadenopathy in a cat with lung abscess and fibrinous pleuritis.

Trauma

Four cats were included in this group, with a mean age of 6.5 years (min-max 3-10). All cats presented with dyspnea. The diagnosis in this group included one cat each with: 1) human abuse causing liver rupture, hemoabdomen and pulmonary contusion, 2) tracheal rupture associated with endotracheal intubation (Figures 16a and b), 3) trapped inside a tumble clothes dryer, and 4) hit by a car.

Accuracy of survey CT was 75% (3/4) and radiography 0% (0/4). Additional correct diagnosis with survey CT (3/4) were trauma (n=2) and tracheal rupture (n=1). The CT findings in this group were variable and included one finding each of peritoneal effusion, pneumothorax, pneumomediastinum, pneumopericardium, rib fracture, bulla, and lung atelectasis. Additional information obtained with CT (4/4) were bulla (n=1), pulmonary contusion (n=1), lung atelectasis (n=1), rib fracture (n=1), discontinuity of tracheal wall (n=1), pneumopericardium (n=1) and lung nodules (n=1). No cats in this group had contrast CT.

Hernia

Three cats were included in this group, with a mean age of 8.3 years (min-max 2-16). Two cats presented dyspneic. Diagnosis in this group included one cat each with: 1) hiatal

hernia, 2) diaphragmatic hernia (Figure 17), and 3) peritoneal pericardial diaphragmatic hernia (PPDH) (Figure 18). The final diagnosis was based on repeated radiographic imaging (hiatal hernia), surgery (DH) and necropsy (PPDH).

Accuracy of survey CT was 66.7% (2/3) and radiography 50% (1/2). Additional correct diagnosis with survey CT (1/2) was diaphragmatic hernia; radiographically, this case was diagnosed as severe pleural effusion of unknown cause. Radiography did correctly diagnose the hiatal hernia.

The CT findings included: disruption of diaphragm (n=2), presence of liver, spleen and fat in the thoracic cavity (n=1), intestinal loops, liver and gallbladder inside the pericardium (n=1), large bulla lesion (n=1), among others. Additional information obtained with CT (1/2) included liver, spleen and fat in the thoracic cavity and disruption of diaphragm.

Contrast CT was performed in the two cats (DH and PPDH), but no different diagnosis or additional information were obtained.

Other

Five cats were included in this group, with a mean age of 6 years (min-max 1-10). Four cats presented with dyspnea. Diagnoses in this group included one cat each with lidocaine toxicity, chylothorax and fibrosing pleuritis, smoke inhalation, pulmonary edema secondary to fluid overload, and normal. The final diagnosis was based on necropsy (pulmonary edema), histopathology (chylothorax) and response to therapy and follow-up (n=3).

Accuracy of survey CT and radiography were both 60% (3/5). No additional correct diagnosis was obtained with either survey CT or radiography. The most common CT findings were patchy alveolar pattern (n=2), bronchial wall thickening (n=2), and one finding each of pneumothorax, pleural effusion, bronchiectasis, hyperlucent lung field. Additional information

obtained with CT (3/5) included: bronchial wall thickening (n=2), lung atelectasis (n=1), patchy alveolar pattern (n=1) hyperlucent lung (n=1) and bronchiectasis (n=1).

Contrast CT was performed in two cats. No additional diagnosis or additional findings were obtained.

4.4 Discussion

A common clinical conundrum is the need to image a clinically unstable patient.[47, 63-65] One of the goals of this study was to describe CT imaging in cats with thoracic disease without the use of sedation or general anesthesia using the VetMouseTrap™. Cats in this study had CT imaging without any complications, including cats with dyspnea. The VetMouseTrap™ provided the environment for imaging without general anesthesia or sedation and allowed constant oxygen and fluid administration throughout the procedure. Computed tomography had very high accuracy, providing a correct diagnosis in 77.8% (42/54) of the cases, while radiography achieved a correct diagnosis in only 58% (29/50). Additional information was obtained with CT in 76% (38/50) of the cases.

In humans, CT has revolutionized the imaging work-up of patients in the emergency department and is now considered to be one of the most valuable imaging tools for trauma patients and patients with non-traumatic emergency conditions. Helical CT offers several advantages for emergency patients: 1) respiratory misregistration due to variations in the depth of inspiration on successive breath holds is essentially eliminated, which decreases the chance of overlooking small injuries; 2) shorter scanning time permits better intravenous contrast media opacification, and 3) improved contrast enhancement of parenchymal organs and multiple consecutive CT examinations on the same patient in a very short period of time.[2]

Survey thoracic radiography is the historical standard for imaging the thorax in veterinary medicine. However, radiography is limited in animals with severe pleural effusion in which the underlying disease can be hidden due to border effacement caused by the fluid.[3, 9, 67-70] Although CT has many advantages over radiography, the need for general anesthesia limits this modality in many unstable animals, including those with dyspnea. Computed tomography using the

VetMouseTrap™ is particularly useful because dyspneic cats can become extremely stressed when handled and restrained for radiographic examination.[62] Four cats in the present study were not considered stable enough to be submitted to a complete thoracic radiography study, but CT was successfully obtained in all cats with no signs of overt stress. This finding was in agreement with a previous study of CT of normal awake cats using the VetMouseTrap™ in which 20 of 22 cats were imaged successfully with no signs of stress.

The most common CT finding of cats with primary lung cancer in the present study was a lung mass (7/8). In a previous CT study in four cats with bronchial adenocarcinoma and one cat with lung metastasis, lung mass was the second most common finding (n=3).[4] In the present study, four cats had a lung mass identified by CT that were not seen radiographically, and in no case was a mass seen radiographically and not identified with CT. Conventional radiography has been reported as an useful imaging modality for identifying thoracic masses, although less useful for differentiating pulmonary, mediastinal or thoracic wall in origin, and for localizing a pulmonary mass to a specific lung lobe.[71]This was not the case in the present study, as a large number of pulmonary masses were not identified with radiography. There are few descriptions of the radiographic appearance of primary lung neoplasia in cats. In one study, pulmonary adenocarcinoma most often appeared as a well-circumscribed and usually cavitated mass in the middle or peripheral portion of the affected lobe, or as a localized alveolar pulmonary infiltrate which was often calcified. Pleural and regional lymph node involvement was more commonly seen with the latter form.[72] Another study describes solitary nodules of one to several centimeters in diameter as the most common radiographic appearance of primary tumors, followed by multiple nodular lesions and disseminated alveolar-interstitial and peribronchial pattern; however, a distinction between the appearance of the tumors in dogs versus cats is not made on

that study.[73] Computed tomographic descriptions of primary lung tumors in cats are even more scarce. To the knowledge of the authors, there is only one study describing the CT appearance in 4 cats with bronchial adenocarcinoma and one cat with lung metastasis, with the most common finding in the first 4 cats being the presence of a lung mass (n= 3) and bilateral or right bronchial lymph node enlargement (n = 4).[4] In three cats with primary lung neoplasia CT detected soft-tissue pulmonary nodules not seen radiographically, which was not unexpected. Computed tomography has been found to be more accurate than thoracic radiography for the detection of pulmonary nodules in human medicine for many years.[14] The improved sensitivity of CT compared with thoracic radiography for detecting pulmonary metastases is due primarily to the superior contrast resolution of CT and the lack of anatomic superimposition on pulmonary parenchyma due to thin-section collimation of CT images. However, the specificity of CT for detecting pulmonary metastatic nodules can be lower than that of thoracic radiography because more small, non-neoplastic, and clinically insignificant nodules are likely to be identified.[14]

None of the 8 cats with primary lung neoplasia in the current study were thought to have thoracic lymphadenopathy with either radiography or survey CT; however, thoracic lymphadenopathy was seen in 5 cats with primary lung carcinoma on contrast CT examinations. This is consistent with previous studies reporting the radiographic and necropsy findings in cats with primary lung tumor, in which thoracic lymphadenopathy is described in a large number of cats and is thought to be the second most common extra pulmonary lesion observed, with pleural effusion being the most common.[72-74] This is also consistent with the previous CT study in cats with bronchial adenocarcinoma and lung metastasis in which bilateral or right bronchial lymph node enlargement were the most common finding (n=4).[4] The reason for not finding lymphadenopathy in these cats during the image evaluation on this study could have been the

absence of contrast CT images or absence of MPR images for interpretation. The visualization of thoracic lymphadenopathy with CT in the present study was possible due to differential attenuation between lymph nodes and surrounding mediastinal fat or pleural effusion. Administration of contrast medium facilitated the diagnosis since all enlarged lymph nodes exhibited some degree of contrast-enhancement. Administering contrast media may be especially important in cats with lung masses, since the presence of thoracic lymphadenopathy is an important prognostic information and it was found in a large number of cats with primary lung neoplasia in the present study.

To the knowledge of the authors this is the first CT study to describe cats with lower airway disease. This report also describes emphysema, bronchiectasis, and tracheal and main stem bronchi stenosis in cats with lower airway disease. Computed tomography had a much higher accuracy for lower airway disease (88.9%) compared to radiography (50%). Diffuse bronchial wall thickening was the most common CT and radiographic finding which is in accordance with the literature.[75, 76] Substantial cellular and architectural changes must occur for pulmonary changes to be radiographically evident in patients with lower airway disease.[71] These changes usually include hyperplasia of the bronchial glands, bronchial wall cellular infiltration, hypertrophy of the bronchial smooth muscles and bronchiectasis. Feline lower airway disease may appear normal radiographically in as many as 23% of cats.[62, 70, 71, 75, 77-80] One third of the cats (3/9) in the present study had a normal radiographic appearance. Computed tomographic findings consistent with asthma in humans include bronchial wall thickening, expiratory air trapping, inspiratory decreased attenuation, and ground glass opacities.[81] Human patients with asthma also show a varying prevalence of emphysematous changes ranging from 15 to 39% in some studies and up to 80% in other studies.[82, 83] Emphysema in humans is well demonstrated

using CT, is known to increase with age and smoking history, and is considered to be an irreversible abnormality in asthma.[82] Subjective descriptions of CT appearances of emphysema include areas of non-peripheral and peripheral low attenuation, pulmonary vascular pruning and distortion, vascular disruption, or obvious bullae.[83]

In the present study hyperlucency diagnosed as emphysema was seen in 44% (4/9) of cats with lower airway disease with CT and in no case with radiography. Retrospective evaluation of lung regions subjectively graded as hyperlucent in all cats with lower airway disease in the present study demonstrated lung densities of less than -900 HU. These areas would be considered emphysema in human CT studies, although no histological correlation was available in any of these cats. Emphysema in cats with lower airway disease have been indicated as a poor prognostic factor and studies are needed to determine the prevalence and characterize the CT appearance of emphysema in cats with lower airway disease.[76]

Three cats in the lower airway group had a patchy alveolar pattern attributed to pneumonia. In previous reports bacterial infections were thought to be uncommon in cats with lower airway disease.[84] Positive bacterial cultures were reported in 25% to 33% of cats with lower airway disease but the significance of such findings was not well determined.[76] *Mycoplasma spp* was previously isolated from cats with signs of lower airway disease and treatment with antibiotics in these cases have been recommended.[84]

Bronchiectasis was detected with CT in four cats and not noted radiographically. Destruction of the bronchial epithelium and cilia and accumulation of secretions in the distal airways that occurs with bronchiectasis predisposes patients to secondary infections. In cats, bronchiectasis has not been reported as common sequella to lower airway disease, but previous studies either used thoracic radiographic as the diagnostic method or were retrospective in nature

and evaluated only cats with a previously established diagnosis of bronchiectasis.[75, 85] In humans, bronchial dilation is reported to occur in up to 80% of patients with asthma and high-resolution computed tomography is superior to bronchography for the evaluation of patients with both bronchiectasis and small-airway disease.[81, 86] Results of the present study suggest that bronchiectasis may be underestimated in cat with lower airway disease.

Tracheal (n=2) and mainstem bronchial (n=3) wall thickening resulting in stenosis was seen on survey CT in 3 cats as evidenced by symmetrical (round) narrowing of the tracheal lumen. These were 2 cats in lower airway disease group and one cat in the infection group. The latter also had tracheal collapse as evidenced by asymmetrical narrowing (U-shaped) of the tracheal lumen. Two of these cats had necropsy and both had findings consistent with tracheitis and bronchitis (one cat from each group). One of these cats was very young (2 months) and thought to have virus infection. This was the only cat for which radiography detected tracheal thickening. In humans, tracheal obstruction, including diffuse or long segment tracheal narrowing is considered a mimic of asthma and the tracheal abnormality is usually diagnosed in thoracic radiographs.[87] We found no studies reporting the presence of tracheal or main stem bronchi collapse thickening or stenosis with concurrent lower airway disease.

Computed tomography had high accuracy in cardiomyopathy and congestive heart failure in cats in this study. This may be important when a confident diagnosis cannot be made radiographically or for patients that are considered unstable for echocardiographic examination. The fact that CT using the VetMouseTrap™ can be performed in awake cats and that highly accurate results were obtained in the absence of contrast administration in this study make CT feasible for dyspneic cats and those for which contrast is contraindicated, including dehydration and anuric renal failure.

Pleural effusion was seen in a large number of cats in this group but was not a limiting factor for CT in evaluating the size and shape of the cardiac silhouette. In the 3 cats with pleural effusion for which radiography was able to detect cardiomegaly, the effusion was graded as mild and this could have been the reason for radiography being able to detect cardiomegaly in this cats.

Another finding of the study was that it was often possible to identify specific cardiac chambers even without contrast administration and cardiomegaly could be readily assessed on the transverse CT images of 8 out of 9 cats in this group. A potential great advantage of CT, although not evaluated in this study, is that fat and pericardial fluid should be easily differentiated from soft-tissue which can make the evaluation of heart size in obese cats and cats with pericardial effusion easier and more accurate than with radiography. A previous study showed that identifying the true cardiac silhouette specially in VD views of obese cats is difficult and can lead to overestimation of cardiac size.[88] Computed tomography can be advantageous in evaluating heart particularly in obese cats in which the cardiac size is difficult to evaluate radiographically, and in cats with congestive heart failure considering that feline cardiogenic pulmonary edema has a variable radiographic appearance making its diagnosis difficult.[65] Furthermore, pulmonary edema must be differentiated from bronchopneumonia and from chronic lower airway disease in cats with bronchial or bronchointerstitial patterns which can be difficult radiographically since pulmonary edema tends to obscure the heart and pulmonary vessels making their radiographic evaluation difficult.[65]

The finding of pleural effusion in seven cats and patchy alveolar pattern in six cats with congestive heart failure is consistent with previous reports. In a study of 23 cats with congestive heart failure, the radiographic appearance of the lung was characterized by an increased opacity

associated with a range of mixed patterns and variable distribution. All cats had evidence of an unstructured interstitial pattern that reduced clarity of margins of the pulmonary vessels and cardiac silhouette. The distribution of pulmonary edema was reported to be diffuse/non-uniform in 61% of cats.[65] Common radiographic findings in 106 cats with feline idiopathic cardiomyopathy were generalized cardiomegaly (67% of the cats), pleural effusion, (29.2%), and pulmonary edema (26.4%). Specific description of the pulmonary pattern associated with the diagnosis of pulmonary edema was not made in this study.[89]

The major advantage of CT imaging of cats with mediastinal masses in the current study was providing additional information, since radiography allowed a correct diagnosis in all but one case. Although no studies evaluating the accuracy of radiography for diagnosing CMM are available, it is reported that most of them can be diagnosed radiographically and the specific location of this masses provides helpful information for formulating differential diagnoses.[7, 71, 90-92] Limitations of radiography in diagnosing CMM include the presence of large amounts of pleural effusion.[5, 67, 68] Because most masses can be diagnosed radiographically, the primary role of CT in the assessment of cranial mediastinal masses is usually to determine invasiveness, particularly regarding vital regional vasculature for which the use of contrast is fundamental.[7, 93]

Cats in the infection group had the lowest number of correct diagnosis achieved by CT (3/7 cats), which could be explained by the common finding of one or multiple lung masses in cats in this group, which was commonly misdiagnosed by CT as being primary lung neoplasia. The differentiation of inflammatory alveolar disease from neoplastic lung mass using CT has not been extensively studied in veterinary medicine. In one study of the use of CT to distinguish a pulmonary mass from alveolar disease the authors did not explain how CT reached a diagnosis of a lung mass other than mentioning the "mass-like appearance" of the lesion.[38] In humans,

diagnosis of pneumonia requires a combination of clinical assessment, radiological imaging, and appropriate microbiological tests. Computed tomography is a valuable adjunct in negative or non-diagnostic thoracic radiography, unresolved pneumonias, and when complications are suspected.[94-96] Findings vary according to the classification and include airspace nodules, lobular opacity, airspace consolidation, ground glass opacities, air bronchograms, interlobular septal thickening and centrilobular or perilobular nodules.[96-98]

Only one study describing the CT findings in a cat with pneumonia was found. This was a case report of a cat with primary Mycoplasma pneumonia associated with respiratory failure in which the CT findings included pleural effusion, subcutaneous emphysema, pneumomediastinum, ground glass attenuation, patchy reticular and ill-defined nodular opacities and patchy regions of air space consolidation. Pneumomediastinum and subcutaneous emphysema were believed to be due to ruptured alveoli or bronchioles with subsequent dissection of air into the mediastinum and along fascial planes.[99] Pleural effusion is not a common finding in cats or dogs with pneumonia and was not found in the current study in cats in this category. Thoracic lymphadenopathy was found with CT in only one cat in this group, diagnosed with suppurative tracheitis and bronchopneumonia.

Although we had a low number of cats (n=4) in the trauma group, the high accuracy of CT in this group indicates that it can be an important imaging modality in the assessment of the trauma patient. The fast, low morbidity acquisition of whole-body images of awake cats allowed CT to be performed in traumatic patients without the risks of general anesthesia or sedation. All cats received supportive treatment, including intravenous fluid and oxygen as clinically indicated, throughout the CT procedure. The incidence of thoracic injury in feline trauma patients varies between 11% and 90%.[100] There are several reports that describe radiographic

findings in dogs and cats with blunt trauma, including injuries seen in canine and feline high-rise syndrome and pulmonary injuries in dogs with fractures as a result of motor vehicle accidents.[47] To the knowledge of the authors, no studies reporting the use of CT to evaluate thoracic injury in cats or dogs with trauma are available and we believe this could be the result of the need of general anesthesia to perform CT. In humans, although thoracic radiography is the primary imaging tool in evaluating patients with thoracic trauma, previous studies have indicated a low sensitivity of chest radiography in the detection of lung injuries in thoracic traumas. Pathologies can be overlooked because of blind spots, like areas neighboring the diaphragm, or retrocardiac and paraspinal regions. Motion artifacts are common in traumatic patients, thus increasing the difficulty of evaluating radiographic images. Furthermore radiography is not reported to be sensitive in the differentiation of contusion, hemorrhage, laceration, hematoma, atelectasis, and hemothorax.[101] Computed tomography is considered superior to routine radiography in detection of lung contusions, pneumothorax, and hemothorax after blunt chest trauma. Computed tomography has also been shown to positively influence therapeutic management in severely injured patients when performed early in management of the case.[102] Therefore, CT evaluation of patients with severe thoracic trauma is believed to be beneficial for diagnosis and treatment planning and is recommended by some authors in the initial diagnostic work-up of patients with multiple injuries and with suspected chest trauma.[101, 102]

CT imaging for the diagnosis of tracheal rupture in a cat has been reported but this is the first report of tracheal rupture detected by CT in an awake cat. The imaging findings were similar to those of the present study, including severe sub-cutaneous emphysema and pneumomediastinum and tracheal tear, detected only with CT in both studies.[103] In the present study no endotracheal tube was placed for CT examination which made evaluation of the trachea

optimal. Tracheal rupture in cats is usually associated with a history of inhalation anesthesia requiring endotracheal intubation with subsequent development of subcutaneous emphysema. Possible explanations include over inflation of the endotracheal tube cuff, change of the cat's recumbent position without proper disconnection of the endotracheal tube from the anesthetic machine, traumatic intubation with a stylet, type of endotracheal tube used, and removal of the endotracheal tube without deflation of the cuff. Subcutaneous emphysema is a consistent clinical sign in these cats because air dissects along connective tissue planes in the cervical area surrounding the trachea, and travels into the mediastinum causing pneumomediastinum. Pneumothorax may develop if pressure is high enough to rupture the mediastinum. Unless confirmed by surgery or tracheoscopy, the diagnosis is usually presumptive, based on the history of recent intubation or recent cervical or thoracic trauma, with the subsequent development of subcutaneous emphysema.[104] Tracheoscopy is reported in some studies to provide an effective means of diagnosing tracheal defects, and in others to be unsuccessful in diagnosing tracheal tears in cats.[103, 104]Computed tomography has been used as a modality to diagnose tracheal tear in humans. The advantages of CT over conventional diagnostic techniques for tracheal evaluation are its ability to provide the location and extent (cervical, intrathoracic, or both) of the tracheal tear, to define and differentiate soft-tissue structures, and to provide secondary reconstructions of extra planes that may help to determine the length of the tear.[103]

The cat with smoke inhalation had pulmonary changes detected on CT and not detected radiographically such as patchy alveolar pattern, emphysema, bronchiectasis and bronchial wall thickening. Smoke inhalation is not very common in dogs and cats. Despite the commonly reported occurrence of fires in United States, only an extremely small percentage of dogs and cats are reported to present to veterinary emergency rooms due to smoking inhalation.[105] Signs of

smoke inhalation may be nonspecific and include cough, dyspnea, tachycardia, tachypnea, and hypoxemia. Almost always signs of conjunctivitis, pharyngitis, and rhinitis are present. Erythema, edema, and soot may be evident on examination of the nose, mouth, and throat. Corneal abrasions are common, and exposure to fire or prolonged heat can produce corneal burns. Mucosal ulcerations and hemorrhagic areas may be present. Signs of laryngotracheal involvement and injury such as drooling, dysphagia, hoarseness, and stridor can be present.[105] Chest radiographs are most commonly normal at the time of and for the first few hours following smoke inhalation. Thus early radiographs are another inaccurate predictor of pulmonary injury. Within 24 to 36 hours of exposure, radiographic changes ranging from patchy atelectasis to diffuse interstitial and alveolar involvement may be evident. Subtle radiographic findings within the first 24 hours of exposure can include perivascular haziness, peribronchial cuffing, bronchial wall thickening, and subglottic edema. The hallmark pulmonary injuries secondary to smoke inhalation usually develop more than 24 hours later and can include acute lung injury, aspiration, infection, volume overload, respiratory distress, and cardiogenic pulmonary edema.[105] In the case we present, CT detected pulmonary changes not seen radiographically therefore it is possible that CT can detect changes earlier than radiographs but future studies with a larger number of cases are required to confirm this.

Computed tomography allowed the diagnosis of hernia in 2 cases, diaphragmatic and peritoneopericardial diaphragmatic hernia (PPDH), the first not reached with radiography and the second in a cat that was not stable enough for radiographic examination. In dogs and cats, diaphragmatic hernia often develops as a result of vehicular or other blunt abdominal trauma. The sudden increase in abdominal pressure at impact is dissipated cranially, resulting in disruption of the diaphragm.[106] Dyspnea was the most frequently reported clinical sign among

dogs (26/63, 41.3%) and cats (21/29, 72.4%) in one study, and present in 38% of the cases in another one.[107, 108] Acute traumatic diaphragmatic hernias may escape detection because owners may be unaware that a traumatic incident has occurred, the condition may be asymptomatic, and a definitive radiographic diagnosis can be difficult to establish.[108] Radiographic diagnosis is the most important diagnostic method of detecting diaphragmatic hernia in dogs and cats nowadays, although it is not always easy to identify diagnostic radiographic signs. Loss of diaphragmatic line and cardiac shadow, increased intrathoracic density, abdominal gas shadow in thorax and empty and wasp-shaped abdomen are characteristic radiographic signs.[109] The presence of pleural effusion or herniation of relatively small volumes of abdominal contents can make diaphragmatic hernias difficult to recognize on thoracic radiographs, particularly if the herniated structures are not gas filled.[108] In one study of chronic diaphragmatic hernia in 34 dogs and 16 cats, approximately one-third of the hernias could not be conclusively demonstrated with thoracic radiography.[108] In the present study radiography detected severe pleural effusion in the cat with DH and the reason could not be determined. The pleural effusion was not confirmed with CT. Other imaging modalities reported for diagnosing DH include upper gastrointestinal (GI) contrast studies, positive-contrast celiography, and ultrasonography, but any of these can be inconclusive and more than one technique may be necessary to confirm the diagnosis.[108]No studies were found of the use of CT to diagnose DH in awake or anesthetized cats.

In the PPDH case, CT allowed a correct diagnosis by direct visualization of gas distended loops of small intestines, part of a liver lobe and the gallbladder inside the pericardium. Peritoneopericardial diaphragmatic hernia occurs when an abnormal communication between the pericardial sac and the peritoneal cavity develops. In dogs and cats, PPDH is solely the result of congenital anomalies since in these species the pericardium and diaphragm are not connected as

in humans, therefore, PPDH as a result of trauma does not occur.[110] Several theories regarding the pathogenesis of PPDH have been proposed; most suggest failure of normal development of the septum transversum, the embryologic structure that forms the ventral portion of the diaphragm.[110] One theory proposes that there is failure in closure of the septum transversum itself, and another proposes that there is failure of fusion of the septum transversum and the pleuroperitoneal folds (the embryologic structures that form the dorsolateral portion of the diaphragm).[110, 111] Radiographic findings of an enlarged cardiac silhouette with loss of visualization of the cranial margins of the diaphragm and cranial shift of abdominal viscera indicate possible PPDH. Abnormal double radiographic cardiac density of soft tissue-gas or soft tissue-fat has been reported. Sonographic evaluation of PPDH may reveal abdominal viscera within the pericardial sac or demonstrate pericardial effusion. Disruption of the diaphragm also supports the diagnosis of herniation. Other tests used to confirm the diagnosis of PPDH include pericardiography, pneumoperitoneography, thoracic tomography, and gastrointestinal contrast studies.[112] The use of CT to diagnose diaphragmatic hernia as well as PPDH in dogs and cats has not been extensively described in veterinary medicine. In the present study, CT allowed promptly identification of both hernias as the presence of abdominal organs such as the liver and spleen and fat inside the thoracic cavity in the case of diaphragmatic hernia, and the presence of small intestinal loops inside the pericardium could be easily seen with CT. These findings are expected considering the superior contrast resolution of CT and the elimination of superimposition with this imaging modality which makes the organs easily to discern and the presence of pleural effusion not to be a major limitation such as with radiography.

Radiography provided a correct diagnosis in the cat with hiatal hernia and this could have been due to the dynamic nature of hiatal hernias since a time difference of four hours between

the two modalities ocurred. A hiatal hernia is defined as an axial displacement of the abdominal part of the esophagus, the esophagogastric junction and/or part of the stomach through the esophageal hiatus of the diaphragm into the thoracic cavity. This condition can be congenital or acquired (mostly older animals) and is rare in dogs and very rare in cats. The most common form is the sliding hiatal hernia which is usually intermittent and can therefore be missed on a single radiographic examination. Another less common form is the paraesophageal hiatal hernia, in which part of the stomach protrudes into the thoracic cavity parallel to the distal esophagus.[113] Radiographs may show an oval homogeneous opacity in the caudal thorax just dorsal to the caudal vena cava. On the ventrodorsal view the opacity is situated in the midline in the caudal mediastinum.[113, 114] Foreign-body obstruction, esophageal neoplasia, or gastro-esophageal intussusception are considered likely differentials.[115] The radiographic findings in the cat in the present study were characteristic for hiatal hernia with a soft-tissue opaque mass present in the caudal thorax in only one lateral view and seen at midline on the VD view. At the time of CT, the esophagus was generalized and mildly gas distended but with no soft-tissue opacity within it which could have made the diagnosis difficult.

Computed tomography provide additional information in the majority of cases in the present study however when comparing imaging modalities, it is important to distinguish the demonstration of new information with the demonstration of clinically important information, or information that could directly change the clinical management of a case. In a human study of the use of CT in the intensive unit care, thoracic radiography detected only 232 of the 482 findings detected with CT, but the majority of the additional CT findings had little clinical importance. These included small amounts of pleural effusion or pneumothorax and minor lung lobe atelectasis, which accounted for 51% of the additional findings.[66] Similarly in the present

study, CT detected several non important findings, such as mild pneumothorax not seen radiographically and presumed to be secondary to thoracocentesis, lung lobe atelectasis, pulmonary nodules in cats already determined to have primary lung neoplasia with pleural metastasis, and bronchitis in cats with a final diagnosis of a different disease, for which this finding was unlikely to have been responsible for the clinical signs presented by the cat or altered the management of the case. Therefore, it is important to find a justification for performing CT in both human and veterinary patients, given the radiation and money concern that this imaging modality represents. In the same previous human study, despite the large number of non important findings, it was found that 72% of the CT examinations demonstrated clinically important information and the CT findings led to a direct change in clinical management in 22% of patients evaluated.[66] In a more recent study of 64 critically ill patients that underwent 82 CT examinations, 85% of the examinations provided information that significantly contributed to clinical decision-making in the treatment of critically ill patients. From these, 61% (50/82) of the examinations resulted in a new treatment intervention.[116] In the present study, additional CT findings were of clinical importance in 40% (20/50) of the cases, by either leading to a different diagnosis or adding important information, such as the presence of metastasis. The main reason for performing most of the CT studies without administration of contrast medium was for fastest, lowest morbidity imaging of cats presented in emergency conditions. In the present study none of the 19 cats receiving contrast showed signs of reactions; however the cats were not specifically monitored for subacute or chronic changes. Additional diagnoses were only reached in 2 of 17 cats with additional contrast CT.

In the current study thoracic CT had better accuracy and provided additional clinically useful information than radiography. This is consistent with previous studies of thoracic CT in

dogs and cats under general anesthesia and humans. [3, 5-7, 9, 66] In one study evaluating the use of radiography in combination with CT for assessment of noncardiac thoracic disease in 28 dogs and 5 cats, CT provided additional information in all but 4 dogs. Based on the CT findings, the imaging diagnosis was changed in 3/5 cats and 13/28 dogs.[5] In another study on 9 dogs and one cat, CT permitted visualization and localization of pulmonary lesions not seen radiographically in 4 cases.[3]

Presence and degree of pleural effusion, peritoneal effusion, pneumomediastinum, mediastinal mass, and pneumothorax had a substantial agreement between radiography and CT. This was unexpected, particularly for the degree of effusion. CT was expected to have a higher sensitivity in detecting mild degrees of pleural lesions. Radiographs are more sensitive than anticipated in detecting pleural and peritoneal effusion, but a larger number of cases should be evaluated before definitive conclusions can be drawn. Although radiography could detect with accuracy the presence and degree of pleural effusion, evaluating underlying disease in this cases can be limited with radiography. This was evident in this study as the presence of pleural effusion was the most common reason for indeterminate findings, including mediastinal lymphadenopathy or masses, cardiomegaly and diaphragmatic rupture. Border effacement is a major limitation of radiographic studies that does not occur with CT due to its higher low contrast resolution. Computed tomography has much higher low-contrast resolution allowing identification of density differences between tissues of about 0.5%, while radiography requires density differences of about 10%.[117] In the present study the majority of cats with pleural effusion were in one of the following 3 groups: cardiomyopathy, mediastinal mass or lung neoplasia. In these groups some of the additional information obtained with CT could have been due to the presence of pleural effusion that made the radiographic diagnosis of such findings

difficult. In some cats, such as in 2 cats with cardiomyopathy, the additional finding with CT of cardiomegaly made the diagnosis of cardiomyopathy possible with this modality but not with radiography. In the cat with diaphragmatic hernia, abdominal organs and fat could be seen in the thoracic cavity with CT allowing the correct diagnosis not achieved radiographically. A severe amount of pleural effusion was diagnosed with radiography in this cat and no pleural free fluid was noted on CT.

The majority of cats in this study presented with dyspnea and this was statistically significant. Dyspnea is most often caused by hypoxemia secondary to cardiovascular or respiratory disorders. Hypoxemia in turn is caused by hypoventilation, diffusion impairment, ventilation-perfusion mismatch, or right-to-left shunting of blood.[62] Feline dyspnea can be due to upper or lower airway disease, pulmonary parenchymal disease, pleural, mediastinal or cardiac diseases, thoracic damage and extra-thoracic diseases.[63] The various causes can dictate different therapies and prognoses, but sometimes can result in similar clinical signs and radiographic appearance. Some conditions such as asthma or hypertrophic cardiomyopathy can appear radiographically normal.[69,70,89] Furthermore, common emergency treatments for some underlying causes of dyspnea can be detrimental if used innapropriety. Corticosteroids, commonly used in the treatment of feline asthma can cause decompensation in the presence of hypertrophic cardiomyopathy leading to congestive heart failure due to plasma volume expansion.[118, 119] This highlights the importance of achieving an accurate and fast diagnosis in cats presented with dyspnea in which case CT can play an important role as demonstrated in the study. Inadequate positioning in 8 of the 50 radiographic studies can be explained by the fact that some cats are less compliant during restraint. Dyspneic cats are less tolerant to handling. The majority of inadequate positioning occurred on VD views which are usually harder to obtain than lateral

views. Positioning was considered adequate in all CT studies confirming the hypothesis that diagnostic CT imaging is feasible in awake cats. With a multi-slice helical CT machine it is possible to reconstruct the images in any desirable plane with similar resolution to the original plane and obliquity can be corrected to some extent during the reconstruction process. The temperament of cats in general also contributes for CT being feasible in this species without the use of sedation or general anesthesia. Cats placed inside the VetMouseTrap^{TM} tended remain in sternal recumbence with minimal to no body movement. Minimal motion artifact was commonly noted when scanning awake cats. This finding was only detected in a small number of CT slices in affected image sets and did not impair imaging evaluation in any case.

The current study had some limitations. Although an overall relatively large number of cats were evaluated, the number of cats in each category of disease was small. Several CT findings and diagnosis are being described for the first time. Future studies using a larger number of cats of each specific disease are necessary before definitive conclusions can be drawn. Thirteen cats had a final diagnosis based on history, response to therapy and follow-up. Most of these cats were in the lower airway disease, trauma or other groups and responded well to medical therapy. In such cases, obtaining a final diagnosis by the means of an invasive test is usually difficult.

In conclusion, results of this study indicate that survey CT is highly accurate (77.8%) for the evaluation of cats with respiratory distress. CT provided additional information in 76% of the cats allowing a correct diagnosis not achieved with radiographs in 28% of cats. Radiography only provided the correct diagnosis in 58% of the cases. CT imaging of cats using the VetMouseTrap^{TM} without general anesthesia or sedation is safe and provides more accurate diagnostic information than radiography.

Footnotes

[*] LightSpeed 16, GE Healthcare, Waukesha, WI

[†] Iohexol, Omnipaque, GE Healthcare, Waukesha, WI

[‡] Carestream Health, Rochester, NY

[§] MedCalc Software, Mariakerke, Belgium; SPSS, IBM Company, Chicago, IL

4.5 Figures

Figure 7. Transverse survey CT image of the cranial thorax of a cat with metastatic lymphoma. Note enlarged sternal lymph node (arrow) and pleural effusion (asterisk). Window width = 400, window level = 40.

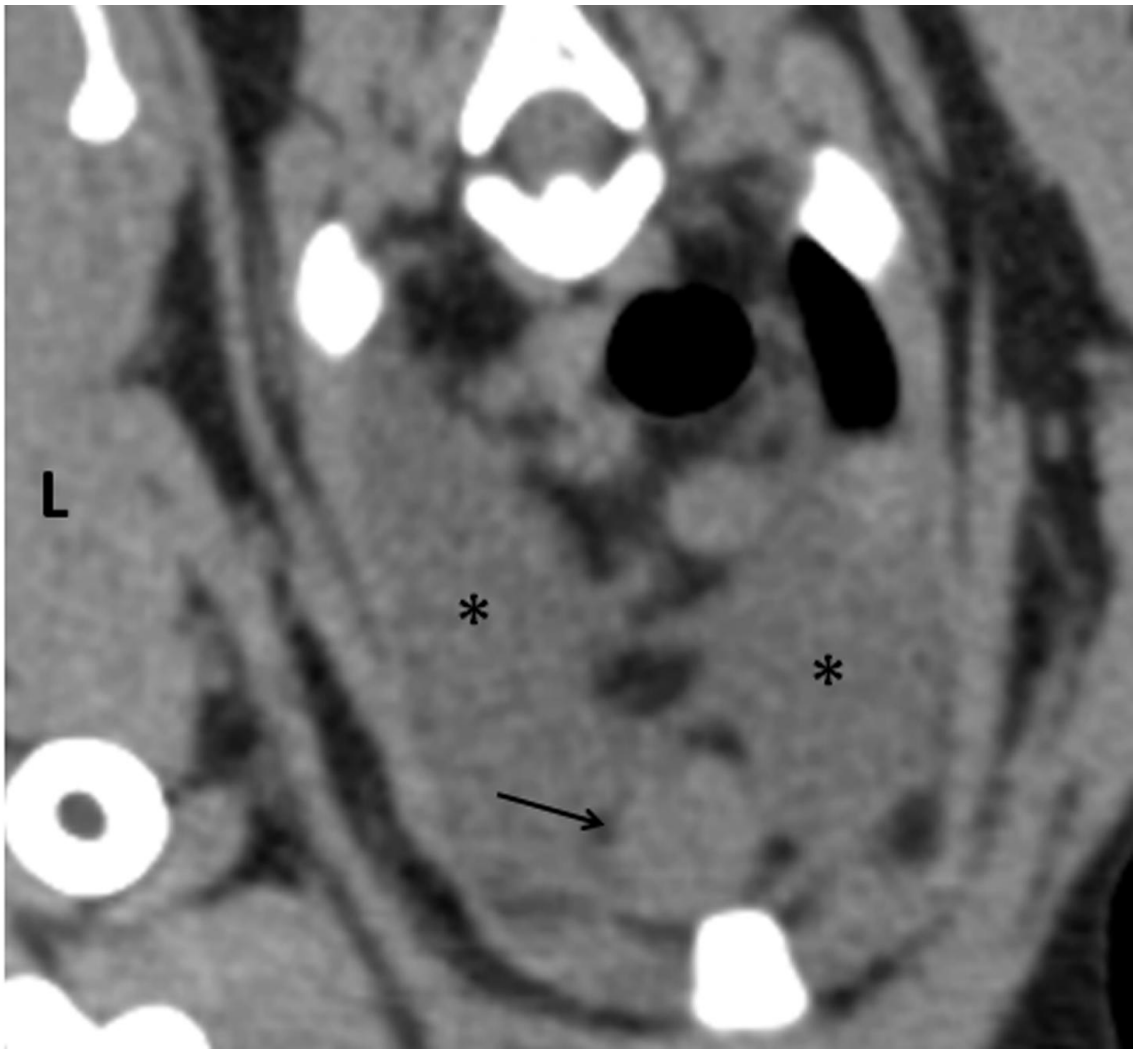

Figure 8. Transverse survey CT image of the caudal thorax of a cat with a cytological diagnosis of pulmonary carcinoma showing a soft-tissue attenuating mass in the left caudal lung lobe (arrow) and pneumothorax (long arrow) not seen radiographically. Note also cavitary mass in the right caudal lung lobe (thick arrow) and pleural effusion (asterisk). Window width = 1600, window level = -600.

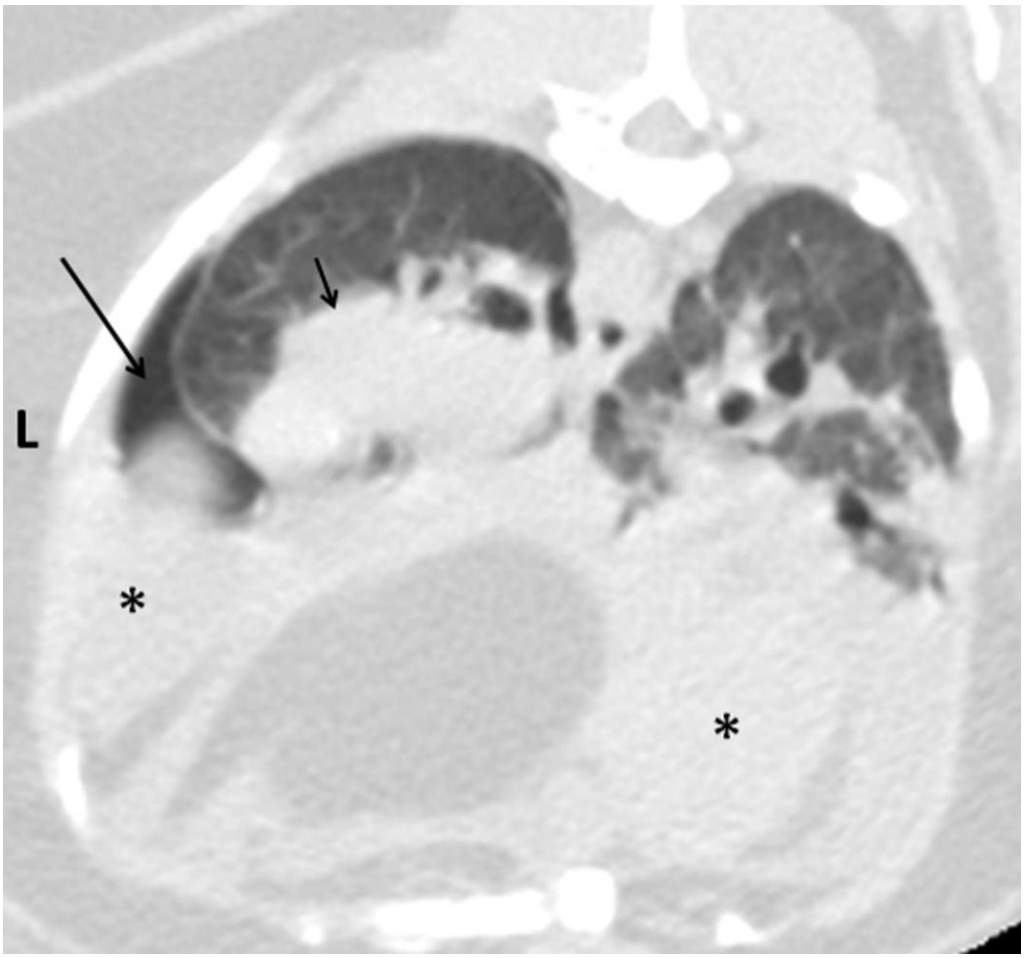

Figures 9a and b. Transverse survey CT images of mid (a) and caudal (b) thorax of two cats with lower airway disease. WW = 1600, WL = -600.

Figure 9a. Note severe diffuse bronchial wall thickening (arrow) and hyperlucent lung field (long arrow).

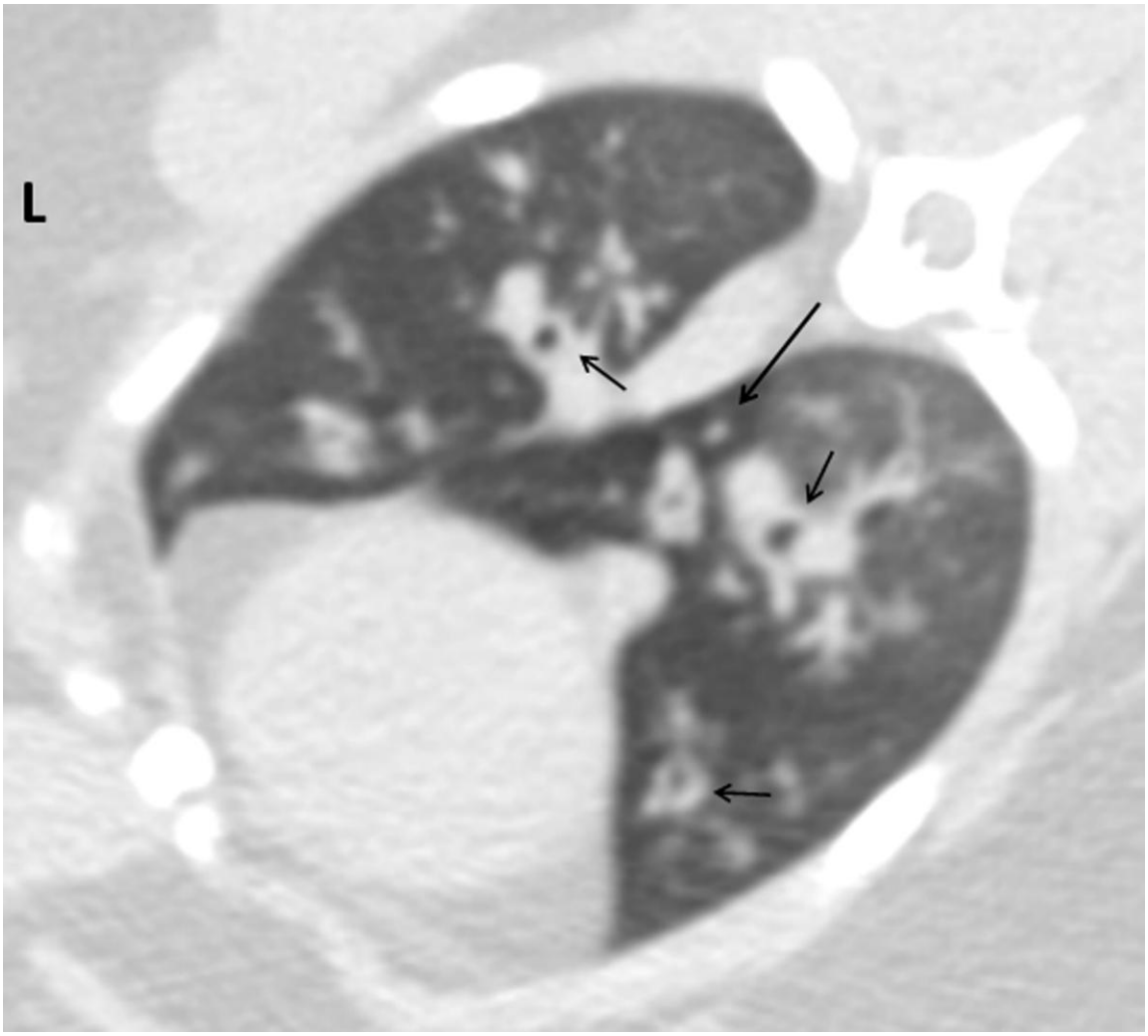

Figure 9b. Note bronchial dilation at the lung periphery (arrow).

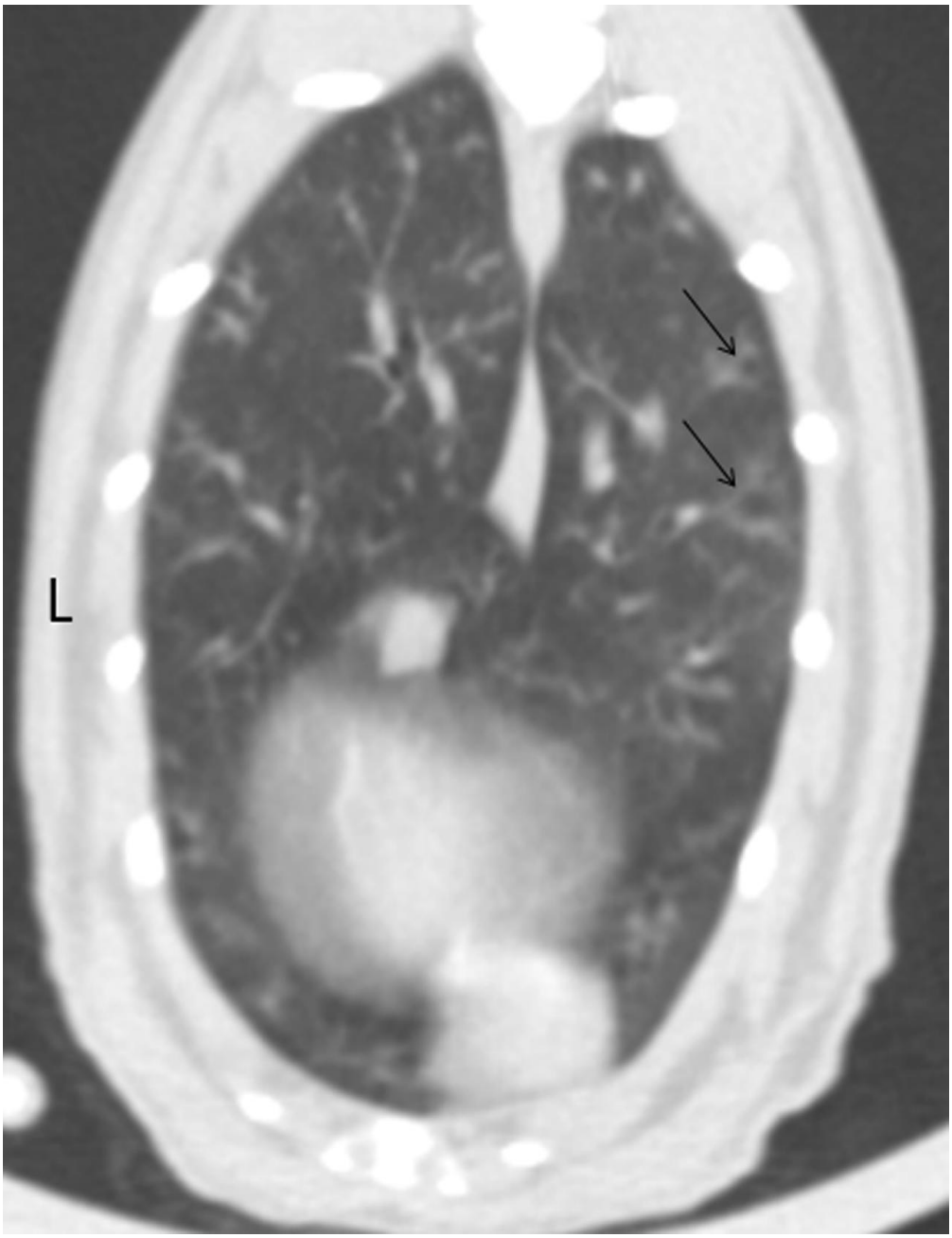

Figures 10a and b. Transverse CT images of the cranial thorax of cat with lower airway disease. Window width = 1600, window level = -600.

Figure 10a. Note tracheal stenosis (arrow); diameter = 2.9 mm (compared with 6.7 mm cranially and 5.9 mm caudally).

Figure 10b. Note severe bilateral mainstem bronchi stenosis (arrows); diameter = 1.7 mm.

Figures 11a and b. Survey CT images of two cats with cardiomyopathy. WW = 400, WL = 40.

Figure 11a. Transverse survey CT image of cat with arrythmogenic right ventricular cardiomyopathy and congestive heart failure. Note severely enlarged right atrium (asterisk).

Figure 11b. Dorsal survey CT image of cat with restrictive cardiomyopathy and congestive heart failure. Cranial is to the top. Note severely enlarged left atrium (arrow) and pleural effusion (asterisk).

Figures 12a - c. Transverse survey CT images of mid (a) and caudal (b, c) thorax of two cats with cardiomyopathy; 6a, b: HCM and, 6c: RCM (c)

6a, b, c. Cardiogenic pulmonary edema seen as variable appearance and distribution of multifocal nonconsolidated alveolar pattern (arrows).

WW= 1600, WL = -600.

Figure 12a. Variable appearance of cardiogenic pulmonary edema (arrows).

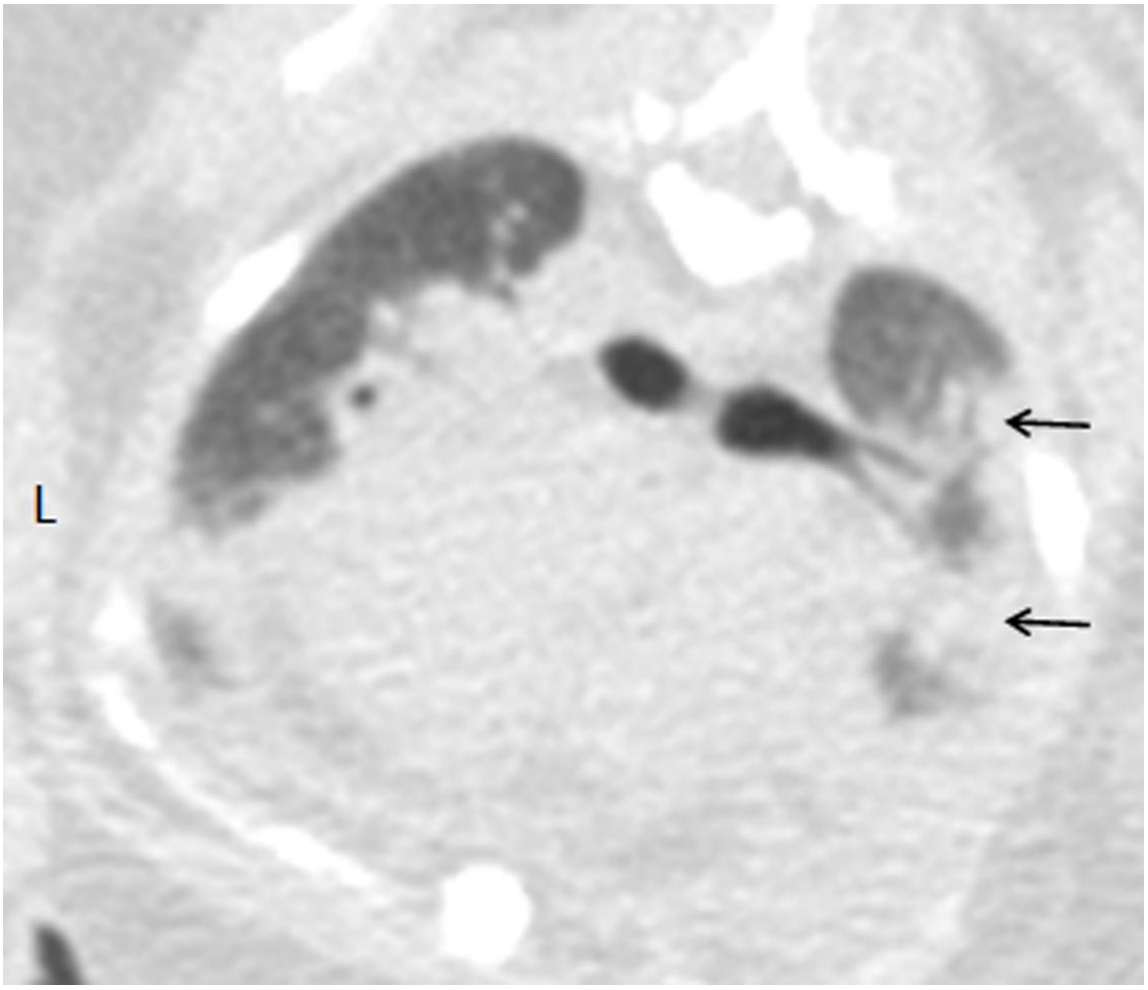

Figure 12b. Variable appearance of cardiogenic pulmonary edema (arrows). Note also pleural free fluid (10-15 HU) (asterisk) and fissure lines (long arrows).

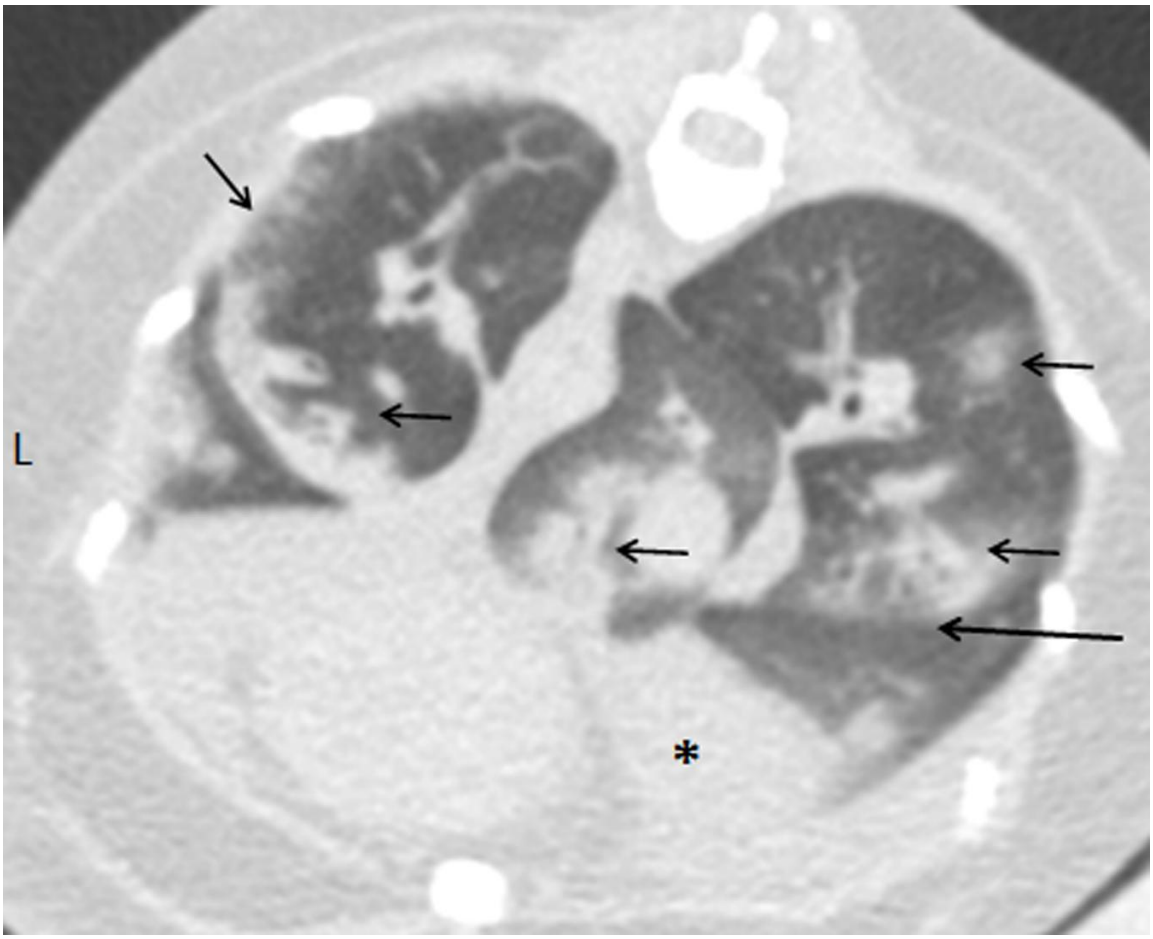

Figure 12c. Variable appearance of cardiogenic pulmonary edema (arrows).

Figure 13. Transverse CT image of the cranial thorax of a cat showing an area of alveolar pattern with reduced size (arrow) of the right cranial lung lobe, diagnosed as atelectasis and not seen with radiography. Note cranial mediastinum mass (asterisk). Window width = 1600, window level = -600.

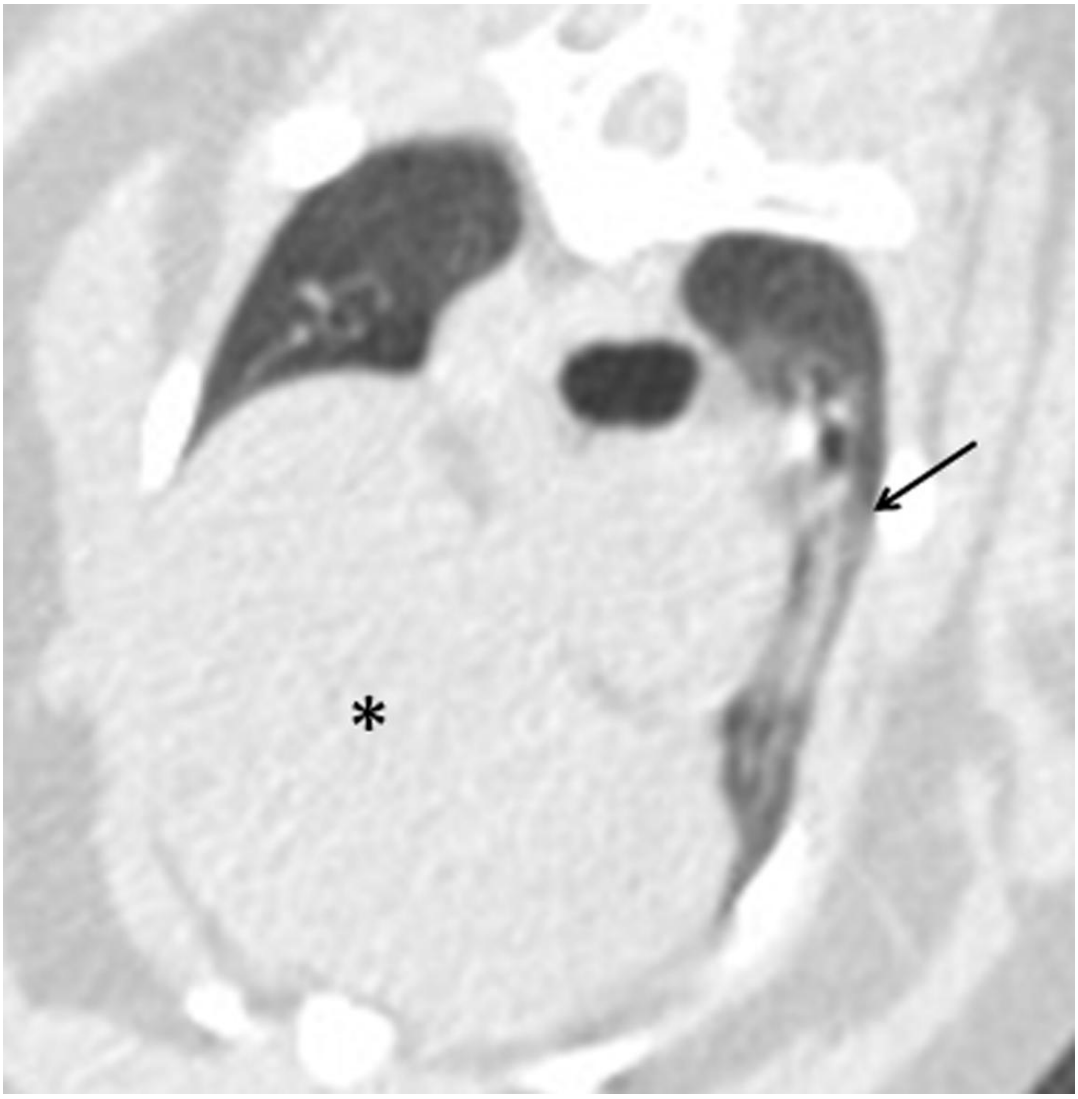

Figures 14a and b. Transverse survey CT images of the cranial thorax of a cat with suppurative tracheitis and bronchitis. Note severe tracheal (a, arrow) and bilateral main stem bronchi narrowing (b, arrows). WW = 1600, WL = -600.

Figure 14a. Severe tracheal narrowing (arrow).

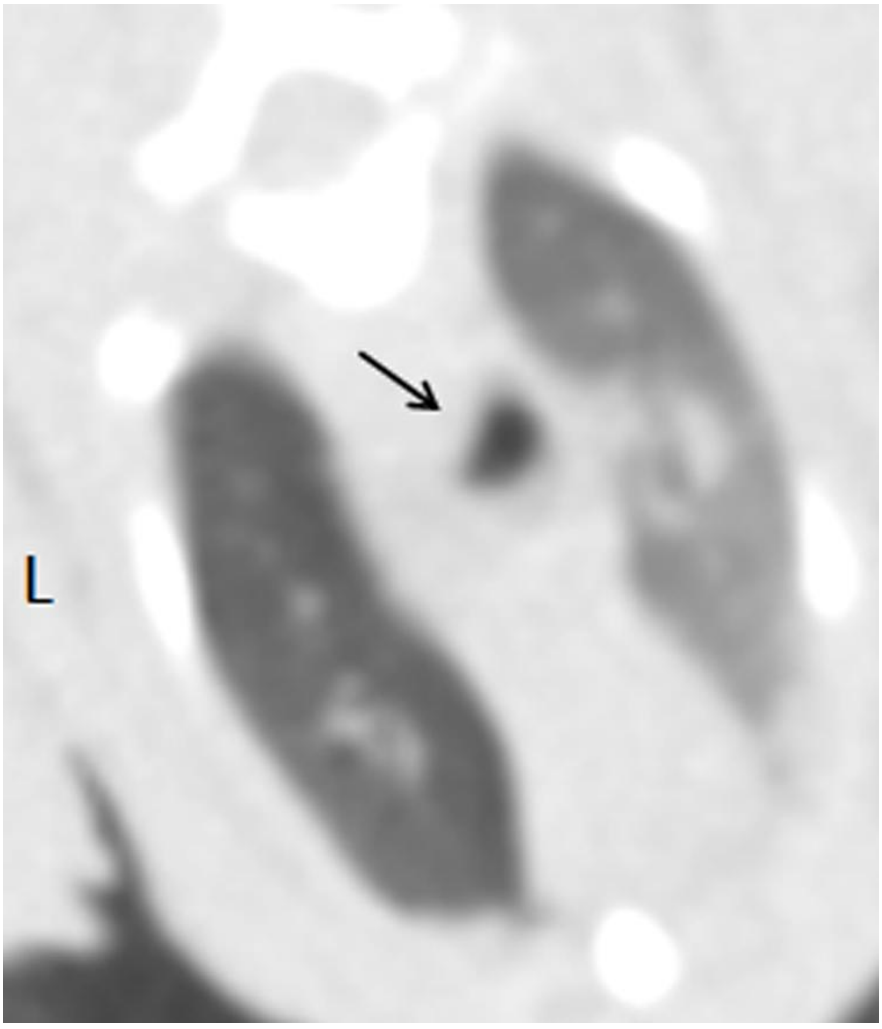

Figure 14b. Severe bilateral main stem bronchi narrowing (arrows).

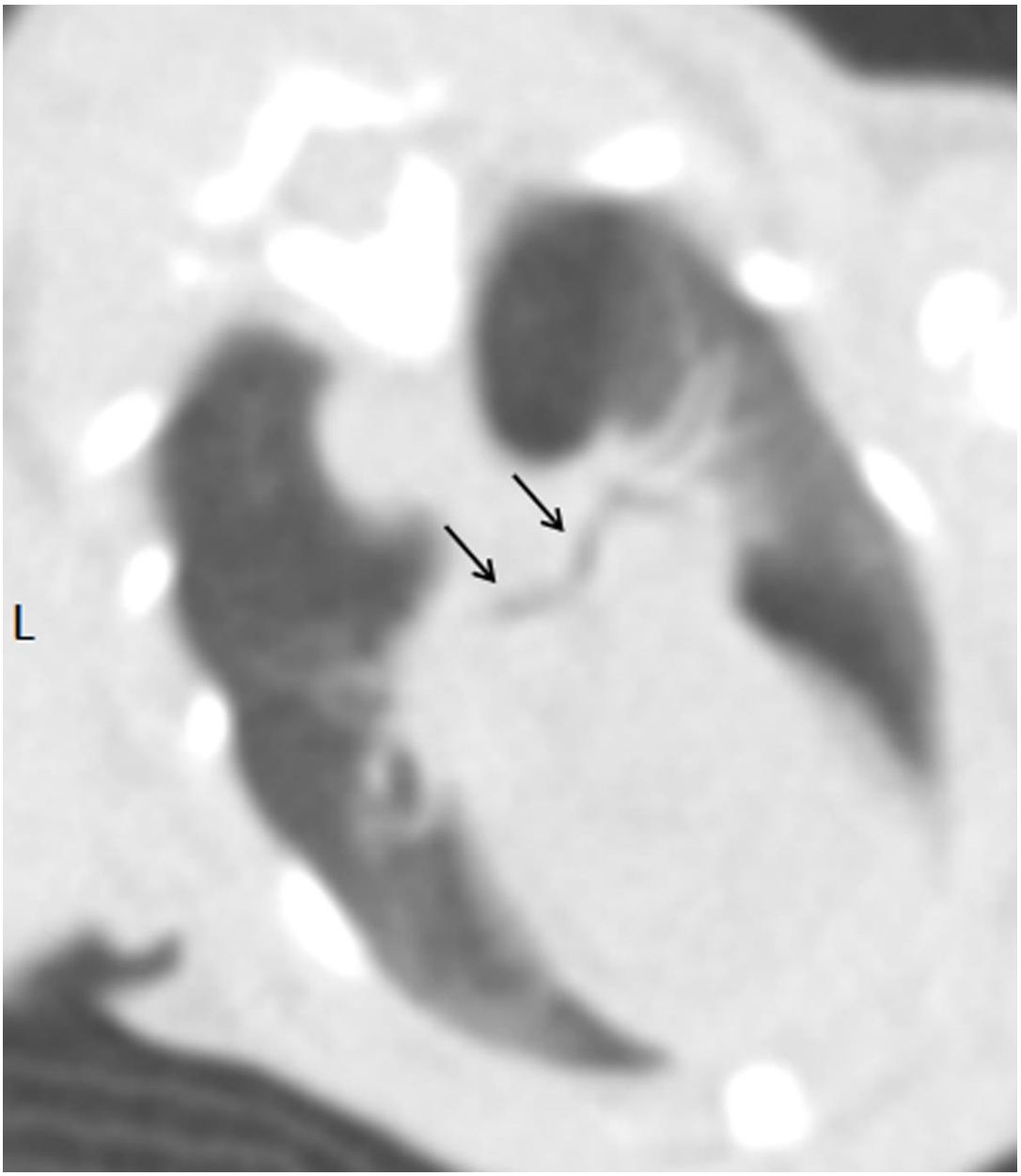

Figures 15a and b. Survey CT images of cat with tracheal rupture. Note tracheal discontinuity (arrows), pneumomediastinum (long arrow), pneumopericardium (thick arrow), and sub-cutaneous emphysema (asterisk). On surgery a 1 cm long tear was present at the dorso-right aspect of the tracheal wall. WW = 1600, WL = -600.

Figure 15a. Transverse CT image: tracheal discontinuity (arrow) and severe pneumomediastinum (long arrow) and sub-cutaneous emphysema (asterisk).

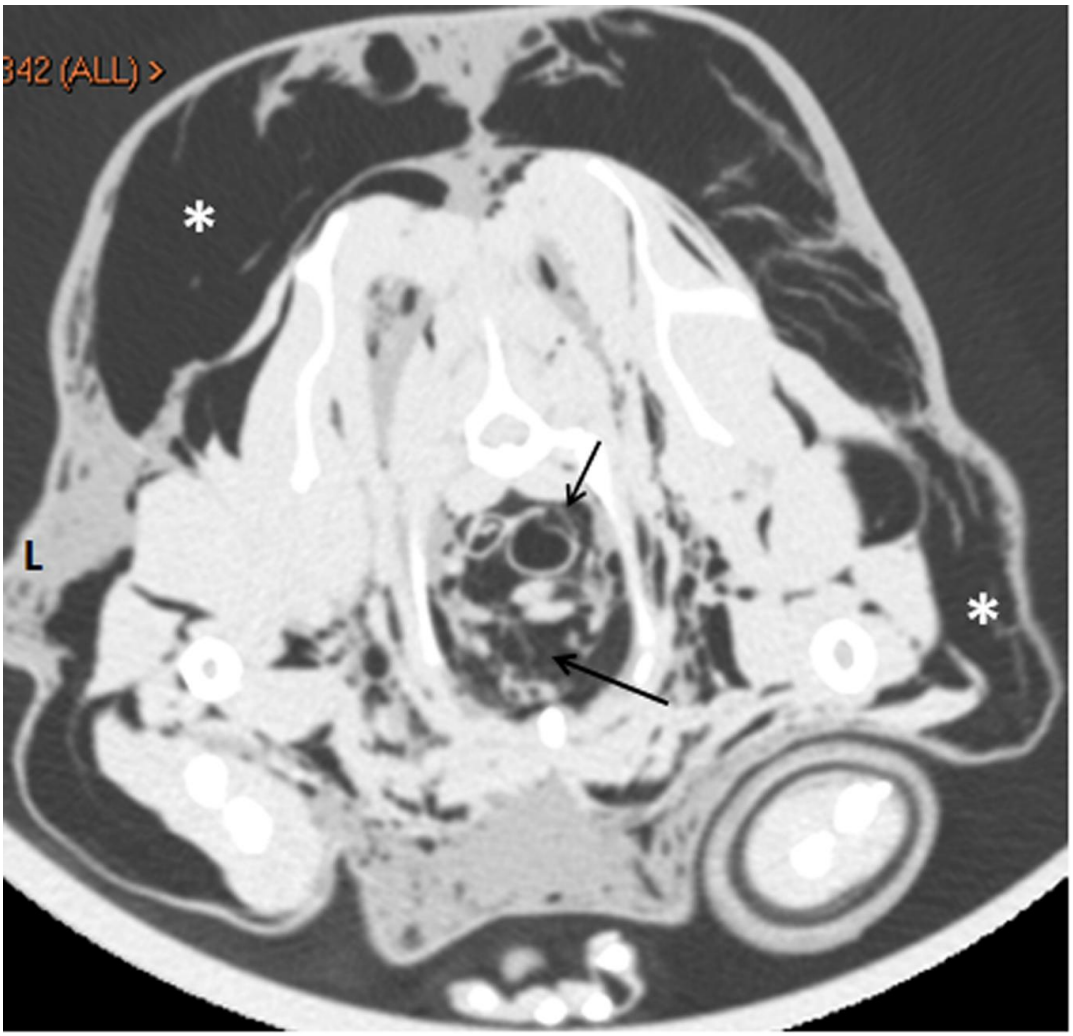

Figure 15b. Sagittal CT image: cranial is to the left. Tracheal discontinuity (arrow), severe pneumomediastinum (long arrow) and pneumopericardium (thick arrow).

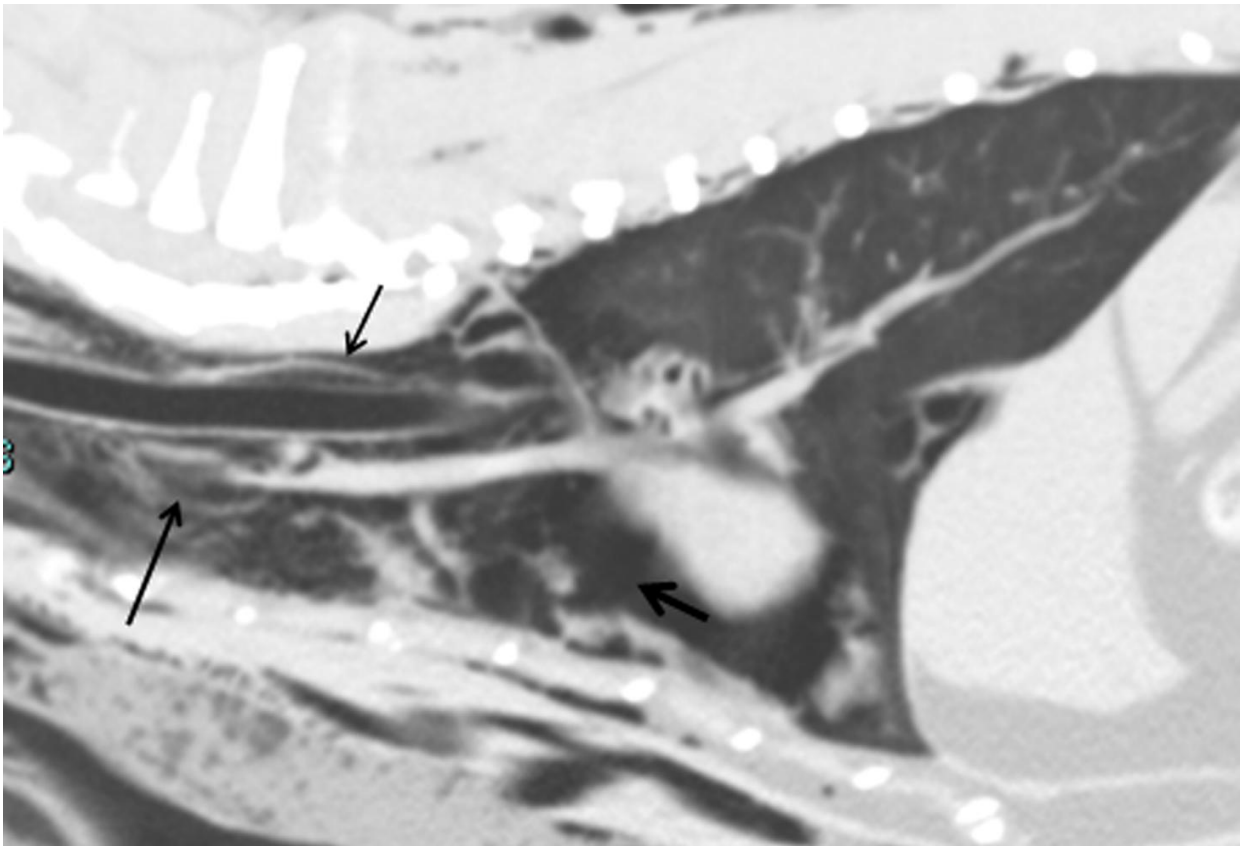

Figure 16. Transverse survey CT image of caudal thorax of a cat with diaphragmatic hernia. Note severe amount of fat attenuating material (-128 HU) in the ventral aspect of the thorax (asterisk). The spleen (arrow) and part of the liver (long arrow) are inside the thorax. The heart is displaced dorsally and to the right (thick arrow). Lung lobe atelectasis is also seen (arrow head). WW = 400, WL = 40.

Figure 17. Transverse contrast CT image of cranial thorax of cat with peritoneal pericardial diaphragmatic hernia. Note distended loops of intestine (arrow) and gallbladder (long arrow) within the pericardium, and large bulla lesion on the right cranial lung lobe (asterisk). On necropsy, segments of ileum, cecum and colon, together with caudate lobe of liver and gallbladder were passing through a 3 x 2 cm hernia. WW = 1600, WL = -600.

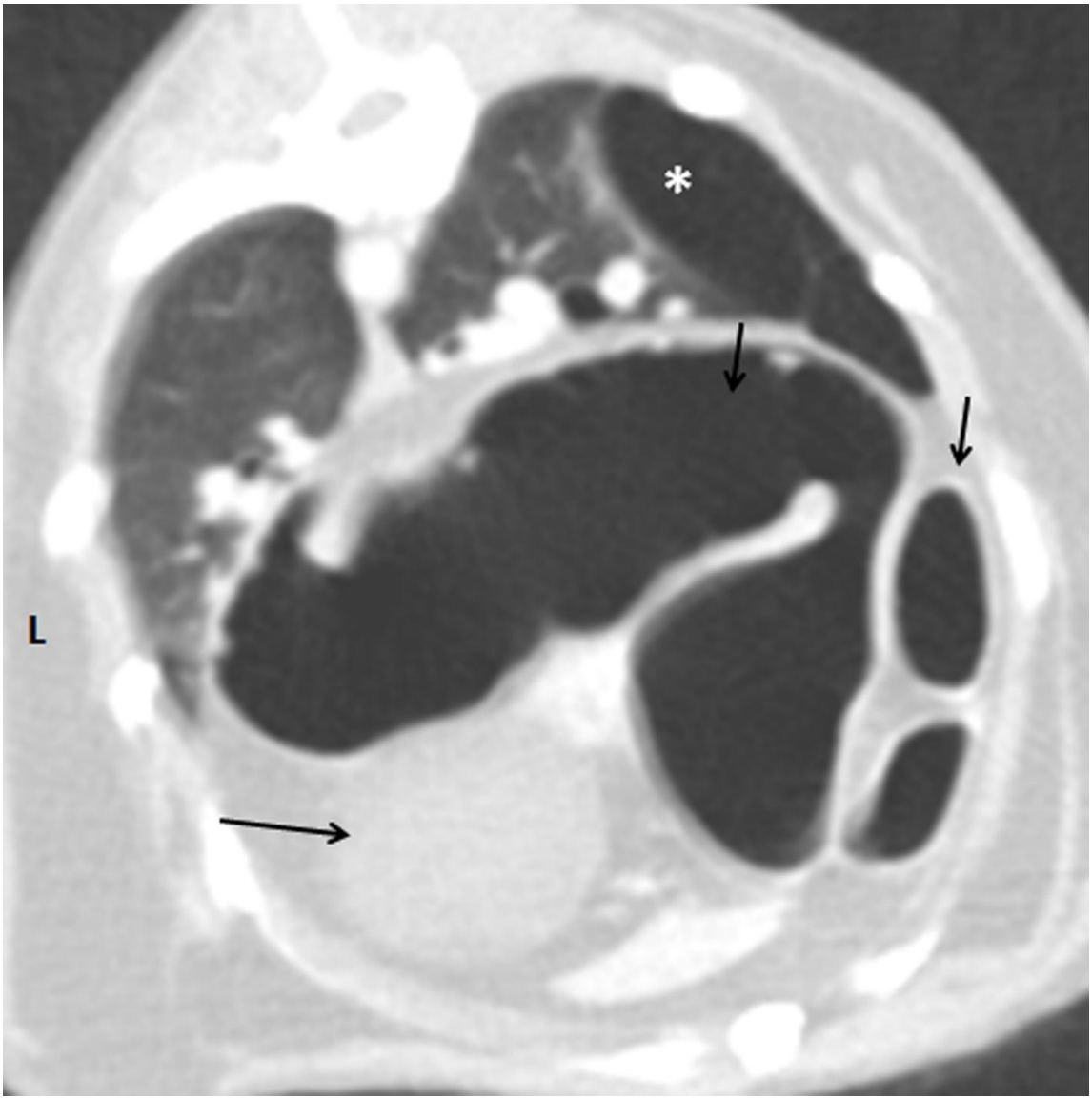

4.6 Tables

Table 10- Disease Groups and Comparison of Modalities

Groups	N	CT Correct Diagnosis	Rad Correct Diagnosis	CT Additional Information	Rad Additional Information
Lung neoplasia	9	8/9 (88.9%)	8/9 (88.9%)	8/9 (88.9%)	0/9 (0%)
Lower Airway	9	8/9 (88.9%)	4/8* (50%)	8/8* (100%)	0/8* (0%)
Cardiomyopathy	9	8/9 (88.9%)	6/8* (75%)	3/8* (37.5%)	2/8* (25%)
Mediastinal mass	8	8/8 (100%)	6/7* (85.7%)	6/7* (85.7%)	1/7* (33.3%)
Infection	7	2/7 (28.6%)	1/7 (14.3%)	5/7 (71.4%)	0/7 (0%)
Trauma	4	3/4 (75%)	0/4 (0%)	4/4 (100%)	0/4 (0%)
Hernia	3	2/3 (66.7%)	1/2* (50%)	1/2* (50%)	0/2* (0%)
Other	5	3/5 (60%)	3/5 (60%)	3/5 (60%)	0/5 (0%)
Total	54	42/54 (77.8%)	29/50 (58%)	38/50 (76%)	3/50 (6%)

Rad= radiography

* One cat did not have radiographs

Table 11- Criteria for Computed Tomography and Radiographic Diagnosis

Imaging modality	Radiography	Computed Tomography
Bronchitis	Bronchial wall thickening*; hyperinflation of lungs**; hyperlucent lung fields**; flattening of diaphragm**; right middle lung consolidation**	Bronchial wall thickening†; bronchial dilation†; right middle lung consolidation**
Cardiomegaly	Round heart*; shift of cardiac apex to the right*; valentine-shaped*	Round heart; valentine-shaped; chamber dilation; segmental wall thickening†
Microcardia	Reduced size of heart*; small vessels*; loss of contact with sternum*; hyperlucent lung fields*	Reduced size of heart*; small vessels*
Bronchiectasis	Enlarged and deformed bronchi*; lack of tapering	Bronchial dilation†; lack of tapering†; visible bronchi in the periphery of lung†; bronchial wall thickening†; mucoid impaction†
Lung mass	Round soft-tissue opacity > 3 cm*; mass effect*; absence of air bronchograms*; consolidated alveolar pattern with increased volume and loss of normal shape**; areas of cavitation**	Round soft-tissue opacity > 3 cm*; mass effect*; absence of air bronchograms*; consolidated alveolar pattern with increased volume and loss of normal shape**; areas of cavitation**
Bulla	Sharply demarcated areas of low attenuation resembling cysts†; disruption of vascular markings	Sharply demarcated areas of low attenuation resembling cysts†; disruption of vascular markings
Emphysema	Hyperlucent, enlarged lung fields*; scant but visible vascular markings*; caudally displaced, flattened diaphragm*	Hyperlucent, enlarged lung fields*; scant but visible vascular markings*; caudally displaced, flattened diaphragm*
Peritoneal effusion	Loss of serosal detail‡	Multiple linear soft-tissue opacities interspersed within the fat; pooling of fluid in the dependent abdomen (aprox. 10 HU); indistinct margins of organs
Pulmonary edema	Patchy alveolar pattern, consolidated alveolar pattern, diffuse in distribution, air bronchograms‡	Patchy alveolar pattern in the hilar region, periphery of lungs or sub-pleural region; consolidated alveolar pattern with air bronchograms
Tracheal collapse	Collapse of cervical segment and dilation of thoracic segment*; undulating dorsal aspect of tracheal wall*	Focal or segmental luminal collapse*; crescent-shaped trachea*, flattening of tracheal cartilage*
Chylothorax	Presence of pleural effusion and rounded lung margins	Presence of pleural effusion and rounded lung margins
Atelectasis	Reduced lung lobe size with alveolar pattern*; affected lobe triangular in shape, broad base and apex toward periphery*; mediastinal shift*	Reduced lung lobe size with alveolar pattern*; affected lobe triangular in shape, broad base and apex toward periphery*; mediastinal shift*
Pneumonia	Bronchial pattern in combination with alveolar*; consolidated alveolar pattern with normal or increased size and normal lung lobe shape*; lobar sign*; patchy alveolar pattern	Bronchial pattern in combination with alveolar*; consolidated alveolar pattern with normal or increased size and normal lung lobe shape*; lobar sign*; patchy alveolar pattern

*BSAVA Manual of Canine and Feline Thoracic Imaging
**Textbook of Respiratory Disease in Dogs and Cats
†Computed Tomography and Magnetic Resonance of the Thorax
‡ Textbook of Veterinary Diagnostic Radiology

Table 12: Kappa Results Between Imaging Modalities

	N*	Radiograph		CT		Kappa
Extra-thoracic		Absent	Present	Absent	Present	
Fracture	46	46	0	45	1	0
Costal arch deformation	46	44	2	42	4	0.292
Sternum deformation	46	45	1	45	1	-0.022
Abdomen						
Peritoneal effusion	46	41	5	42	4	0.877
Pneumoperitoneum	46	46	0	45	1	0
Mass	46	46	0	45	1	0
Aerophagia	46	31	15	32	14	0.346
Mediastinum						
Esophageal dilation	46	40	6	29	17	0.084
Pneumomediastinum	46	44	2	44	2	1
Mass	42	36	6	38	4	0.774
Lymphadenopathy	40	40	0	37	3	0
Cardiomegaly	42	37	5	35	7	0.419
Microcardia	46	41	5	44	2	0.238
Pleural cavity						
Effusion	46	30	16	31	15	0.951
Pneumothorax	46	43	3	41	5	0.728
Diaphragm						
Hernia	40	40	0	40	0	**
Flattening	43	37	6	43	0	0
Tenting	44	43	1	44	0	0
Asymmetry	46	46	0	46	0	**
Upper Airway						
Tracheal narrowing	46	45	1	44	2	0.657
Tracheal deviation	46	42	4	45	1	-0.036
Main stem bronchi narrowing	46	46	0	43	3	0
Lower Airway						
Bronchial wall thickening	45	36	9	34	11	0.359
Bronchiectasis	46	44	2	40	6	-0.07
Alveolar pattern	44	22	22	10	34	0.364
Lung mass	44	38	6	34	10	0.548
Unstructured interstitial	45	43	2	32	13	0.205
Structured interstitial	45	40	5	36	9	0.167
Vascular pattern	46	44	2	44	2	0.477
Bulla	44	43	1	41	3	-0.035
Hyperlucency	46	46	0	36	10	0

*Indeterminate answers resulted in some findings having less than 46 cats
**Insufficient number to perform test

Table 12 (cont.)- Kappa Results Between Imaging Modalities

	N	Absent		Mild		Moderate		Severe		Kappa
		Rad	CT	Rad	CT	Rad	CT	Rad	CT	
Degree of bronchial wall thickening	46	37	35	3	5	3	4	3	2	0.449
Degree of pneumomediastinum	46	44	44	0	0	1	1	1	1	1
Degree of pneumothorax	46	41	41	4	3	0	0	1	2	0.577
Degree of pleural effusion	46	30	31	7	7	6	3	3	5	0.809
Degree of esophageal dilation	46	40	30	5	13	1	3	0	0	0.170
	N	**Absent**		**Cranial**		**Middle**		**Caudal**		**Kappa**
Alveolar pattern distribution	46	23	11	12	10	1	2	10	23	0.329

Rad= radiography

Table 13- Indeterminate Answers

Outcome	Radiograph	CT
Mediastinal lymphadenopathy	16% (8/50)	0% (0/54)
Diaphragmatic hernia	16% (8/50)	0% (0/54)
Mediastinal mass	10% (5/50)	0% (0/54)
Cardiomegaly	10% (5/50)	0% (0/54)
Diaphragmatic flattening	8% (4/50)	1.9% (1/54)
Lung mass	6% (3/50)	0% (0/54)
Diaphragmatic tenting	4% (2/50)	1.9% (1/54)
Alveolar pattern	4% (2/50)	0% (0/54)
Bulla	4% (1/50)	0% (0/54)
Esophageal dilation	2% (1/50)	0% (0/54)
Bronchial wall thickening	2% (1/50)	0% (0/54)
Unstructured interstitial pattern	2% (1/50)	0% (0/54)
Structured interstitial pattern	2% (1/50)	0% (0/54)

Table 14- Results for Comparison of Proportions for Image Quality

	Radiography	CT	% Difference	95% CI	Chi-square*	Significance
Technique adequate	96%	100%	4%	-5.4% to 10.6%	0	P = 1
Positioning adequate	84%	100%	16%	4.7% to 29.1%	6.658	P = 0.0099
Motion artifact	0%	50%	50%	34.4% to 63.9%	31.215	P < 0.0001
Complete study	96%	100%	4%	-3.9% to 13.7%	0.510	P = 0.4751

Outcomes indicate presence

*Degrees of freedom= 1

CHAPTER 5

CONCLUSIONS

The VetMouseTrap™ is a safe device that provides effective oxygen and catheter-based therapy while keeping safe temperature and CO_2 levels. The construction has no moving parts or hinges and has a secure closure without additional metallic or plastic components. The sides are not sealed, which allows excess gas to escape, and prevents pressure, heat and humidity accumulation. The cats can be monitored visually throughout the imaging procedure and removed quickly in case of an emergency. The device has low attenuation (approximately 54 Hounsfield units) and did not cause visible artifacts during CT image acquisition, permitting CT imaging of non-sedated, unanesthetized cats.

The VetMouseTrap™ allowed whole-body images to be successfully acquired in a very short period of time in 90.9% (20/22) of awake normal cats with excellent spatial resolution in all three planes and negligible motion artifact when using a 16-slice CT scanner. Protocols with 1.75 pitch had significant windmill and helical-helical artifact that compromised image quality and therefore are not recommended. With 0.562 pitch, windmill and helical artifacts were almost absent and motion, although statistically higher compared to 1.75 pitch, was overall minimal and not considered to be clinically relevant. Based on these results and on the literature, we recommend a protocol of 80 kV, 130 mA, 0.5 s, and 0.562 pitch with a 1.25 mm slice thickness, and a 0.625 mm slice reconstruction interval for helical thoracic CT examination of awake cats using the VetMouseTrap™. The VetMouseTrap™ has the potential to make a significant impact on the safety of the diagnostic imaging and case management of cats with respiratory compromise.

Survey CT is highly accurate (77.8%) for the evaluation of cats with respiratory distress. Computed tomography provided additional information in 76% of the cats allowing a correct diagnosis not achieved with radiographs in 28% of cats. Radiography only provided the correct diagnosis in 58% of the cases. Computed tomographic imaging of cats using the VetMouseTrap^{TM} without general anesthesia or sedation is safe and provides more accurate diagnostic information than radiography.

REFERENCES

1. White CS, Kuo D. Chest Pain in the Emergency Department: Role of Multidetector CT. *Radiology*. 2007;245: 672-681.
2. Novelline RA, Rhea JT, Rao PM, Stuk JL. Helical CT in Emergency Radiology. *Radiology*. 1999;213: 321-339.
3. Cipone M, Diana A, Gandini G, Fava D, Trenti F. Use of Computed Tomography in Thoracic Diseases of Small Animals. *Vet Res Commun*. 2003;27: 381-384.
4. Henninger W. Use of computed tomography in the diseased feline thorax. *J Small Anim Pract*. 2003;44: 56-64.
5. Prather AB, Berry CR, Thrall DE. Use of radiography in combination with computed tomography for the assessment of noncardiac thoracic disease in the dog and cat. *Vet Radiol Ultrasound*. 2005;46: 114-121.
6. Burk RL. Computed tomography of thoracic diseases in dogs. *J Am Vet Med Assoc*. 1991;199: 617-621.
7. Yoon J, Feeney DA, Cronk DE, Anderson KL, Ziegler LE. Computed tomographic evaluation of canine and feline mediastinal masses in 14 patients. *Vet Radiol Ultrasound*. 2004;45: 542-546.
8. De Rycke LM, Gielen IM, Simoens PJ, van Bree H. Computed tomography and cross-sectional anatomy of the thorax in clinically normal dogs. *Am J Vet Res*. 2005;66: 512-524.
9. Johnson VS, Ramsey IK, Thompson H, Cave TA, Barr FJ, Rudorf H, et al. Thoracic high-resolution computed tomography in the diagnosis of metastatic carcinoma. *J Small Anim Pract*. 2004;45: 134-143.
10. Eisenkraft JB. Effects of anaesthetics on the pulmonary circulation. *British Journal of Anaesthesia*. 1990;65: 63-78.
11. Staffieri F, Franchini D, Carella GL, Montanaro MG, Valentini V, Driessen B, et al. Computed tomographic analysis of the effects of two inspired oxygen concentrations on pulmonary aeration in anesthetized and mechanically ventilated dogs. *Am J Vet Res*. 2007;68: 925-931.
12. Hedenstierna G, Rothen H. Atelectasis Formation During Anesthesia: Causes and Measures to Prevent It. *Journal of Clinical Monitoring and Computing*. 2000;16: 329-335.
13. Johnston C, Carvalho WBd. Atelectasias em pediatria: mecanismos, diagnóstico e tratamento. *Revista da Associação Médica Brasileira*. 2008;54: 455-460.
14. Nemanic S, London CA, Wisner ER. Comparison of thoracic radiographs and single breath-hold helical CT for detection of pulmonary nodules in dogs with metastatic neoplasia. *J Vet Intern Med* 2006;20: 508-515.
15. Flohr TG, Schaller S, Stierstorfer K, Bruder H, Ohnesorge BM, Schoepf UJ. Multi-Detector Row CT Systems and Image-Reconstruction Techniques. *Radiology*. 2005;235: 756-773.
16. Rydberg J, Liang Y, Teague SD. Fundamentals of multichannel CT. *Radiol Clin North Am*. 2003;41: 465-474.

17. Lee KSMD, Boiselle PMMD. Update on Multidetector Computed Tomography Imaging of the Airways. *Journal of Thoracic Imaging*.25: 112-124.
18. Siegel MJ. Multiplanar and Three-dimensional Multi-Detector Row CT of Thoracic Vessels and Airways in the Pediatric Population. *Radiology*. 2003;229: 641-650.
19. Goldman LW. Principles of CT and CT Technology. *J Nucl Med Technol*. 2007;35: 115-128.
20. Seeram E. Computed tomography: physical principles, clinical applications, and quality control St. Louis, Missouri: Saunders Elsevier, 2009;536.
21. Beckmann EC. CT scanning the early days. *The British Journal of Radiology*. 2006;79: 5–8.
22. Ohlerth S, Scharf G. Computed tomography in small animals--basic principles and state of the art applications. *Vet J*. 2007;173: 254-271.
23. Seibert JA. X-Ray Imaging Physics for Nuclear Medicine Technologists. Part 1: Basic Principles of X-Ray Production. *J Nucl Med Technol*. 2004;32: 139-147.
24. Miracle AC, Mukherji SK. Conebeam CT of the Head and Neck, Part 1: Physical Principles. *AJNR Am J Neuroradiol*. 2009;30: 1088-1095.
25. Tidwell AS. Advanced imaging concepts: A pictorial glossary of CT and MRI technology. *Clinical Techniques in Small Animal Practice*. 1999;14: 65-111.
26. Jerrold Bushberg JAS, Edwin M. Leidholdt, John M. Boone. The essential physics of medical imaging. Philadelphia: Lippincott Willians and Wilkins, 2001;933.
27. Ohkubo M, Wada S, Matsumoto T, Nishizawa K. An effective method to verify line and point spread functions measured in computed tomography. *Medical Physics*. 2006;33: 2757-2764.
28. Ohkubo M, Wada S, Ida S, Kunii M, Kayugawa A, Matsumoto T, et al. Determination of point spread function in computed tomography accompanied with verification. *Med Phys*. 2009;36: 2089-2097.
29. Suetens P. Fundamentals of Medical Imaging. Cambridge University Press, 2009;264.
30. Jerrold Bushberg JAS, Edwin M. Leidholdt, John M. Boone. The essential physics of medical imaging. *Williams and Wilkins*. 1994
31. Thomas Newton DGP. Radiology of the skull and brain: technical apects of computed tomography. The C.V. Mosby Company, 1981.
32. Bourne R. Fundamentals of Digital Imaging in Medicine. Springer-Verlag London Limited
2010;200.
33. Barrett JF, Keat N. Artifacts in CT: Recognition and Avoidance. *Radiographics*. 2004;24: 1679-1691.
34. Seibert JA, Boone JM. X-Ray Imaging Physics for Nuclear Medicine Technologists. Part 2: X-Ray Interactions and Image Formation. *J Nucl Med Technol*. 2005;33: 3-18.
35. Silver MD, Taguchi K, Hein IA, Chiang B, Kazama M, Mori I. Windmill artifact in multislice helical CT. *Medical Imaging 2003: Image Processing*. San Diego, CA, USA: SPIE, 2003;1918-1927.
36. Rivero MA, Ramirez JA, Vazquez JM, Gil F, Ramirez G, Arencibia A. Normal anatomical imaging of the thorax in three dogs: computed tomography and macroscopic cross sections with vascular injection. *Anat Histol Embryol*. 2005;34: 215-219.

37. Samii VF, Biller DS, Koblik PD. Normal cross-sectional anatomy of the feline thorax and abdomen: comparison of computed tomography and cadaver anatomy. *Vet Radiol Ultrasound*. 1998;39: 504-511.
38. Spann DR, Sellon RK, Thrall DE, Bostian AE, Boston GT. Computed tomographic diagnosis: use of computed tomography to distinguish a pulmonary mass from alveolar disease. *Vet Radiol Ultrasound*. 1998;39: 532-535.
39. Zekas LJ, Crawford JT, O'Brien RT. Computed tomography-guided fine-needle aspirate and tissue-core biopsy of intrathoracic lesions in thirty dogs and cats *Vet Radiol Ultrasound*. 2005;46: 200-204.
40. Morandi F, Mattoon JS, Lakritz J, Turk JR, Wisner ER. Correlation of helical and incremental high-resolution thin-section computed tomographic imaging with histomorphometric quantitative evaluation of lungs in dogs. *Am J Vet Res*. 2003;64: 935-944.
41. Schultz RM, Peters J, Zwingenberger A. Radiography, computed tomography and virtual bronchoscopy in four dogs and two cats with lung lobe torsion. *J Small Anim Pract*. 2009;50: 360-363.
42. Oliveira CR, Ranallo FN, Pijanowski GJ, Mitchell MA, O'Brien MA, McMichael M, et al. The VetmouseTrap™: a device for computed tomographic imaging of the thorax of awake cats. *Vet Radiol Ultrasound*."in press".
43. Brody ASMD. Thoracic CT Technique in Children. *Journal of Thoracic Imaging*. 2001;16: 259-268.
44. Frush DP, Donnelly LF. Helical CT in children: technical considerations and body applications. *Radiology*. 1998;209: 37-48.
45. Mann FA, Wagner-Mann CC, Branson KR. Transcutaneous Oxygen and Carbon Dioxide Monitoring in Normal Cats. *Journal of Veterinary Emergency and Critical Care*. 1997;7: 99-109.
46. Berent AC, Todd J, Sergeeff J, Powell LL. Carbon monoxide toxicity: a case series. *Journal of Veterinary Emergency and Critical Care*. 2005;15: 128-135.
47. Sigrist NE, Doherr MG, Spreng DE. Clinical findings and diagnostic value of post-traumatic thoracic radiographs in dogs and cats with blunt trauma. *J Vet Emerg Crit Care* 2004;14: 259-268.
48. Rydberg J, Sandrasegaran K, Ying J, Akisik F, Choplin RH, Tarver RD. Isotropic chest CT examination: diagnostic quality of reformats. *Clinical Radiology*. 2006;61: 588-592.
49. Szucs-Farkas Z, Kurmann L, Strautz T, Patak MA, Vock P, Schindera ST. Patient exposure and image quality of low-dose pulmonary computed tomography angiography: comparison of 100- and 80-kVp protocols. *Invest Radiol*. 2008;43: 871-876.
50. Viera AJ, Garrett JM. Understanding interobserver agreement: the kappa statistic. *Fam Med*. 2005;37: 360-363.
51. Sigal-Cinqualbre AB, Hennequin R, Abada HT, Chen X, Paul JF. Low-Kilovoltage Multi-Detector Row Chest CT in Adults: Feasibility and Effect on Image Quality and Iodine Dose. *Radiology*. 2004;231: 169-174.
52. Kalva SPMD, Sahani DVMD, Hahn PFMDP, Saini SMD. Using the K-edge to Improve Contrast Conspicuity and to Lower Radiation Dose With a 16-MDCT: a Phantom and Human Study. *Journal of Computer Assisted Tomography May/June*. 2006;30: 391-397.

53. Heyer CM, Mohr PS, Lemburg SP, Peters SA, Nicolas V. Image Quality and Radiation Exposure at Pulmonary CT Angiography with 100- or 120-kVp Protocol: Prospective Randomized Study. *Radiology*. 2007;245: 577-583.
54. Polacin A, Kalender WA, Marchal G. Evaluation of section sensitivity profiles and image noise in spiral CT. *Radiology*. 1992;185: 29-35.
55. Joly H, D'Anjou M-A, Alexander K, Beauchamp G. Comparison of Single-Slice Computed Tomography Protocols for Detection of Pulmonary Nodules in Dogs. *Vet Radiol Ultrasound*. 2009;50: 279-284.
56. Drees R, Dennison SE, Keuler NS, Schwarz T. Computed tomographic imaging protocol for the canine cervical and lumbar spine. *Vet Radiol Ultrasound*. 2009;50: 74-79.
57. Zamyatin AA, Hein IA, Silver MD, Nakanishi S. Up-sampling with Shift Method for Windmill Correction. *Nuclear Science Symposium Conference Record, 2006 IEEE*, 2006;2293-2295.
58. Mori I. Antialiasing backprojection for helical MDCT. *Medical Physics*. 2008;35: 1065-1077.
59. Dalrymple NC, Prasad SR, El-Merhi FM, Chintapalli KN. Price of Isotropy in Multidetector CT1. *Radiographics*. 2007;27: 49-62.
60. Paulson EK, Jaffe TA, Thomas J, Harris JP, Nelson RC. MDCT of Patients with Acute Abdominal Pain: A New Perspective Using Coronal Reformations from Submillimeter Isotropic Voxels. *Am J Roentgenol*. 2004;183: 899-906.
61. Szucs-Farkas Z, Verdun FR, von Allmen G, Mini RL, Vock P. Effect of X-ray tube parameters, iodine concentration, and patient size on image quality in pulmonary computed tomography angiography: a chest-phantom-study. *Invest Radiol*. 2008;43: 374-381.
62. Forrester SD, Moon ML, Jacobson JD. Diagnostic evaluation of dogs and cats with respiratory distress. *Compendium* 2001;23: 56-69.
63. Swift S, Dukes-McEwan J, Fonfara S, Loureiro JF, Burrow R. Aetiology and outcome in 90 cats presenting with dyspnoea in a referral population. *J Small Anim Pract*. 2009;50: 466-473.
64. Vilafranca M, Font A. Thymolipoma in a cat. *J Feline Med Surg* 2005;7: 125-127.
65. Benigni L, Morgan N, Lamb CR. Radiographic appearance of cardiogenic pulmonary oedema in 23 cats. *J Small Anim Pract*. 2009;50: 9-14.
66. Miller WT, Jr., Tino G, Friedburg JS. Thoracic CT in the intensive care unit: assessment of clinical usefulness. *Radiology*. 1998;209: 491-498.
67. Myer W. Radiography review: pleural effusion. *Vet Radiol Ultrasound*. 1978;19: 75-79.
68. Groves TF, Ticer JW. Pleural fluid movement. *Vet Radiol Ultrasound*. 1983;24: 99-105.
69. Damama-Moraitou KK, Patsikas MN, Koutinas AF. Feline lower airway disease: a retrospective study of 22 naturally occurring cases from Greece. *J Feline Med Surg* 2004;6: 227-233.
70. Corcoran BM, Foster DJ, Fuentes VL. Feline asthma syndrome: A retrospective study of the clinical presentation in 29 cats. *J Small Anim Pract*. 1995;36: 481-488.
71. Johnson EG, Wisner ER. Advances in respiratory imaging. *Vet Clin North Am Small Anim Pract* 2007;37: 879-900.
72. Koblik PD. Radiographic appearance of primary lung tumors in cats. *Vet Radiol Ultrasound*. 1986;27: 66-73.

73. Peter F. Suter CBC, Timothy R. O'Brien, Daniel Koller,. Radiographic recognition of primary and metastatic pulmonary neoplasms of dogs and cats. *Vet Radiol Ultrasound*. 1974;15: 3-24.
74. Miles KG. A review of primary lung tumors in the dog and cat. *Vet Radiol Ultrasound*. 1988;29: 122-128.
75. Gadbois J, D'Anjou MA, Dunn M, Alexander K, Beauregard G, D'Astous J, et al. Radiographic abnormalities in cats with feline bronchial disease and intra- and interobserver variability in radiographic interpretation: 40 cases (1999-2006). *J Am Vet Med Assoc*. 2009;234: 367-375.
76. Dye JA. Feline bronchopulmonary disease. *Vet Clin North Am Small Anim Pract Small Anim Pract*. 1992;22: 1187-1201.
77. Moses BL, Spaulding GL. Chronic bronchial disease of the cat. *Vet Clin North Am Small Anim Pract* 1985;15: 929-948.
78. Padrid P. Feline asthma diagnosis and treatment. *Vet Clin North Am Small Anim Pract* 2000;30: 1279-1293.
79. Moise NS, Wiedenkeller D, Yeager AE, Blue JT, Scarlett J. Clinical, radiographic, and bronchial cytologic features of cats with bronchial disease: 65 cases (1980-1986). *J Am Vet Med Assoc*. 1989;194: 1467-1473.
80. Evaluation of biomarkers in bronchoalveolar lavage fluid for discrimination between asthma and chronic bronchitis in cats. *Am J Vet Res*.71: 583-591.
81. Jensen SP, Lynch DA, Brown KK, Wenzel SE, Newell JD. High-resolution CT features of severe asthma and bronchiolitis obliterans. *Clin Radiol*. 2002;57: 1078-1085.
82. Harmanci E, Kebapci M, Metintas M, Ozkan R. High-resolution computed tomography findings are correlated with disease severity in asthma. *Respiration*. 2002;69: 420-426.
83. McLean AN, Sproule MW, Cowan MD, Thomson NC. High resolution computed tomography in asthma. *Thorax*. 1998;53: 308-314.
84. White HL, Rozanski EA, Tidwell AS, Chan DL, Rush JE. Spontaneous pneumothorax in two cats with small airway disease. *J Am Vet Med Assoc*. 2003;222: 1573-1575.
85. Norris CR, Samii VF. Clinical, radiographic, and pathologic features of bronchiectasis in cats: 12 cases (1987-1999). *J Am Vet Med Assoc*. 2000;216: 530-534.
86. Ooi GC, Khong PL, Chan-Yeung M, Ho JCM, Chan PKS, Lee JCK, et al. High-Resolution CT Quantification of Bronchiectasis: Clinical and Functional Correlation. *Radiology*. 2002;225: 663-672.
87. Woods AQ, Lynch DA. Asthma: an imaging update. *Radiol Clin North Am*. 2009;47: 317-329.
88. Litster AL, Buchanan JW. Radiographic and echocardiographic measurement of the heart in obese cats. *Vet Radiol Ultrasound*. 2000;41: 320-325.
89. Ferasin L, Sturgess CP, Cannon MJ, Caney SMA, Gruffydd-Jones TJ, Wotton PR. Feline idiopathic cardiomyopathy: a retrospective study of 106 cats (1994-2001). *J Feline Med Surg* 2003;5: 151-159.
90. Patnaik AK, Lieberman PH, Erlandson RA, Antonescu C. Feline cystic thymoma: a clinicopathologic, immunohistologic, and electron microscopic study of 14 cases. *J Feline Med Surg* 2003;5: 27-35.
91. Davies C, Forrester SD. Pleural effusion in cats: 82 cases (1987 to 1995). *J Small Anim Pract*. 1996;37: 217-224.

92. Zekas LJ, Adams WM. Cranial mediastinal cysts in nine cats. *Vet Radiol Ultrasound*. 2002;43: 413-418.
93. Scherrer W, Kyles A, Samii V, Hardie E, Kass P, Gregory C. Computed tomographic assessment of vascular invasion and resectability of mediastinal masses in dogs and a cat. *N Z Vet J*. 2008;56: 330-333.
94. Banker P, Jain V, Haramati L. Impact of chest CT on the clinical management of immunocompetent emergency department patients with chest radiographic findings of pneumonia. *Emerg Radiol* 2007;14: 383-388.
95. Hayden GE, Wrenn KW. Chest Radiograph vs. Computed Tomography Scan in the Evaluation for Pneumonia. *J Emerg Med*. 2009;36: 266-270.
96. Sharma S, Maycher B, Eschun G. Radiological imaging in pneumonia: recent innovations. *Curr Opin Pulm Med*. 2007;13: 159-169.
97. Ito I, Ishida T, Togashi K, Niimi A, Koyama H, Ishimori T, et al. Differentiation of bacterial and non-bacterial community-acquired pneumonia by thin-section computed tomography. *Eur J Radiol*. 2009;72: 388-395.
98. Reittner P, Ward S, Heyneman L, Johkoh T, Müller N. Pneumonia: high-resolution CT findings in 114 patients. *Eur Radiol*. 2003;13: 515-521.
99. Trow AV, Rozanski EA, Tidwell AS. Primary mycoplasma pneumonia associated with reversible respiratory failure in a cat. *J Feline Med Surg* 2008;10: 398-402.
100. Zulauf D, Kaser-Hotz B, Hassig M, Voss K, Montavon PM. Radiographic examination and outcome in consecutive feline trauma patients. *Vet Comp Orthop Traumatol*. 2008;21: 36-40.
101. Elmali M, Baydin A, Nural MS, Arslan B, Ceyhan M, Gurmen N. Lung parenchymal injury and its frequency in blunt thoracic trauma: the diagnostic value of chest radiography and thoracic CT. *Diagn Interv Radiol*. 2007;13: 179-182.
102. Trupka A, Waydhas C, Hallfeldt KK, Nast-Kolb D, Pfeifer KJ, Schweiberer L. Value of thoracic computed tomography in the first assessment of severely injured patients with blunt chest trauma: results of a prospective study. *J Trauma*. 1997;43: 405-411; discussion 411-402.
103. Bhandal J, Kuzma A. Tracheal rupture in a cat: diagnosis by computed tomography. *Can Vet J*. 2008;49: 595-597.
104. Mitchell SL, McCarthy R, Rudloff E, Pernell RT. Tracheal rupture associated with intubation in cats: 20 cases (1996-1998). *J Am Vet Med Assoc*. 2000;216: 1592-1595.
105. Fitzgerald KT, Flood AA. Smoke Inhalation. *Clin Tech Small Anim Pract* 2006;21: 205-214.
106. Schmiedt CW, Tobias KM, Stevenson MAM. Traumatic diaphragmatic hernia in cats: 34 cases (1991-2001). *J Am Vet Med Assoc*. 2003;222: 1237-1240.
107. Gibson TWG, Brisson BA, Sears W. Perioperative survival rates after surgery for diaphragmatic hernia in dogs and cats: 92 cases (1990-2002). *J Am Vet Med Assoc*. 2005;227: 105-109.
108. Minihan AC, Berg J, Evans KL. Chronic Diaphragmatic Hernia in 34 Dogs and 16 Cats. *J Am Anim Hosp Assoc*. 2004;40: 51-63.
109. Hyun C. Radiographic diagnosis of diaphragmatic hernia: review of 60 cases in dogs and cats. *J Vet Sci*. 2004;5: 157-162.

110. Reimer SB, Kyles AE, Filipowicz DE, Gregory CR. Long-term outcome of cats treated conservatively or surgically for peritoneopericardial diaphragmatic hernia: 66 cases (1987-2002). *J Am Vet Med Assoc*. 2004;224: 728-732.
111. Evans SM, Biery DN. Congenital peritoneopericardial diaphragmatic hernia in the dog and cat: a literature review and 17 additional case histories. *Vet Radiol Ultrasound*. 1980;21: 108-116.
112. Hodges RD, Tucker RL, Brace JJ. Radiographic diagnosis. *Vet Radiol Ultrasound*. 1993;34: 249-252.
113. Dongen Pv. What is your diagnosis? [Sliding hiatal hernia in a cat]. *J Small Anim Pract*. 1997;38: 379.
114. Ackerman N. Esophageal hiatal hernia in a dog. *Vet Radiol Ultrasound*. 1982;23: 107-108.
115. Owen MC, Morris PJ, Bateman RS. Concurrent gastro-oesophageal intussusception, trichobezoar and hiatal hernia in a cat. *N Z Vet J*. 2005;53: 371-374.
116. AhvenjÄRvi LK, Laurila JJ, Jartti A, Ylipalosaari P, Ala-Kokko TI, SyrjÄLÄ HP. Multi-detector computed tomography in critically ill patients. *Acta Anaesthesiol Scand*. 2008;52: 547-552.
117. Hounsfield G. Potential uses of more accurate CT absorption values by filtering. *Am J Roentgenol*. 1978;131: 103-106.
118. Ployngam T, Tobias AH, Smith SA, Torres SMF, Ross SJ. Hemodynamic effects of methylprednisolone acetate administration in cats. *Am J Vet Res*. 2006;67: 583-587.
119. Smith S, Tobias, AH, Fine, DM, Jacob, KA, Ployngam, T. Corticosteroid-Associated Congestive Heart Failure in 12 Cats. *Intern J Appl Res Vet Med*. 2004;*Vol. 2*: 159-170.